APPLICATION OF NEURAL NETWORKS TO PREDICT THE PERFORMANCE OF A RUN-AROUND MEMBRANE ENERGY EXCHANGER (RAMEE)

A Thesis Submitted to the College of

Graduate Studies and Research

In Partial Fulfillment of the Requirements

For the Degree of Master of Science

In the Department of Mechanical Engineering

University of Saskatchewan

Saskatoon

By

SOHEIL AKBARI

Permission to Use

In presenting this thesis in partial fulfilment of the requirements for a Postgraduate degree from the University of Saskatchewan, I agree that the Libraries of this University may make it freely available for inspection. I further agree that permission for copying of this thesis in any manner, in whole or in part, for scholarly purposes may be granted by the professors who supervised my thesis work or, in their absence, by the Head of the Department or the Dean of the College in which my thesis work was done. It is understood that any copying or publication or use of this thesis or parts thereof for financial gain shall not be allowed without my written permission. It is also understood that due recognition shall be given to me and to the University of Saskatchewan in any scholarly use which may be made of any material in my thesis.

Requests for permission to copy or to make other use of material in this thesis in whole or part should be addressed to:

Head of the Department of Mechanical Engineering

University of Saskatchewan

57 Campus Drive, Saskatoon, Saskatchewan, Canada (S7N 5A9)

ABSTRACT

The objective of this thesis is to develop a fast model to predict the performance of a Run-Around Membrane Energy Exchanger (RAMEE). The RAMEE is a novel air-to-air energy recovery system that is capable of transferring both heat and moisture between two air streams. The utilization of a properly controlled RAMEE in the HVAC system of a building can significantly reduce the required energy to condition the ventilation air of the buildings. A neural network (NN) approach is applied to model the steady-state and transient performance of the RAMEE under a wide range of operating and system parameters.

In order to approximate the underlying function of a physical system using a NN approach, a set of examples (data points) that describes the behavior of the system is required to train NNs. In this study, two separate numerical models that predict the steady-state and transient effectiveness of the RAMEE are utilized to generate the required training data sets. The Back-Propagation algorithm is applied to feed-forward NNs of different architectures to minimize the errors between the predicted effectivenesses by the numerical models and the NN models. Root Mean Squared Error (RMSE) between the results of steady-state NN models and the steady-state simulations are 0.05 °C for the sensible NN and 0.02 g_v/kg_a for the latent NN. The accuracy of the transient NNs are reported in terms of Mean Absolute Difference (MAD) which are 0.5 °C for the sensible model and 0.2 g_v/kg_a for the latent NN. The steady-state NN models show an excellent accuracy and the accuracy of transient NN models are quite acceptable for energy transfer calculation purposes, which is the main application of the NN models.

The main advantage of NNs over numerical models is the non-iterative nature of the NN models that provides a very fast feed-forward model that can generalize

and predict the RAMEE effectiveness for any practical operating condition in a fraction of second. This simplicity of predictions allowed the steady-state NN models to be used with a simple optimization algorithm to find the optimal performance of RAMEE during each operational hour. The TRNSYS computer simulations used the output of the optimized NNs to predict the annual energy savings caused by an optimally controlled RAMEE for an office building as well as a hospital. The results for an office building show up to 43% heating energy saving in cold climates, and up to 15% cooling energy saving in hot climates. The same analysis for the application of an optimally controlled RAMEE in the HVAC system of a hospital shows even more energy savings. The optimized RAMEE reduces the annual heating energy by 58 - 66% in cold climates, and the annual cooling energy by 10 - 18% in hot climates. The RAMEE allows the heating system to be downsized by 45% in cold climates, and the cooling system to be downsized by 25% in hot climates.

ACKNOWLEDGMENTS

I am deeply grateful to my supervisor, Professor Carey Simonson, who helped me with his valuable ideas, friendly manner, and patience. His understanding of different aspects of my life significantly helped me to complete my studies. Meeting somebody like Carey is not a chance that happens often in my life! I would like to thank my co-supervisor Professor Robert Besant for his deep knowledge and improving comments. I believe this world needs more people like Professor Besant to discover and deal with unknown problems.

I am thankful to all students at University of Saskatchewan RAMEE research group that I learned a lot from them. The interactions between the students in our research group were a very effective educative experience.

I also appreciate the financial support by the National Science and Engineering Research Council of Canada (NSERC) and Venmar CES, Inc., Saskatoon, SK, Canada.

To the people whom I like!

TABLE OF CONTENTS

page

LIST OF TABLES

LIST OF FIGURES

NOMENCLATURE

Acronyms

ACH	Air Change per Hour
AHRI	Air-Conditioning, Heating and Refrigeration Institute
ANN	Artificial Neural Network
ASHRAE	American Society of Heating, Refrigerating and Air-conditioning Engineers
BP	back-propagation
CAV	Constant Air Volume
CBECS	Commercial Buildings Energy Consumption Survey
EPA	Environment Protection Agency
ERV	Energy Recovery Ventilator
FD	Finite Difference
HVAC	Heating, Ventilation and Air-Conditioning;
IAQ	Indoor Air Quality
LAMEE	Liquid to Air Membrane Energy Exchanger
LCEA	Life-Cycle Environmental Assessment
LCC	Life-Cycle Cost
MAD	Mean Absolute Difference
MLP	Multi Layer Perceptron
MSE	Mean Squared Error
NN	Neural Network
PNL	Pacific Northwest Lab
RAHE	Run-Around Heat recovery Exchanger
RH	Relative Humidity
RAMEE	Run-Around Membrane Energy Exchanger
RMSE	Root Mean Squared Error
TESS	Thermal Energy System Specialists
TMY	Typical Meteorological Year
TNM	Transient Numerical Model
US	United States
VAV	Variable Air Volume

English Symbols

$\dot{m}$	Mass flow rate (kg/s)
A	Membrane surface area in the exchanger (m^2)
B	Intercept of the linear trend line
$b_{\{i\}}$	Bias to layer i
C_{air}	heat capacity rate of air, [W/°C]
C_p	Specific heat capacity of air (J/kg.K)

C_{salt}	heat capacity rate of salt solution, [W/°C]
Cr*	heat capacity rate ratio
Eff.	Effectiveness
H	Enthalpy (kJ/kg)
h	Enthalpy of air (J/kg dry air)
h_{fg}	Enthalpy of phase change (J/kg)
H*	Operating Condition Factor
h	Air side convective heat transfer coefficient [$W/m^2.°C$]
h_m	Air side convective mass transfer coefficient [$kg/(m^2.s)$]
$iw_{\{1,i\}}$	weights to layer 1 from input layer (input weight)
K	Kelvin
k	Membrane heat conductivity [W/(m.°C)]
k_m	Membrane mass conductivity (water vapor permeability) [kg/(m.s)]
Lat.	Latent
$lw_{\{2,1\}}$	weights to layer 2 from layer 1 (layer weight)
$lw_{\{3,2\}}$	weights to layer 3 from layer 2 (layer weight)
$lw'_{\{3,2\}}$	transpose of weights matrix to layer 3 from layer 2
M	Slope of the linear trend line
NTU	Number of Heat Transfer Units
NTU_m	Number of Mass Transfer Units
OC	Operational costs ($US)
PBP	Payback period (yr)
Q	Energy transfer via the RAMEE system (W)
$Q_{sens,rec}$	Sensible heat recovery (J/s)
$Q_{lat,rec}$	Latent energy recovery (J/s)
r	linear correlation coefficient
R	Bypass fraction (dimensionless)
U'	Overall convective mass transfer coefficient (kg/m^2 s)
Sen.	Sensible
T	temperature, [°C] or [F]
t	time (s)
th	air channel thickness (m)
U	overall heat transfer coefficient, [$W/(m^2.°C)$]
U_m	overall mass transfer coefficient, [$kg/(m^2.s)$]
W	humidity ratio, [kg_v/kg_a]
x	volume of salt solution in each exchanger (m^3)
x_i	LAMEE entrance length [m]
x_i/x_0	entrance ratio
x_0	LAMEE length [m]
y_0	LAMEE height [m]
y_0/x_0	aspect ratio

Greek Symbols

ΔT	the difference between outdoor and indoor air temperature ($T_{In,S} - T_{In,E}$)
ΔT_{diff}	the absolute difference between supply side temperature variation predicted by neural network model and finite difference model ($\Delta T_{diff} = \left\lvert \Delta T_{s,net} - \Delta T_{s,sim} \right\rvert$)
ΔT_s	the supply side temperature difference ($T_{In,S} - T_{out,S}$)
ΔW	the difference between outdoor and indoor air humidity ratio ($W_{In,S} - W_{In,E}$)
ΔW_{diff}	the absolute difference between supply side humidity ratio variation predicted by neural network model and finite difference model ($\Delta W_{diff} = \left\lvert \Delta W_{s,net} - \Delta W_{s,sim} \right\rvert$)
ΔW_s	the supply side humidity ratio difference ($W_{In,S} - W_{out,S}$)
δ	Membrane thickness [m]
ε	Effectiveness (%)
ε_l	Latent effectiveness (%)
ε_s	Sensible effectiveness (%)

Subscript

a	air
air	Refers to the air properties or air side properties
ave	Average
C	counter flow
CC	cross-counter flow
E	exhaust side
exh,in	The exhaust air at the inlet of the energy exchanger, i.e., indoor air
In	inlet
in	Refers to indoor condition (temperature, humidity ratio or enthalpy)
l	Latent
m	moisture
mem	membrane
net	value determined by the neural network model
Out	outlet
out	Refers to outdoor condition (temperature, humidity ratio or enthalpy)

oa	Outdoor ventilation air
opt	Optimal
S	supply side
s	Sensible
sim	by finite difference simulations
sol	Refers to the solution properties
sup	The air supplied to the conditioned space
sup,in	The supply air at the inlet of the energy exchanger, i.e., outdoor air
t	Total
sup,out	The supply air at the outlet of the energy exchanger
v	water vapor
w	water

CHAPTER 1

INTRODUCTION

1.1. An Overview on Energy Recovery in Buildings

Energy is one of the crucial concerns for the future of the world. Around 40 percent of the energy used by humans is consumed in buildings and almost half of this amount is used by the Heating Ventilating and Air-Conditioning (HVAC) systems of buildings [1.1]. A growing population requires more buildings and more energy. At the same time, the demand for a good thermal comfort and better Indoor Air Quality (IAQ) for occupants of buildings is changing HVAC standards (e.g. ASHRAE std. 55-2010, ASHRAE std. 62.1-2010, ASHRAE std. 90.1 2010) in a way that increases the required energy for air conditioning buildings.

With new and revised standards and increasing prices of energy, engineers have been trying to design and develop energy efficient systems to meet occupant comfort and IAQ standards for buildings. One method to save energy in buildings is called 'return air recirculation'. In this method the HVAC system uses a portion of the return air to mix with the supply air stream. This method is easy and cheap to implement but has two main problems. First, the other portion of the return air that is not being used for mixing with the supply air is discharged as exhaust air and all of its energy is lost. Second, since the return air may contain some airborne, it does not enhance the IAQ, health, and comfort for occupants in the building.

Over the last few decades energy recovery from exhaust air has been used in devices called Energy Recovery Ventilators (ERVs). ERVs are divided into two

main categories: heat recovery ventilators and heat and moisture recovery ventilators. Heat recovery ventilators transfer only sensible energy (heat) between supply and exhaust air streams using some specific types of heat exchangers (e.g. heat pipe and metal flat plate heat exchangers). The main advantage of this method is that there is little or no contaminant transfer from exhaust to supply air. In warm humid climates heat exchanger devices are being replaced by heat and moisture recovery ventilators since researches [1.2,1.3] show that a properly controlled heat and moisture exchanger can recover higher amounts of energy. The most commonly used heat and moisture exchanger is the 'energy wheel' (Figure 1.1) which makes up about ¾ of the new building market in North America. The energy wheel is a regenerative rotating wheel, comprised of numerous narrow desiccant coated channels that can transfer heat and moisture between two adjacent air streams as the wheel rotates between the supply and exhaust air flows. The advantages of this system are high performance, low cost, simplicity, and the possibility of defining a relatively simple control strategy for its optimum operation. The main disadvantages of energy wheels are the necessity of having adjacent supply and exhaust ducts, and the transfer of a small fraction of contaminants from the exhaust duct to the supply duct due to seal leakage and carry over.

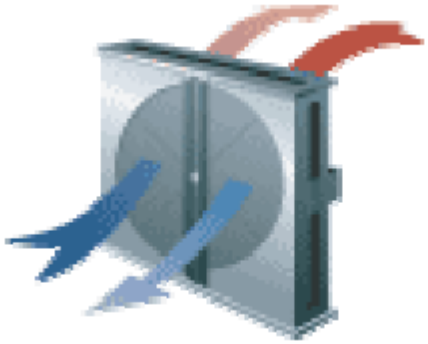

Figure 1.1. Energy wheel (from www.venmarces.com)

In this thesis, extensive research has been conducted on a new type of heat and moisture ERV, called a Run-Around Membrane Energy Exchanger (RAMEE), which does not have the disadvantages of energy wheels. Next section explains the principals about the RAMEE since.

1.2. Run-Around Membrane Energy Exchanger (RAMEE)

A Run-Around Membrane Energy Exchanger (RAMEE) is a novel air-to-air heat and moisture recovery system that consists of two separate liquid-coupled membrane-based energy exchangers, called LAMEEs, which each allow the transfer of both heat and water vapor as shown in Figure 1.2. RAMEEs do not need an adjacent supply and exhaust air ducting and can be installed for retrofit applications where supply and exhaust ducts may not be adjacent. Also for applications in buildings with more than one exhaust or supply duct, RAMEEs are easily applicable.

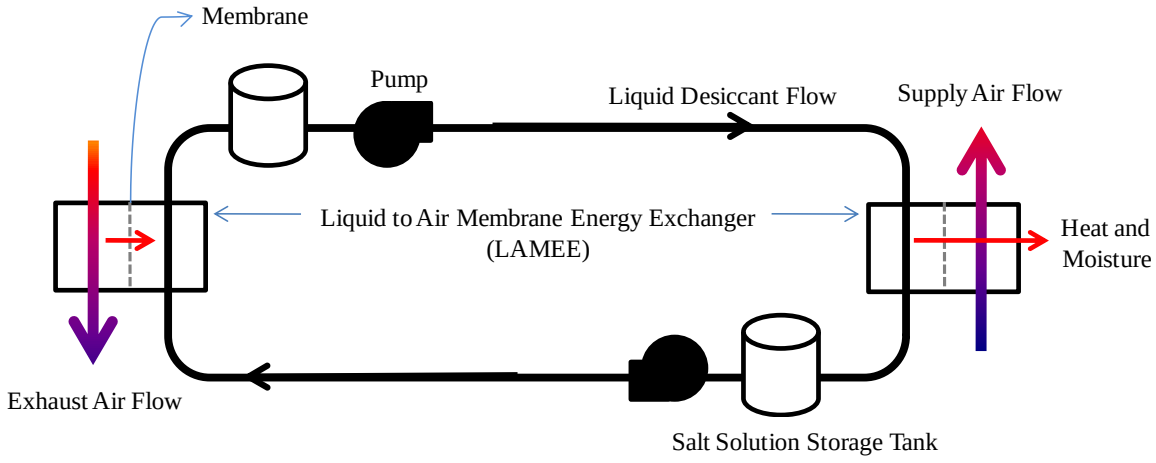

Figure 1.2. Schematic illustration of a RAMEE with all main components.

As is shown in Figure 1.2, each LAMEE in the RAMEE system transfers heat and moisture between each air stream and the pumped liquid desiccant salt solution flow. Assuming a winter operating condition when the indoor air is warmer and more humid than the outdoor air, the RAMEE preconditions the supply air by transferring heat and moisture from the exhaust to the supply air flow. During

summer outdoor conditions, the supply air is preconditioned by transferring heat and moisture to cooler and dryer exhaust flow.

1.3. The Importance of Controlling and Modeling the RAMEE System

Since the RAMEE is a coupled heat and moisture transfer system, the performance of the RAMEE is characterized by two effectiveness values for energy transfer, called sensible effectiveness and latent effectiveness for sensible energy and phase change energy transfer, respectively.

Effectiveness of the RAMEE depends on many parameters including operating conditions (outdoor and indoor air temperature and humidity), air flow rate, and solution flow rate. In many cases, uncontrolled operation of a RAMEE can increase the energy consumption of the HVAC system. For instance when the system is operating under a part load condition (the building needs cooling and the outdoor air is cool enough (e.g. 16 °C) to overcome internal loads) an uncontrolled RAMEE warms up the supply air, then the cooling unit has to cool down the supply air to adjust it to set-point temperature that causes a waste of energy. In many similar cases heat transfer, moisture transfer, or both may not be desired or heat transfer should be minimized and at the same time moisture transfer has to be maximized etc. For such conditions, an appropriate control strategy should be determined to maximize the RAMEE energy savings.

The first step for controlling any system is to realize the system behavior under different practical operating conditions. Therefore, representing models are required to predict the RAMEE effectivenesses. Some graduate students at Venmar CES student research group at the University of Saskatchewan have developed numerical models for the steady-state and transient performance of RAMEE [1.4-1.8].

1.4. Thesis Objectives and Overview

As mentioned in section 1.3, extensive research has been conducted to model and predict RAMEE performance. All the researchers have used experimental or numerical approaches (finite difference solutions) for the coupled heat and moisture transfer to quantify RAMEE performance. The numerical models are comprehensive and suitable for sensitivity studies, but due to their iterative nature, these codes are not fast enough to predict the RAMEE performance for some specific applications like calculating annual energy savings using transient building simulation tools (TRNSYS) and optimization of the RAMEE performance for different operating conditions where the system effectiveness for many hours of operation is required.

In order to develop a fast model to predict the performance of the RAMEE, a Neural Network (NN) approach is implemented in this thesis to map some of the inputs of numerical models to the corresponding desired outputs.

The objectives of this M.Sc. study are to:

1. Model the steady-state performance of RAMEE using NN approach over a wide range of operating conditions
2. Model the transient performance of a specific design of RAMEE using NNs for a practical transient operating conditions

The details of the methods implemented to meet the objectives of this research are described in chapter 2 for the steady-state NN model and chapter 3 for the transient NN model. Chapter 4 is an example for the application of the model presented in chapter 2, which shows the annual energy savings in a health-care facility with an optimally controlled RAMEE in its HVAC system.

This thesis is compromised of four manuscripts. As listed below, manuscript #1, #2, and #3 are presented in chapter 2, 3, and 4 respectively, while manuscript #4 which is a similar study to manuscript #3, is attached as Appendix A.

1. **S. Akbari**, H.B. Hemingson, D. Beriault, C.J. Simonson, R.W. Besant, Application of neural networks to predict the steady state performance of a Run-Around Membrane Energy Exchanger, *Int. J. Heat Mass Transfer* **55** (2012), pp. 1628–1641.
2. **S. Akbari**, C.J. Simonson, R.W. Besant, Application of neural networks to predict the transient performance of a Run-Around Membrane Energy Exchanger for yearly non-stop operation, Submitted to Int. J. Heat Mass Transfer for publication (Mar. 2012).
3. M. Rasouli, **S. Akbari**, C.J. Simonson and R.W. Besant. Analysis of a health-care facility HVAC system equipped with a run-around membrane energy exchanger, submitted to Energy and Buildings (Nov. 2010)
4. M. Rasouli, **S. Akbari**, H. Hemingson, R.W. Besant and C.J. Simonson. 2010. Application of a run-around membrane energy exchanger in an office building HVAC system, ASHRAE Transactions, 117 (2) (2012), pp. 686-703.

Appendix B is presenting the data needed to reproduce the steady-state and transient models presented in chapter 2 and 3. Appendix C covers the computer codes developed to optimize the RAMEE performance in chapter 4 and appendix A. Appendix D presents the copyright permissions from the publishers of manuscript #1 and #4 and the co-authors who contributed to manuscripts # 2 and #3.

1.5. References of Chapter 1

[1.1] L. Perez-Lombard, J. Ortiz, C. Pout, A review of buildings energy consumption information, 40 (2008), pp. 394-398.

[1.2] L.Z. Zhang , J.L. Niu, Energy requirements for conditioning fresh air and the longterm savings with a membrane-based energy recovery ventilator in Hong Kong, Energy 26 (2001), pp. 119–135.

[1.3] M. Rasouli, C. J. Simonson, R. W. Besant, Applicability and optimum control strategy of energy recovery ventilators in different climatic conditions, Energy and Buildings 42 (2010), pp. 1376–1385.

[1.4] M. Seyed Ahmadi, B. Erb, C.J. Simonson, R.W. Besant, Transient behavior of run-around heat and moisture exchanger system. Part I: Model formulation and verification, International Journal of Heat and Mass Transfer 52 (2009), pp. 6000-6011.

[1.5] M. Seyed Ahmadi, B. Erb, C.J. Simonson, R.W. Besant, Transient behavior of run-around heat and moisture exchanger system. Part II: Sensitivity studies for a range of initial conditions, International Journal of Heat and Mass Transfer 52 (2009), pp. 6012-6020.

[1.6] B. Erb, C.J. Simonson, M. Seyed Ahmadi, R.W. Besant, Experimental Measurements of a Run-Around Membrane Energy Exchanger (RAMEE) with Comparison to a Numerical Model, ASHRAE Transactions, 115(2009).

[1.7] A. Vali, Modeling a Run-around Heat and Moisture Exchanger Using Two Counter/Cross Flow Exchangers, M.Sc. thesis, University of Saskatchewan, Saskatoon, Sk, Canada, 2010.

[1.8] H.B. Hemingson, The Impacts of Outdoor Air Conditions and Non-Uniform Exchanger Channels on a Run-Around Membrane Energy Exchanger, M.Sc. Thesis, University of Saskatchewan, Saskatoon, SK, 2010.

CHAPTER 2

STEADY STATE PERFORMANCE OF RAMEE

2.1. Overview of Chapter 2

This chapter contains manuscript #1, which provides a detailed description of the methods applied to develop neural networks (NNs) that predict the steady-state performances of the RAMEE over a wide range of affecting parameters.

After a literature review, this chapter presents the physical description of the RAMEE and introduces the numerical model for the RAMEE. The parameters that may affect the performance of the RAMEE are studied in sections 2.4.3 and 2.4.4 followed by the selected inputs and outputs for the NN models and the description of NNs architecture and training process. Finally, numerical and experimental validation of the NN models are presented in section 2.8.

The required data to train NN models is provided using the latest version of steady-state model available in Venmar CES student research group (this version is the last version before the EPS 1.3.1). The Neural Network Toolbox of MATLAB® version 7.10.0 is used to train the data provided by steady-state numerical model.

The contributions of each author to this research work are as follows:

Soheil Akbari, M.Sc. student and main author, generated and processed the numerical data, trained the networks, developed the figures and tables, and wrote the paper.

Howard B. Hemingson, M.Sc. student, helped the main author to understand the physical problem more profoundly, debugged and supported the numerical model, and helped the main author to generate the numerical data.

David Beriault, M.Sc. student, provided the experimental data to validate the NN models (Figure 2.12)

Carey J. Simonson, and **Robert W. Besant**, the research group supervisors, conceived the research study, read and edited the paper and improved this study with their valuable comments.

MANUSCRIPT # 1

Application of neural networks to predict the steady state performance of a Run-Around Membrane Energy Exchanger

Soheil Akbari, Howard B. Hemingson, David Beriault, Carey J. Simonson[*]*, Robert W. Besant*

2.2. Abstract

Modeling the performance characteristics of thermal systems has been a research interest for many decades with moisture transfer systems experiencing a resurgence over the last decade, especially in heating, ventilating, and air conditioning (HVAC) applications. In this study, a Neural Network (NN) model is developed to predict the heat and moisture transfer performances (i.e., the sensible and latent effectivenesses) of a novel HVAC energy exchanger called the Run-Around Membrane Energy Exchanger (RAMEE) which is able to transfer both heat and moisture between exhaust and supply air streams. The training data set for the NN model covers a wide range of design and operating parameters and is produced using an experimentally validated finite difference (FD) model. Two separate NNs (one for sensible and one for latent energy transfer) each with five inputs and one output, are selected to represent the RAMEE. The results from NN models are numerically and experimentally validated. The root mean squared error (RMSE) between the FD and NN models are 0.05 °C and 2×10^{-5} kg_v/kg_a, indicating satisfactory agreement for energy exchange calculations. The paper reports the weights and biases to make the results of this study reproducible. These NN models are very fast and easy to use therefore, they might be used for design and for estimating the annual energy savings in different buildings which use the RAMEE in their HVAC system. Additionally, the NN models can be used with optimization

algorithms to maximize energy savings and minimize life-cycle costs for a given system.

2.3. Introduction

With increasing emphasis on reducing energy consumption, extensive research has been done to model heat and energy exchangers. Zhang et al. [2.1] studied the conjugate heat and mass transfer in membrane-formed channels for different flow configurations using a CFD model. Zhang [2.2] also modeled heat and mass transfer in plate-fin enthalpy exchangers and compared different plate and fin materials. Several researchers have measured and modeled heat and mass transfer characteristics of a rotating regenerative total energy wheel [2.3-2.7].

The use of computational intelligence techniques like neural networks (NNs), instead of conventional methods, is sharply increasing, since they have many interesting advantages [2.8]. NNs are easy to implement and use. Also a correctly designed NN can approximate any complex, continuous, and nonlinear function to a pre-specified accuracy and can generalize underlying functions describing a physical phenomenon (e.g. the performance function of a thermal and/or moisture transfer system).

Kalogirou [2.8] discuses various applications of neural networks in energy analysis problems. During recent years, many researchers have used neural networks to predict the performance of thermal systems using experimental or numerical data [2.9-2.14]. Ning and Zaheeruddin [2.15] developed a dynamic neural model to determine the optimal control of a variable-air-volume HVAC system in a building.

Using numerical simulation methods, Vali et al. [2.16] studied the effectiveness of a Run-Around Heat recovery Exchanger (RAHE) system with combined counter and cross flow exchangers. They also developed a new

effectiveness correlation for counter/cross flow configuration. Fan et al. [2.17] developed a finite difference (FD) model to predict the performance of a Run-Around Membrane Energy Exchanger (RAMEE) system using cross flow exchangers for simultaneous heat and moisture transfer for air-to-air energy recovery. The transient performance of the RAMEE was developed by Seyed Ahmadi et al. [2.18] and a complete study about the steady state performance under different outdoor air conditions was presented by Hemingson et al. [2.19, 2.20].

Although a numerical model for performance prediction of counter flow RAMEE system exists, it is too computationally intensive to be used by design engineers. Also working with this code for performance and energy consumption optimization purposes would be even more time consuming. For example, in order to maximize annual energy savings in a building using the RAMEE system, the optimum performance of the system during every operational hour through the year is required. Therefore, having a computationally fast model that relates the operating conditions to performance of RAMEE would be very useful.

Such a desired correlation would be very complex because the behavior of the RAMEE system is non-linear and there are many parameters that affect the performance of the RAMEE and each of these vary over wide ranges. Therefore, finding correlations with desired accuracy using conventional methods for a RAMEE system is likely very difficult or impractical.

The purpose of this study is to correlate the performance characteristics (i.e. sensible and latent effectivenesses) of a counter flow RAMEE system for a covering and practical range of independent parameters that affect the system performance using a multi-layer perceptron (MLP) neural network [2.21], trained with a back-propagation algorithm [2.22].

2.4. Description of RAMEE

2.4.1. Main Components

As can be seen in Figure 2.1, the RAMEE is composed of two exchangers, which simultaneously transfer heat and moisture between two air streams using an aqueous salt solution as a coupling liquid. For example in HVAC applications during winter operating condition, the outdoor air (inlet of supply exchanger) is usually cooler and dryer than the indoor air (inlet of exhaust exchanger). During such conditions, the RAMEE recovers heat and moisture from the exhaust air and transfers this recovered heat and moisture to the supply air. Therefore it saves energy and increases the indoor comfort for occupants.

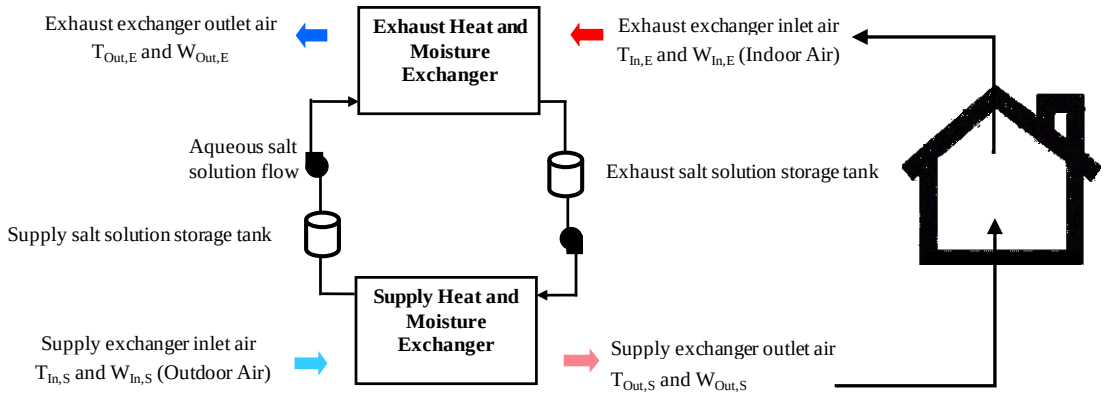

Figure 2.1. Schematic view of RAMEE components and inlet and outlet air conditions.

Each exchanger is made up of many air and liquid flow channels, each separated by a semi-permeable membrane (Figure 2.2). These membranes allow water vapor to transfer between the fluid streams but they prevent liquid transfer [2.23]. Such a heat and moisture exchanger is called a Liquid-to-Air Membrane Energy Exchanger (LAMEE). An individual LAMEE can have different flow configurations. Figure 2.2a and b show counter and cross-counter flow configurations respectively.

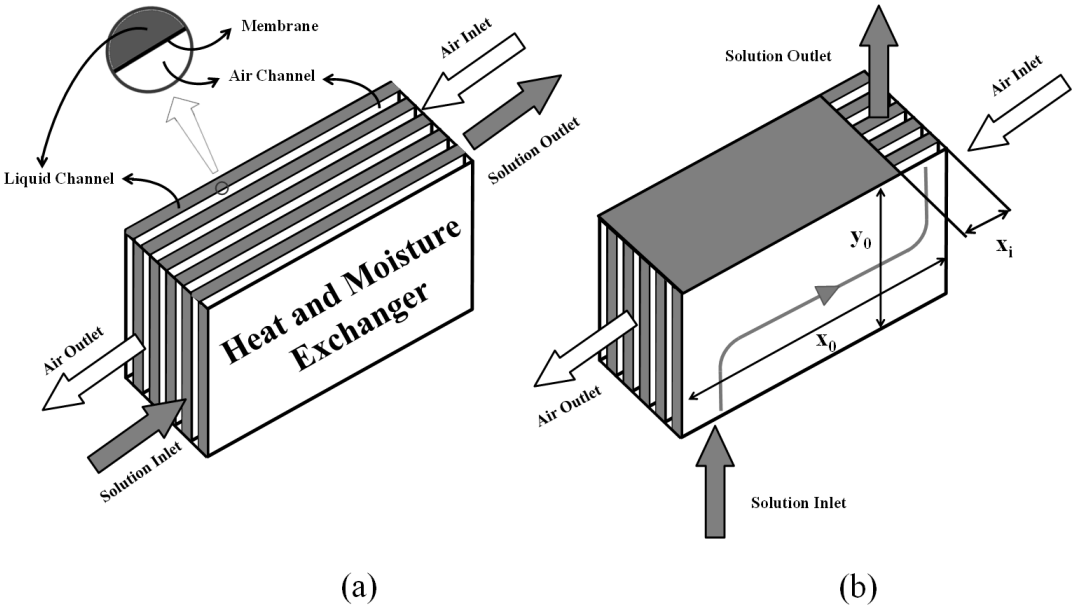

Figure 2.2. More details for structure and operation of a) counter flow LAMEE b) cross-counter flow LAMEE.

The RAMEE system which is studied and modeled in this paper has two identical LAMEEs with equal mass flow rates of air.

2.4.2. Numerical Model

A numerical model which solves the governing physical equations for steady-state coupled heat and mass transfer through the RAMEE system is presented by Hemingson et al. [2.19, 2.20]. This model predicts the sensible and latent effectivenesses of the RAMEE system defined in equations 2.1 and 2.2 where the mass flow rate of supply and exhaust air streams are equal.

$$\varepsilon_s = \frac{\Delta T_S}{\Delta T} = \frac{T_{In,S} - T_{Out,S}}{T_{In,S} - T_{In,E}} \quad (2.1)$$

$$\varepsilon_l = \frac{\Delta W_S}{\Delta W} = \frac{W_{In,S} - W_{Out,S}}{W_{In,S} - W_{In,E}} \quad (2.2)$$

Where, ΔT_S and ΔW_S are the air temperature and humidity ratio difference between the inlet and outlet of supply LAMEE, and ΔT and ΔW are the air

temperature and humidity ratio difference between the inlets of supply and exhaust LAMEEs. ΔT and ΔW can be considered as the driving potentials for heat and moisture transfer in RAMEE system. The other symbols are defined in the nomenclature. In this study, the results from this numerical model are used to develop the NN models.

2.4.3. Parameters Affecting RAMEE Performance

Hemingson et al. [2.19, 2.20] showed that many parameters affect the performance of the RAMEE. The purpose of studying the effect of these parameters is to determine the importance of each parameter. It helps us to simplify the predicting model by eliminating the parameters that are not important. Here we categorize them into two groups, first *design parameters* and second *operating parameters*.

2.4.3.1. Design Parameters

There are four important dimensionless design parameters that affect the performance of the RAMEE as listed below.

$$NTU = \frac{UA}{C_{air}} = \frac{UA}{\dot{m}_a C_{P,a}} \tag{2.3}$$

$$NTU_m = \frac{U_m A}{\dot{m}_a} \tag{2.4}$$

$$Aspect\ Ratio = \frac{Y_0}{X_0} \tag{2.5}$$

$$Entrance\ Ratio = \frac{X_i}{X_0} \tag{2.6}$$

where *NTU* is the number of heat transfer units of each LAMEE and NTU_m is the number of mass transfer units.

The aspect ratio is the ratio of the height to the length of the LAMEEs and the entrance ratio is the ratio of solution flow entrance length to the length of LAMEE (Figure 2.2).

2.4.3.2. Operating Parameters

Operating parameters are parameters that may change during the operation of a RAMEE in a building. These parameters include the temperature and humidity ratio of the outdoor and indoor air (Figure 2.1) and the heat capacity rate ratio, *Cr**, as defined in equation 2.7.

$$Cr^* = \frac{C_{sol}}{C_a} \tag{2.7}$$

C_a and C_{sol} are respectively heat capacity rate of air and salt solution flows. *Cr** is an operating parameter because the solution flow rate may be changed to maximize or minimize heat and moisture transfer depending on the building needs [2.24].

2.4.4. Effects of Design Parameters

2.4.4.1. Effect of *NTU* and NTU_m

According to equations 2.3 and 2.4 the ratio of NTU_m and *NTU* would be

$$\frac{NTU_m}{NTU} = C_{p,a}\ \frac{U_m}{U} \tag{2.8}$$

where $C_{p,a}$ is the thermal capacity of air and can be assumed as a constant value. The ratio of U_m and *U* is equal to

$$\frac{U_m}{U} = \frac{\left[\frac{1}{h_{m,air}}+\frac{\delta}{km}\right]^{-1}}{\left[\frac{1}{h_{air}}+\frac{\delta}{k}\right]^{-1}} \tag{2.9}$$

where h_{air} and $h_{m,air}$ are air-side convective heat and moisture transfer coefficients respectively. For the practical operation range of RAMEE, the air and salt solution flow are laminar and mainly fully developed therefore the convective heat and mass transfer coefficients for a *given design* are constant since the Nusselt number is

constant and equal to 8.24 [2.25]. Thus, h_{air} and $h_{m,air}$ are only a function of air channel thickness, the thickness of membrane, δ, and the heat conductivity and mass conductivity of the membrane, k and k_m. Therefore, for a given membrane and air channel thickness the ratio of U_m and U is constant. It means that NTU_m and NTU for a given LAMEE are always proportional therefore, only one of these design parameters needs to be known or used as input to the NN model. In this paper NTU will be used as an input parameter for the NN model and NTU_m/NTU will be constant and equal to 0.26 based on the specifications of the LAMEEs presented in table 2.1.

Table 2.1. Membrane and air gap properties of each LAMEE.

Property	Value
LAMEE Dimensions	
Length	1800 [mm]
Width	200 [mm]
Entrance Length	76 [mm]
Channel Thickness	
Air	4.4 [mm]
Solution	2.7 [mm]
Membrane Properties	
Thickness	0.2 [mm]
Thermal Conductivity	0.334 [W/(m·K)]
Water Vapour Permeability	1.66×10^{-6} [kg/(m·s)]

Aspect and entrance ratios affect the solution flow distribution through counter-cross flow LAMEEs therefore they change the performance of counter-cross flow RAMEE systems only. The effect of aspect and entrance ratios on the performance of RAMEE is presented in section 2.4.2.

2.4.4.2. Effect of Aspect and Entrance Ratios

As was discussed in the previous section, entrance and aspect ratios can change the performance of the RAMEE by changing the solution flow distribution. In order to quantify the effect of these parameters the simulated effectiveness values for a cross-counter flow RAMEE using different entrance and aspect ratios are compared to effectiveness values for a counter flow RAMEE in Figure 2.3. This

sensitivity study is based on the system performance at different outdoor air conditions defined by AHRI summer and winter test conditions [2.26].

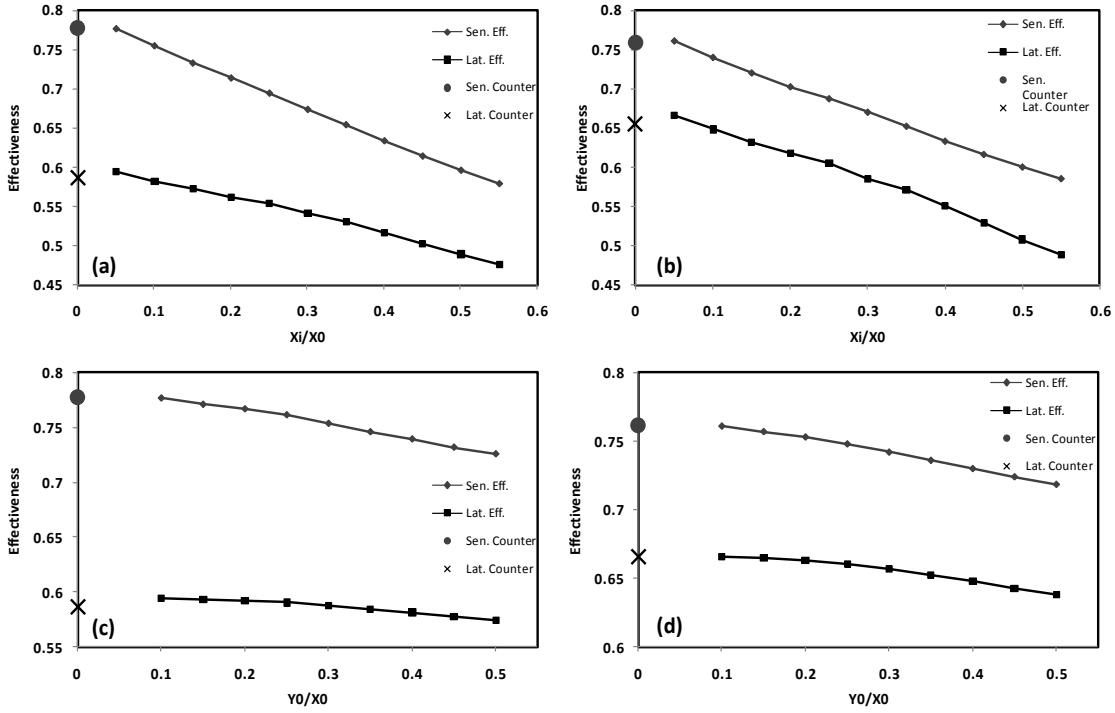

Figure 2.3. RAMEE sensible and latent effectivenesses with two cross-counter flow LAMEEs with different entrance ratio ((a) and (b)) and aspect ratio ((c) and (d)). The numerical data is generated with *NTU=10*, and (a) *Cr*=2.5*, aspect ratio=0.1, and AHRI summer condition, (b) *Cr*=1.5*, aspect ratio=0.1 and AHRI winter condition, (c) *Cr*=2.5*, entrance ratio=0.05 and AHRI summer condition, and (d) *Cr*=1.5*, entrance ratio=0.05 and AHRI winter condition. The effectivenesses for the RAMEE with two pure counter flow LAMEEs are included for comparison.

According to the sensitivity study in Figure 2.3, it can be concluded that the sensible and latent effectiveness values for counter flow RAMEE can be used to predict the performance of cross-counter flow RAMEE systems of sufficiently small aspect and entrance ratios i.e. for entrance ratios less than 0.1 (when the aspect ratio is 0.1) the difference between cross-counter and counter flow RAMEE systems for both sensible and latent effectiveness values is less than 5%. Also for aspect ratios less than 0.2 (when the entrance ratio is 0.05) this difference is not more than 1%. The NN models presented in this study are based on counter flow numerical model therefore the entrance and aspect ratios are not included in the NN model. Although,

this sensitivity study shows that the NN model can predict the effectivenesses for cross-counter flow RAMEEs of sufficiently small aspect and entrance ratios.

2.5. Back-Propagation Algorithm

Neural networks are a non-algorithmic modeling method and can learn based on examples. Among various types of NNs, Multi Layer Perceptrons [2.21], using back-propagation (BP) [2.22] method, are being widely used to solve many engineering modeling problems [2.9-2.14]. The main idea of the back-propagation method is to update the matrices of weights and biases based on the error between desired output values (targets) and NN outputs. Different error functions can be applied to achieve a neural model of desired accuracy. In order to simply implement the back-propagation algorithm, equation 2.10 can be considered.

$$F_{n+1} = F_n + \Delta F \tag{2.10}$$

where F_n is the current weights and biases matrix and ΔF is the update matrix which mainly depends on the error gradient vector and the type of training and performance functions. Reference [2.22] provides a more detailed description about the BP method.

One of the most popular applications of NNs in engineering is called *function approximation.* In this study the BP algorithm will be applied to approximate the underlying function describing the RAMEE sensible and latent effectivenesses. To achieve this, the inputs and outputs of the neural model have to be selected then a training data set including inputs and corresponding outputs is required.

2.6. Neural Model, Inputs and Outputs, and Data Generation Process

The training data set used in this study is provided using the FD model presented by Hemingson [2.20]. The training data set has a key role in the training

process and should have two important properties. First, the inputs should include all the parameters which affect the performance of the system. Second, every input parameter should cover a practical range with reasonable increments because the number of training data points depends on both the range of input parameters and the size of increments. Smaller increments provide a higher accuracy but require more training data. Therefore it is important to choose reasonable increments to achieve acceptable accuracy and training time.

In order to determine a practical range with reasonable increments Figure 2.4 was plotted. It shows that the slope of the effectiveness-*Cr** curves is decreasing when *Cr** passes the peak *Cr** value. This slope is very small for *Cr** values around 5. Therefore the model was limited to Cr* values less than 5. Also with the increase in *NTU* the effectiveness curves tend to be very similar. It shows that it is not necessary to include higher *NTUs* in the model. According to Figure 2.4 it can be concluded that the ranges for *NTU* and *Cr** are completely covering for the purpose of this study because the variations in effectivenesses are very slight for *NTUs* and *Cr*s* higher than 14 and 5. The increment of 0.2 for *Cr** is shown in the curves with *NTU*=1. As can be observed the points are quite close therefore increments smaller than 0.2 is not necessary.

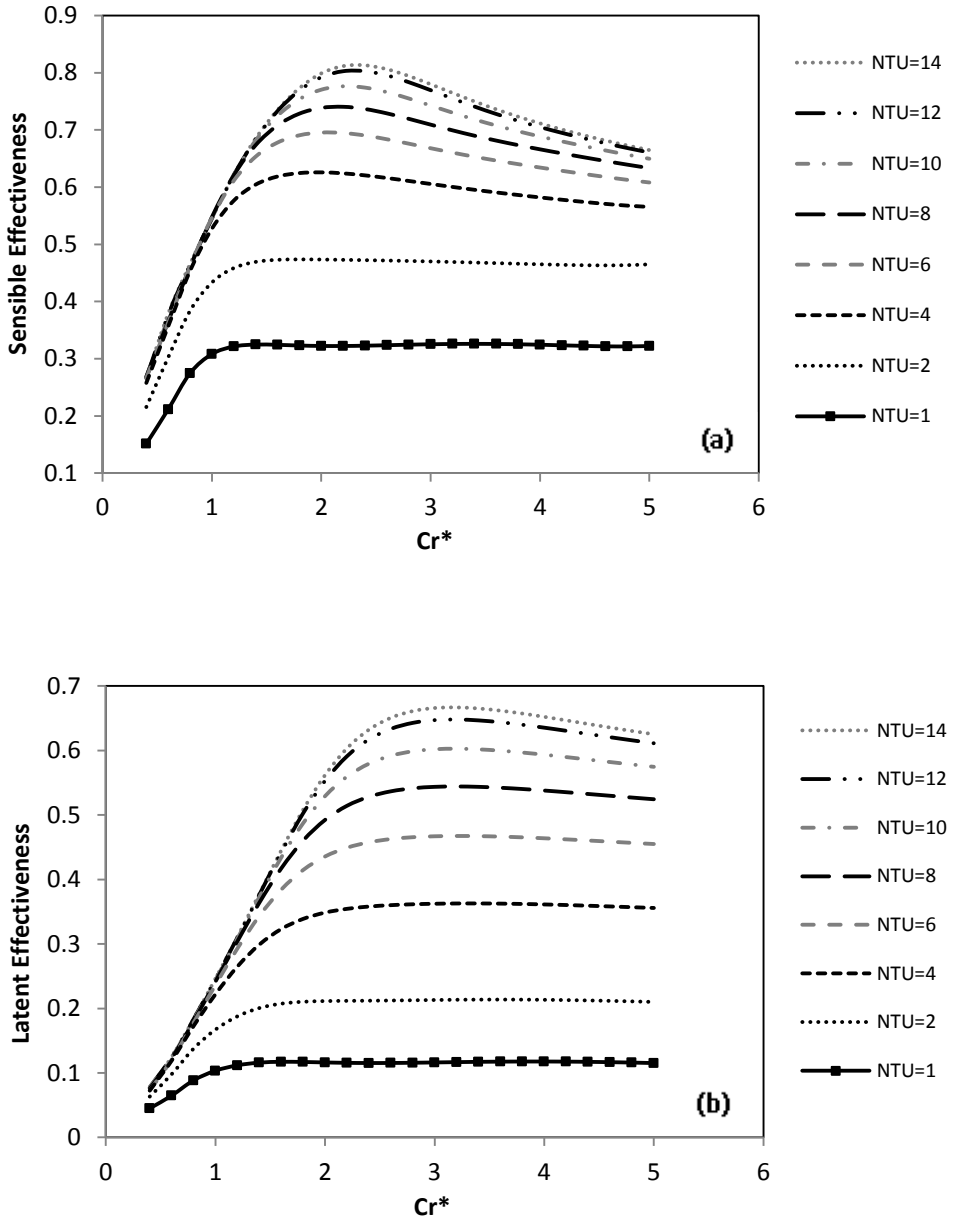

Figure 2.4. RAMEE (a) sensible and (b) latent effectivenesses, for different *NTUs*, versus *Cr for AHRI summer condition presenting the training data set range and increments.**

As was mentioned before, the *design parameters* affecting the RAMEE performance are *NTU, NTU_m, aspect ratio, and entrance ratio*. The results of the sensitivity study (section 2.4.2) showed that the difference between effectivnesses of counter flow RAMEE and cross-counter flow one of small aspect and entrance ratios is negligible. Therefore, these two geometrical parameters which describe the geometry of counter-cross flow LAMEEs were not assumed as the inputs of neural model and the neural model was developed based on counter flow numerical model.

Also, as was discussed in section 2.4.1, NTU_m and NTU are proportional so we only used NTU as the neural network model input. Table 2.2, shows the range and increment values for NTU as a design parameter and Cr^*as an operating parameter.

Table 2.2. The range and increment values for *NTU, Cr*,* and indoor humidity ratio used to provide the training data set.

Input Parameter	Minimum Value	Maximum Value	Increment
NTU	1	15	2
Cr*	0.4	5	0.2
$W_{In,E}$	0	0.012 kg_v/kg_a	0.002 kg_v/kg_a

In addition to NTU and Cr^*, the ranges and increments for the other effecting parameters have to be included. Since the variations in indoor temperature are usually smaller than ±2°C, the indoor temperature is assumed to be constant and equal to 23°C in this study (based on the average of ASHRAE winter and summer indoor comfort temperature [2.27]). The main advantage of this assumption is that it decreases the size of training data set and subsequently training process time. The validity of this assumption will be verified in results and discussion section.

Although indoor temperature is almost constant and will be controlled in buildings, the indoor humidity is often free-floating. Furthermore, according to ASHRAE summer and winter indoor comfort zones [2.27, 2.28], the humidity ratio of indoor air (Figure 2.1, $W_{In,E}$), ranges from 0 to 0.012 kg_v/kg_a. In developing the training set, the indoor humidity ratio was varied between 0 to 0.012 kg_v/kg_a with the increment of 0.002 kg_v/kg_a.

Finally, practical values for the other operating parameters (outdoor temperature, $T_{In,S}$, and outdoor humidity ratio, $W_{In,S}$) that represent different outdoor operating conditions for various climates throughout the year should be obtained. In Figure 2.5, circles show the outdoor operating cases on the psychometric chart used to provide the training data set for NN model. As is depicted in Figure 2.5, these 110

points range from -16 to 50 °C and fall between the aqueous salt solution (Lithium Bromide) saturation line [2.29] and the air saturation line.

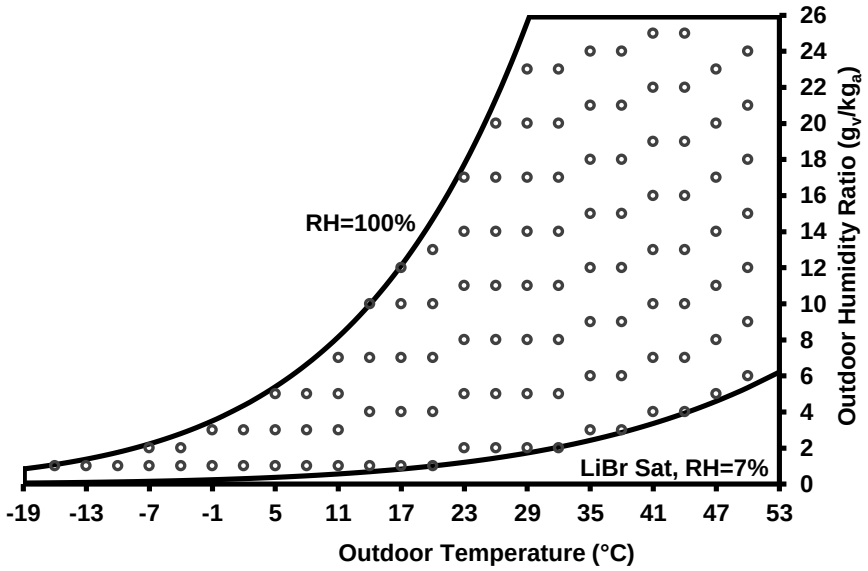

Figure 2.5. Outdoor temperature and humidity ratio conditions on the psychometric chart, used to provide the training data set.

In order to make sure that the cases presented in Figure 2.5 cover the outdoor operating conditions for different climates, these operating points are compared with the yearly hour by hour (8760 hr) outdoor temperature and humidity conditions for four cities of different climates based on Typical Meteorological Year [2.30] (Figure 2.6). Saskatoon, Chicago, Phoenix, and Miami are selected for comparison as they represent cold and dry, cold and humid, hot and dry, and hot and humid climates respectively [2.31].

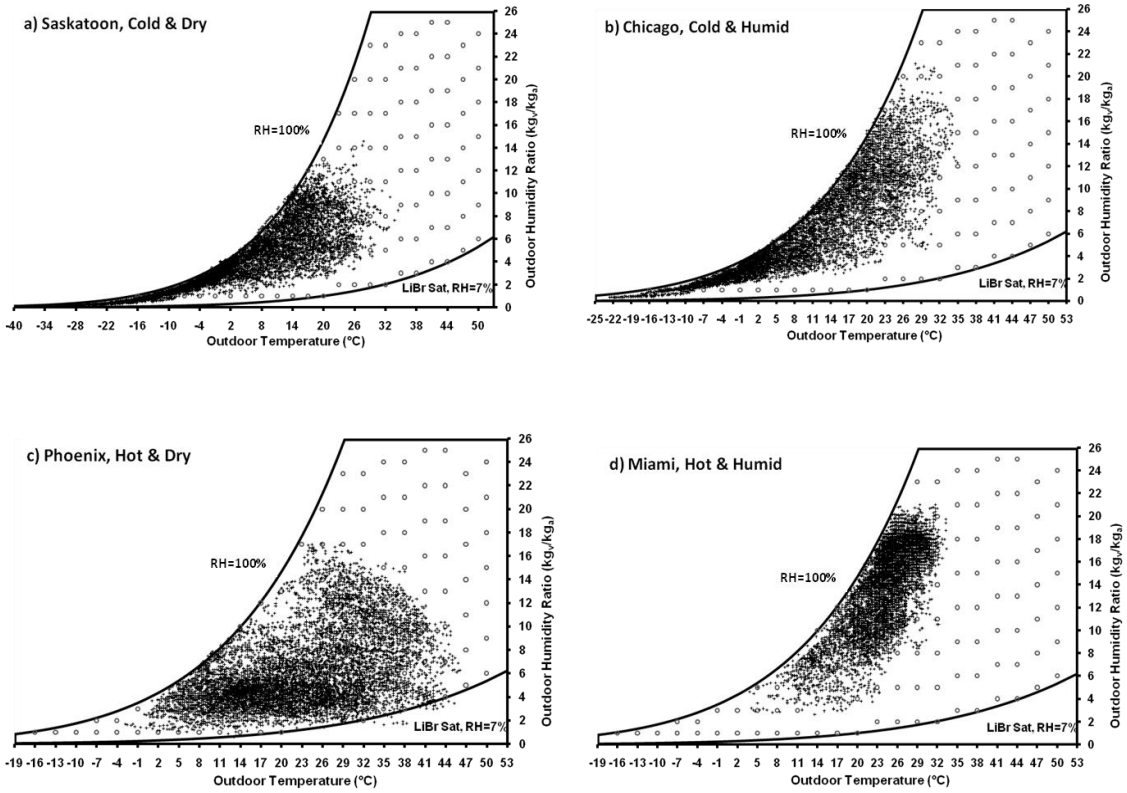

Figure 2.6. Outdoor conditions for different cities compared to the outdoor conditions used in the training data set.

As can be seen in Figure 2.6, the selected range of outdoor conditions for training the NN model almost covers all outdoor temperature and humidity ratio conditions for the different climates except for operating hours of temperatures below -16 °C. In very cold climates like Chicago and Saskatoon only 1% and 11% of the hours are colder than -16 °C respectively. Therefore the applied outdoor condition to develop the NN model sufficiently covers the different climates.

Using these ranges for input data and their corresponding increments a data set of approximately 140,000 points, which represents and covers the real physical problem was provided to train the NN model.

According to what was discussed in section 2 and section 4, the inputs for the NN model would be *NTU, Cr*,* ΔT*,* $W_{In,S}$, and $W_{In,E}$. In this study instead of using sensible and latent effectivenesses as outputs of NN models, for simplicity ΔT_S and ΔW_S were used which can be easily used to calculate sensible and latent

effectivenesses using equations 2.1 and 2.2. The acceptable output range for sensible and latent networks are ΔT_s = -32.9 to 24.8 °C and ΔW_s = -0.008 to 0.0155 kg_v/kg_a.

2.7. NN Architecture and Training Process

2.7.1. NN Architecture

Two separate Multi Layer Perceptron feed-forward networks using the well-known Levenberg-Marquardt [2.32-2.34] training algorithm were used to map the inputs of the network (*NTU, Cr*,* ΔT*,* $W_{In,S}$, and $W_{In,E}$) to their corresponding targets (ΔT_S or ΔW_S). Figure 2.7 shows a simplified schematic view of the NN model which has two hidden layers and one output layer. In this figure, for simplicity, the biases are not shown. The network with an output of ΔT_S is called the sensible network and the other network (with ΔW_S as output) is called the latent network. For more information about the mathematical model of neural networks a block diagram for a single neuron is included in the appendix B1.

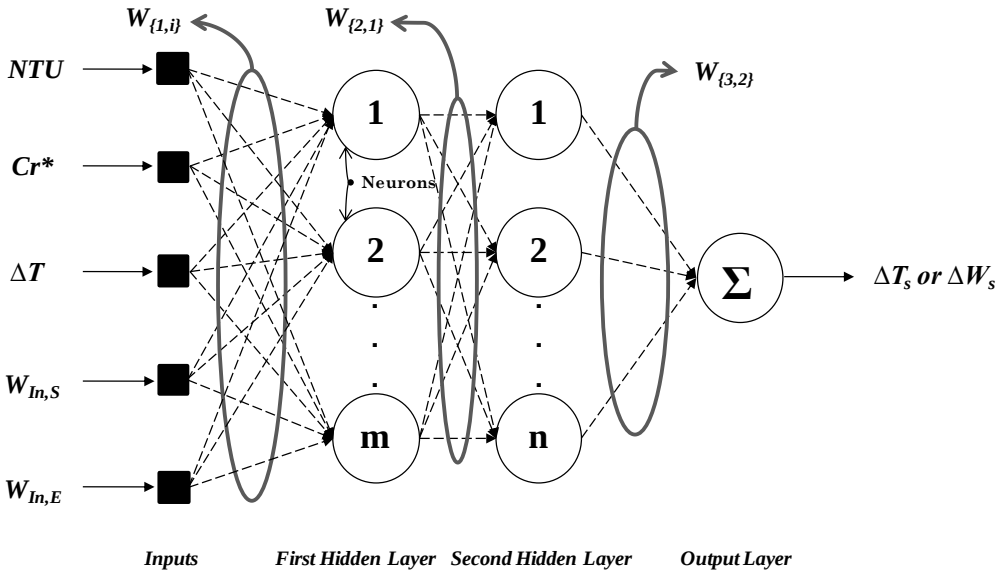

Figure 2.7. Architecture of a fully connected three layer neural network with five inputs, m neurons in the first hidden layer, n neurons in the second hidden layer, and one neuron in the output layer which might be written as a 5-m-n-1 network.

It would be possible to develop a single neural model to predict both ΔT_S and ΔW_S at once. But defining a network with multiple outputs may decrease the

accuracy of the results because the hidden neurons would have difficulty to model at least two functions at the same time. Therefore it is very common to train separate networks for each output, then to combine them into a package and run them as a unit. This is the method used in this study. We have developed two different models that target the sensible and latent performance of RAMEE separately. The training data set is the same for both sensible and latent networks and it represents a coupled heat and moisture transfer action. For example the sensible network presents the sensible performance of a system that transfers heat and moisture at the same time. It is not a model for sensible heat transfer of a heat exchanger.

Generally speaking, there is no proven method to find the optimum neural model (the simplest model with the highest accuracy) for different problems. Thus, for every specific problem a pre-defined desired accuracy would be a reasonable stopping criterion. Finding a neural model to represent a real and unique problem is basically a trial and error process and depends on the type and complexity of the problem as well as the experience of the trainer. To reach the desired accuracy, different topologies for the neural models were tried.

2.7.2. Training process

To improve the generalization of the neural model, the early stopping method [2.35] was applied. In this method, the generated data set is divided into three subsets. The first subset is called the training subset, which is used for back-propagating the errors and updating weights and biases during the training session. The second subset is called the validating set which is monitored during the training session by the early stopping method to prevent the network from over-fitting the training subset. The third subset is called the test set. The test set is the “unseen” by the NN because it is not used for either updating weights or stopping the training.

The error of the test set is very important because it is monitored by the trainer to make sure that the accuracy of network is acceptable for unseen data. This error facilitates the comparison of different neural models for a specific problem and allows the researcher to choose the most accurate one.

In this paper, the generated data set was divided into three subsets (training, validating, and testing). Different dividing ratios were applied to the data set to get the best results. In this study, the tried NN models were not very sensitive to slight variations in dividing ratios (due to the large number of data points) although, the lowest errors were reached using training subset, 70%, validating, 15 %, and testing, 15% of the whole generated data set.

In order to make the computations easier all input and corresponding outputs were normalized to [-1,1] range using a simple linear function which, for every parameter, sets the minimum value as -1 and maximum value as +1 and linearly maps other values between -1 and +1.

After dividing and normalizing the training data set, different architectures for sensible and latent networks were applied and the errors were compared to each other. The nonlinearity and complexity of the problem didn't let the authors to use linear neurons in hidden layers since the networks with linear hidden neurons caused much bigger errors than the desired values. Also networks with one hidden layer failed to provide the desired accuracy. Thus, networks with more hidden layers (2 or 3 layers) of different number of neurons in each layer were trained and tested. Finally a 5-10-10-1 model for both sensible and latent networks was found as an appropriate architecture. Table 2.3 shows the training set error compared to the test set error for different architectures of the sensible network. These values are the best results of around 10 runs for each architecture.

Table 2.3. Result of linear regression along with MSE for different architectures for training and test sets. M and B are the slope and intercept of the linear trend line respectively. R and MSE are the correlation coefficient and Mean Squared Error between the NN and FD model results respectively.

No.	Architecture For Sensible Net.	Training Set Error				Test Set Error			
		M	B	r	MSE $(°C)^2$	M	B	r	MSE $(°C)^2$
1	5-20-1	0.908	0.483	0.928	1.1136	0.909	0.491	0.925	1.1541
2	5-40-1	0.962	0.237	0.957	0.9135	0.955	0.244	0.944	0.9732
3	5-10-10-1	1.000	0.001	0.999	0.0018	1.000	0.002	0.999	0.0021
4	5-16-14-1	1.000	0.001	1.000	0.0007	0.999	0.001	0.998	0.0029
5	5-8-12-8-1	0.997	0.003	0.993	0.0082	0.995	0.004	0.988	0.0088

Note that in Table 2.3, M and B are the slope and intercept of the linear trend line respectively and 'r' is the correlation coefficient. These three parameters show the average accuracy of the different architectures while the Mean Squared Error (MSE) shows the scatter of the prediction. Architectures number 1 and 2 have only one hidden layer and their accuracy is lower than number 3 and 4 which have two hidden layers. Number 5 shows higher errors, although it has three hidden layers. Number 4 shows higher accuracy than number 3 on the training set while it has higher error for the test set. Therefore network number 3 is proposed as the one with preferred architecture.

Another important parameter in determining the configuration of a neural network is the type of the transfer functions of its neurons. In this study different common transfer functions for hidden and output layers were applied. The best obtained combination was the hyperbolic tangent function (see the appendix B1) for hidden layers and linear function for output layer. In order to make the results of this study reproducible, the architecture and properties of both sensible and latent models along with matrices of weights and biases are reported in appendix B2.

After completely defining and presenting the developed NN models the accuracy of their predictions is discussed in the next section and the results from these models are verified.

2.8. Verification and Application of the NN Model

2.8.1. Accuracy of the NN Models

To make sure that the performances of the sensible and latent NN models are acceptable for a complete range of unseen data, an unseen test data set of 9000 data points were created using the FD model. The 30 outdoor temperature and humidity ratio conditions used to create the new unseen test set are shown in Figure 2.8 along with the condition used for the training data set.

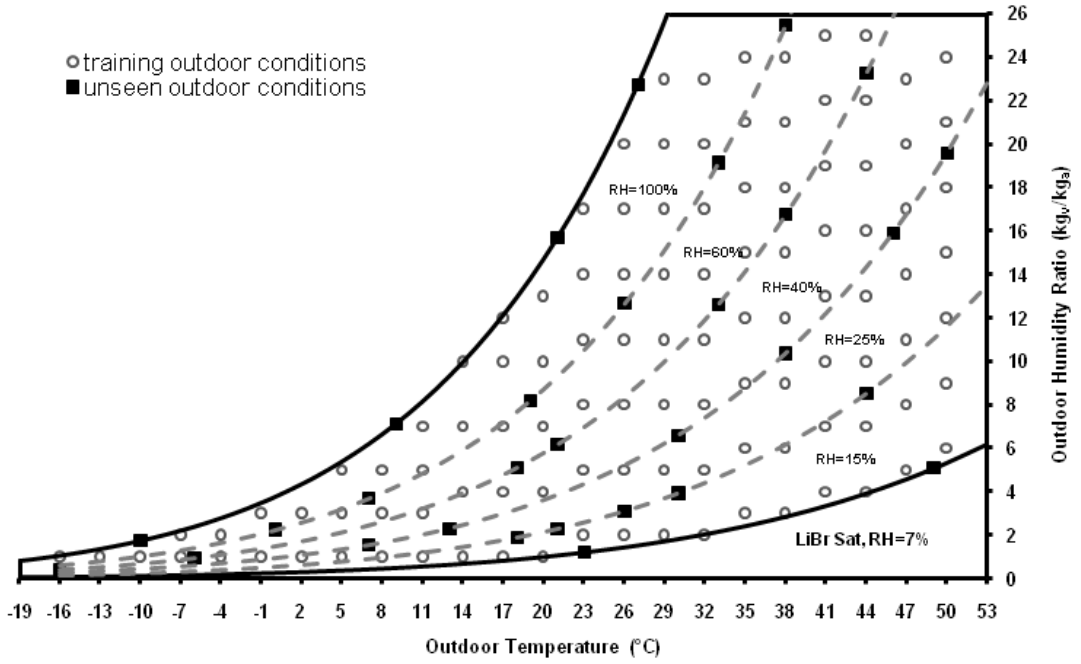

Figure 2.8. Outdoor operating conditions used to create the unseen test set compared to conditions used to create the training data set.

As can be seen in Figure 2.8, the unseen data set covers a wide range of temperatures and relative humidity conditions. Also the locations of the squares (unseen points) are chosen in a way that are between circles (training points) and not too close to them.

For every outdoor condition ($T_{In,s}$ and $W_{In,s}$) other input parameters (*NTU, Cr**, and $W_{In,E}$) were systematically changed in a way that almost cover all possible input cases. For this purpose, five values of *NTU* (ranging from 3 to 15 in increments

of 3), five values of *Cr**, (ranging from 1 to 5 in increments of 1), two values of $T_{In,E}$ (21 and 25 °C), and six values of $W_{In,E}$ (ranging from 0.001 to 0.011 kg_v/kg_a in increments of 0.002 kg_v/kg_a) were applied to get the unseen data set. Therefore, with 30 outdoor conditions, 5 *NTUs*, 5 *Cr*s*, 2 $T_{In,E}$, and 6 $W_{In,E}$, the unseen set has a total of 9000 points.

This test set, that has quite different input vectors than the test set used in training process, was used to evaluate the performance of the neural models. Figure 2.9 presents a frequency distribution histogram showing the difference between the NN and the FD model where the terms ΔT_{diff} and ΔW_{diff} are defined by equations 2.11 and 2.12.

$$\Delta T_{diff} = \left|\Delta T_{S,net} - \Delta T_{S,sim}\right| \tag{2.11}$$

$$\Delta W_{diff} = \left|\Delta W_{s,net} - \Delta W_{s,sim}\right| \tag{2.12}$$

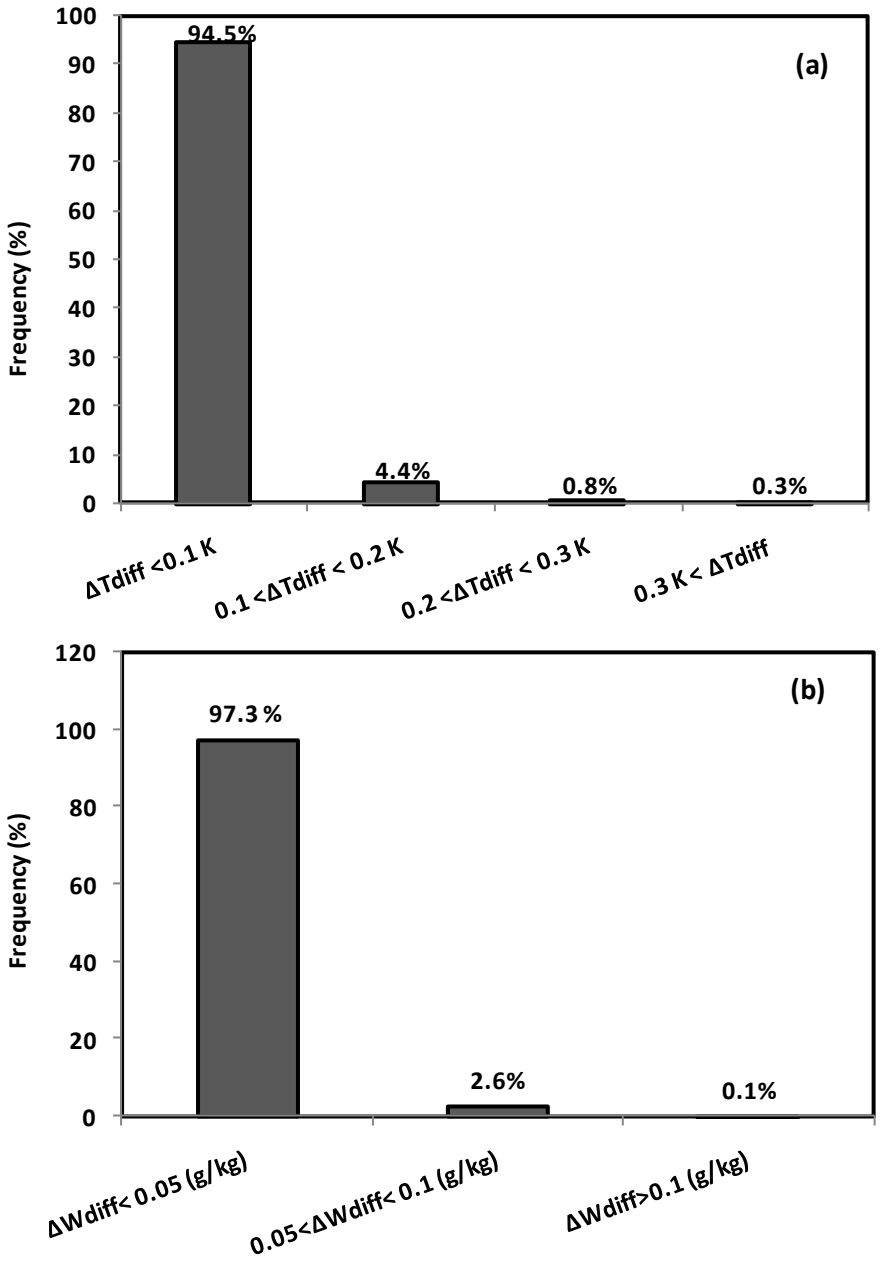

Figure 2.9. Frequency of absolute difference between predicted values by NN model and numerically simulated values for (a) the sensible NN (b) the NN model.

In Figure 2.9, the absolute difference between predicted and simulated supply side temperature variations (ΔT_{diff}), for 94.5% of the 9000 test points is less than 0.1 °C which gives a desired accuracy for the purpose of this study. The absolute humidity ratio difference (ΔW_{diff}), for 97.3% of test cases is less than 5×10^{-5} kg_v/kg_a.

For the unseen 9000-point test set, table 2.4 shows four different error types that all verify a very good agreement between the results from NN model and FD model outputs.

Table 2.4. Error values between the results from NN model and FD model outputs for both sensible and latent networks tested using 9000 test points.

Error Type	Error Value For Sensible NN Model	Error Type	Error Value For Latent NN Model
Max. of ΔT_{diff}	0.49 °C	**Max. of ΔW_{diff}**	1.2×10^{-4} kg_v/kg_a
MSE	0.0026 (°C) ^{2}	**MSE**	3.92×10^{-10} $(kg_v/kg_a)^2$
RMSE	0.05 °C	**RMSE**	2×10^{-5} kg_v/kg_a
Mean ΔT_{diff} = $\frac{\sum_{i=1}^{9000}(\Delta T_{diff})_i}{9000}$	0.03 °C	**Mean ΔW_{diff} =** $\frac{\sum_{i=1}^{9000}(\Delta W_{diff})_i}{9000}$	1.4×10^{-5} kg_v/kg_a

According to the high accuracy of the results, assuming constant indoor temperature ($T_{In,E}$ = 23°C) to provide the training data set is valid. Because the models were tested using a data set of two different indoor temperatures (21 and 25 °C) and the results were acceptable. On the other hand, assuming constant indoor temperature helped to shrink the training data set and subsequently decrease the training time.

2.8.2. Comparing the NN and FD Models for Different Operating Condition Factors

After making sure about the accuracy of the NN model in previous section, it is interesting to compare NN model outputs with FD model results for some sample cases. In order to do this comparison Figure 2.10 and 2.11 are plotted. In these figures dashed lines show the results from NN model while solid ones are representative of the FD model outputs.

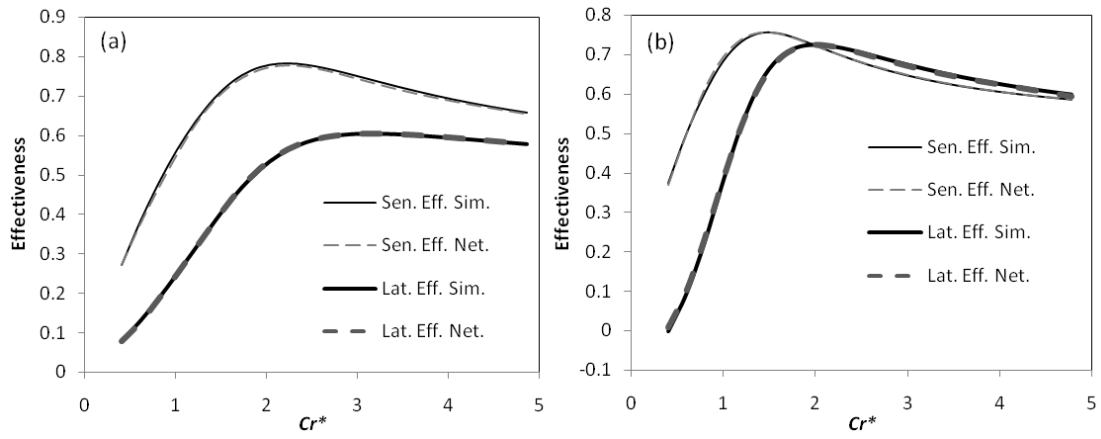

Fig. 2.10. Comparison between numerical and NN model effectivenesses with *NTU=10* for a) AHRI summer condition. b) AHRI winter condition.

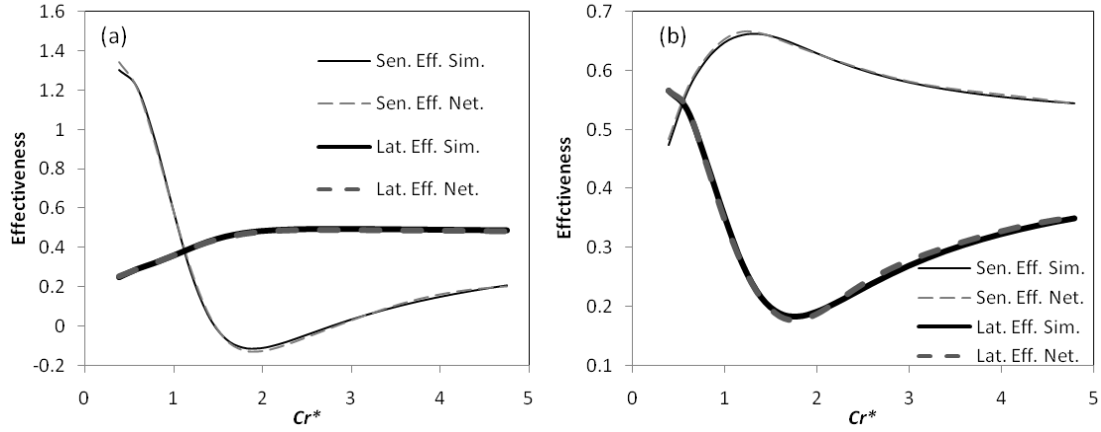

Fig. 2.11. Comparison between numerical and NN model effectivenesses with *NTU=10* for (a) *H*=7*. (b) *H*=-0.4*.

Figure 2.10 shows a very good agreement between the NN model and simulation results for *NTU*=10, variable *Cr** between 0.4 and 5, and AHRI summer and winter operating conditions. In this figure, a usual trend for variation of effectivenesses with *Cr** is shown. The sensible and latent effectivenesses increase with *Cr** and reach a maximum value then slightly decrease. This trend depends on the operating condition.

Equation 2.13 defines a factor called operating condition factor [2.19,2.20] which is the ratio of latent to sensible energy differences between the indoor and outdoor air.

$$H^* = \frac{\Delta H_{Lat.}}{\Delta H_{Sen.}} \approx 2500 \frac{W_{In,S} - W_{In,E}}{T_{In,S} - T_{In,E}} \quad (2.13)$$

According to equation 2.13, outdoor air conditions that are warmer and more humid or cooler and drier than the indoor condition have a positive *H** value and all other conditions have a negative *H** value. Positive values for *H** mean that the driving potentials for heat and moisture transfer are in the same direction (e.g. both heat and moisture transfer flow are from supply air to exhaust air when the supply is warmer and more humid than the exhaust air) while the negative *H** values mean that the driving potentials for heat and moisture transfer are in the opposite direction. The behaviour of RAMEE is very different when *H** is positive than when *H** is negative as documented and explained in references [2.19] and [2.20]. Figure 2.11 shows a comparison between simulated and network results for two different operating condition factors.

Figure 2.11a presents good agreement for *H**=7 (i.e. latent to sensible enthalpy difference between indoor and outdoor air) where the sensible effectiveness has an unusual trend (see Figure 2.12a), and Figure 2.11b is for *H**= -0.4 with an unusual trend for latent effectiveness. This figure implies that NN models show good agreement in both trend and value over different operating condition factors.

2.8.3. Experimental Validation

The experimental results developed by Beriault [2.36] are used to validate the results from the NN models. An extreme experimental case with *H**=-0.68 is chosen to test the ability of NN models in predicting the behaviour of the RAMEE. The experimental results, consisting of some measurements taken at constant *NTU* and *H** but different *Cr*s*, were produced by a counter/cross flow RAMEE system with aspect and entrance ratios of 0.25 and 0.05. Figure 2.12 shows a high degree of

scatter for the experimental results and very big experimental uncertainties due to small differences between humidity ratios and temperatures of two air flows.

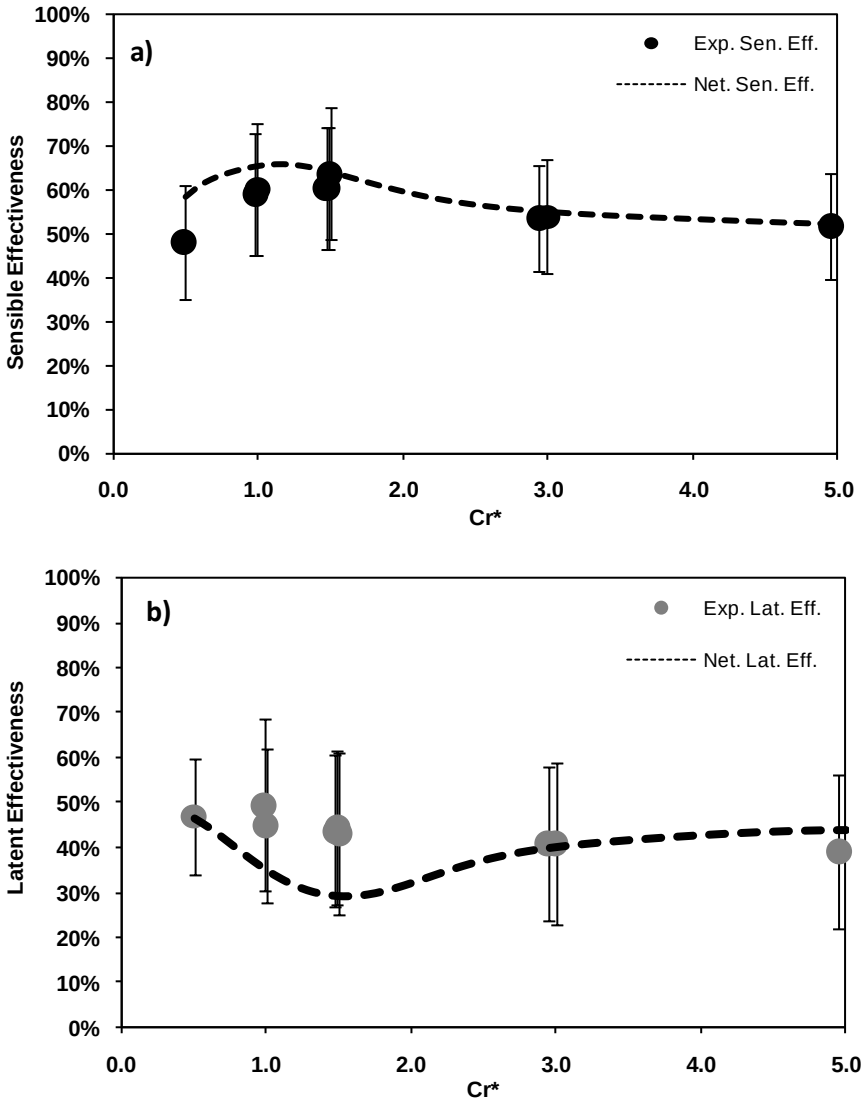

Fig. 2.12. Experimental results for *NTU=17* and *H*=-0.68* compared to a) sensible NN model b) latent NN model.

The scatter and deviation from NN results can result from many reasons like flow maldistribution in the channels, salt solution leakage from the liquid channels, deformation of the channels and the membranes [2.37], and heat transfer between the system and the environment [2.38]. Table 2.5 contains dimensions of the exchangers and the membrane properties of the Beriault's LAMEE prototype.

Detailed information about the experimental set-up, and testing condition and procedure is presented in [2.36].

Table 2.5. Specifications of Beriault's prototype used to develop the experimental validation data points.

Property	Value
LAMEE Dimensions	
Length	1220 [mm]
Width	305 [mm]
Entrance Length	64 [mm]
Channel Thickness	
Air	5.4 [mm]
Solution	2.6 [mm]
Membrane Properties	
Thickness	0.5 [mm]
Thermal Conductivity	0.334 [W/(m·K)]
Water Vapour Permeability	3.4×10^{-6} [kg/(m·s)]

Although an extreme operating condition (H^*=-0.68 means an opposite direction in heat and moister transfer with small temperature and humidity ratio differences [2.20]) was chosen to experimentally validate the NN results (membrane water vapour permeability, and air and solution thicknesses of Beriault's model are slightly different from the values were used to provide the training data set but NTU_m/NTU value for these two prototypes are equal to 0.26), a reasonable agreement for both sensible and latent effectivenesses can be seen in Figure 2.12. In this figure trends for NN model and experimental results are similar and the values are in agreement within the uncertainty bounds.

2.8.4. Application of the NN Model

Generally speaking, NNs can simply interpolate any new pattern that falls in the domain of input parameters. Unlike the FD model, the NN models predict the sensible and latent performance of the RAMEE system at a very high speed due to their non-iterative data processing (The NN models are approximately 10^7 times faster than the FD model). For example the NNs presented in this paper take less

than one second to produce the results for 8760 points (i.e. hourly effectiveness values for one year) using a common Pentium desktop, while the FD model takes a few days to produce the same data.

One of the most important applications of the NN models is to predict annual energy savings by the RAMEE. The definition of the optimal system performance for the RAMEE, operating under different outdoor and indoor conditions, is developed by Rasouli et al. [2.39]. This definition can vary depending on building demand. For example in the hours that the building needs sensible heating (i.e. only heat transfer from exhaust air to supply air is important and moisture transfer does not matter) the optimum performance is to maximize the sensible effectiveness of the RAMEE. As is discussed in previous sections (see Figs. 2.10 and 2.11) the sensible or latent effectiveness of the system can be maximized or minimized changing the Cr^* (or salt solution flow rate). Using an optimization algorithm applied to the neural network models, the optimum effectiveness values for RAMEE under different operating conditions are obtained. These optimum values are used for TRNSYS computer simulation of the RAMEE system when operating in an office building in four different climates to estimate the annual savings by RAMEE [2.39]. The results show up to 43% heating energy saving in cold climates, and up to 15% cooling energy saving in hot climates. The same analysis for the application of a RAMEE system in the HVAC system of a hospital shows even more savings [2.40]. The optimized RAMEE saves the annual heating energy by 58% to 66% in cold climates, and the annual cooling energy by 10% to 18% in hot climates. The RAMEE can also downsize the heating system by 45% in cold climates, and the cooling system by 25% in hot climates [2.40].

2.9. Conclusions

In this study, sensible and latent effectiveness of a Run-Around Membrane Energy Exchanger (RAMEE) were predicted using two separate neural network (NN) models. A training data set of approximately 140,000 points, provided using a Finite Difference (FD) model, was subjected to a back-propagation algorithm to minimize the error between the outputs of the FD model and the NN. Finally, a 5-10-10-1 configuration was concluded to result in a NN model of satisfactory accuracy for both sensible and latent energy transfer in the RAMEE.

The ability of the trained NN models to predict the effectiveness of the RAMEE was double checked numerically and experimentally. A completely unseen test set of 9000 data points which covers a wide range of parameters (i.e. *NTU* from 1 to 15, *Cr** from 0.4 to 5, and outdoor and indoor conditions covering different climates) was used to test the accuracy of the NN models. The root mean squared error (RMSE) and average absolute error between the results from FD and NN models were 0.05 °C and 0.03 °C for the sensible NN model and 2×10^{-5} kg_v/kg_a and 1.4×10^{-5} kg_v/kg_a for the latent neural network. Also the results from NN model show a reasonable agreement with experimental data.

Such a fast and non-iterative mathematical model can be used as a computational component in commercial building energy simulation packages to estimate the possible annual energy savings using a RAMEE [2.39]. Also the NN models can be used to find the optimum design or operating parameters (*NTU and Cr**) of RAMEE for various outdoor and indoor air conditions.

2.10. References of chapter 2

[2.1] L.Z. Zhang, C.H. Liang, L.X. Pei, Conjugate heat and mass transfer in membrane-formed channels in all entry regions, International Journal of Heat and Mass Transfer 53 (2010) 815–824.

[2.2] L.Z. Zhang, Heat and mass transfer in plate-fin enthalpy exchangers with different plate and fin materials, International Journal of Heat and Mass Transfer 52 (2009) 2704–2713.

[2.3] E.M. Sparrow, J.C.K. Tong, M.R. Johnson, G.P. Martin, Heat and mass transfer characteristics of a rotating regenerative total energy wheel, International Journal of Heat and Mass Transfer 50 (2007) 1631–1636.

[2.4] S. Nair, S. Verma, S.C. Dhingra, Rotary heat exchanger performance with axial heat dispersion, International Journal of Heat and Mass Transfer 41 (1998) 2857–2864.

[2.5] M. Porowski, E. Szczechowiak, Influence of longitudinal conduction in the matrix on effectiveness of rotary heat regenerator used in air-conditioning, Heat and Mass Transfer 43 (2007) 1185–1200.

[2.6] C.J. Simonson, R.W. Besant, Energy wheel effectiveness: part i – development of dimensionless groups, International Journal of Heat and Mass Transfer 42 (1999) 2161–2170.

[2.7] C.J. Simonson, R.W. Besant, Energy wheel effectiveness: part ii – correlations, International Journal of Heat and Mass Transfer 42 (1999) 2171–2185.

[2.8] S. A. Kalogirou, Applications of artificial neural networks in energy systems, Energy Conversion & Management 40 (1999) 1073–1087.

[2.9] G. Xie, B. Sunden, Q. Wang, L. Tang, Performance predictions of laminar and turbulent heat transfer and fluid flow of heat exchangers having large tube-diameter and large tube-row by artificial neural networks, International Journal of Heat and Mass Transfer 52 (2009) 2484–2497.

[2.10] H. Peng, X. Ling, Neural networks analysis of thermal characteristics on plate-fin heat exchangers with limited experimental data, Applied Thermal Engineering 29 (2009) 2251–2256.

[2.11] C.K. Tan, J. Ward, S.J. Wilcox, R. Payne, Artificial neural network modelling of the thermal performance of a compact heat exchanger, Applied Thermal Engineering 29 (2009) 3609–3617.

[2.12] G. Diaz, M. Sen, K.T. Yang, R.T. McClain, Simulation of heat exchanger performance by artificial neural networks, International Journal of HVAC&R Research 5 (1999) 195–208.

[2.13] A. Pacheco-Vega, G. Diaz, M. Sen, K.T. Yang, R.T. McClain, Heat rate predictions in humid air–water heat exchangers using correlations and neural networks, ASME Journal of Heat Transfer 123 (2001) 348–354.

[2.14] Y. Islamoglu, A. Kurt, Heat transfer analysis using ANNs with experimental data with air flow in corrugated channels, International Journal of Heat and Mass Transfer 47 (2004) 1361–1365.

[2.15] M. Ning, M. Zaheeruddin, Neuro-optimal operation of a variable air volume HVAC&R system, Applied Thermal Engineering 30 (2010) 385–399.

[2.16] A. Vali, C. J. Simonson, R. W. Besant, G. Mahmood, Numerical model and effectiveness correlations for a run-around heat recovery system with combined counter and cross flow exchangers, International Journal of Heat and Mass Transfer 52 (2009) 5827–5840.

[2.17] H. Fan, C.J. Simonson, R.W. Besant, W. Shang, Performance of a run-around system for HVAC heat and moisture transfer applications using cross-flow plate exchangers coupled with aqueous lithium bromide, HVAC&R Research 12 (2006) 313–336.

[2.18] M. Seyed Ahmadi, B. Erb, C.J. Simonson, R.W. Besant, Transient behavior of run-around heat and moisture exchanger system, Part I: Model formulation and verification, International Journal of Heat and Mass Transfer 52 (2009) 6000-6011.

[2.19] H.B. Hemingson, C.J. Simonson, R.W. Besant, Steady-state performance of a run-around membrane energy exchanger for a range of outdoor air conditions, International Journal of Heat and Mass Transfer 54 (2011) 1814-1824.

[2.20] H.B. Hemingson, The impacts of outdoor air conditions and non-uniform exchanger channels on a run-around membrane energy exchanger, M.Sc. thesis, University of Saskatchewan, Saskatoon, SK, 2010.

[2.21] Y. Wang, A neural network adaptive control based on rapid learning method and its application, Advances in Modeling and Analysis 46 (1994) 27–34.

[2.22] M.T. Hagan, H.B. Demuth, M.H. Beale, Neural Network Design, PWS Publishing, Boston, MA, 1996, pp. 11-2 -12-52.

[2.23] M.D. Larson, C.J. Simonson , R.W. Besant, P.W. Gibson, The elastic and moisture transfer properties of polyethylene and polypropylene membranes for use in liquid-to-air energy exchangers, Journal of Membrane Science 302 (2007) 136-149.

[2.24] M. Rasouli, C.J. Simonson, R.W. Besant, Applicability and optimum control strategy of energy recovery ventilators in different climatic conditions, Energy and Buildings 42 (2010), 1376-1385.

[2.25] F.P. Incropera, D.P. DeWitt, Fundamentals of Heat and Mass Transfer, Sixth ed., John Wiley & Sons, New York, 2007, pp. 518-521.

[2.26] AHRI. 2005. ANSI/ARI Standard 1060, Standard for Rating Air-to-Air Exchangers for Energy Recovery Ventilation Equipment. Arlington, VA: Air-Conditioning & Refrigeration Institute.

[2.27] ASHRAE Standard 55-2004, Thermal Environmental Conditions for Human Occupancy, American Society of Heating, Refrigerating and Air-Conditioning Engineers, Inc., Atlanta, Georgia, 2004.

[2.28] ASHRAE Handbook Fundamentals, Chapter 9: Thermal Comfort, ASHRAE (2009), Atlanta.

[2.29] M. Afshin, C.J. Simonson, R.W. Besant, Crystallization limits of LiCl-water and MgCl2-water salt solutions as operating liquid desiccant in the RAMEE system, ASHRAE Transactions 116 (2010), Part 2, 494-506.

[2.30] W. Marion, K. Urban, User's Manual for TMY2s, 1995, National Renewable Energy Laboratory.

[2.31] R.S. Briggs, R.G. Lucas, T.Z. Todd, Climate classification for building energy codes and standards: Part 2 - Zone definitions, maps, and comparisons, ASHRAE Transactions 109 (2003) 122-130.

[2.32] K. Levenberg, A method for the solution of certain problems in least squares, Quarterly of Applied Mathematics 2 (1944) 164-168.

[2.33] D. Marquardt, An algorithm for least-squares estimation of nonlinear parameters, SIAM Journal of Applied Mathematics 11 (1963) 431-441.

[2.34] M.T. Hagan, H.B. Demuth, M.H. Beale, Neural Network Design, PWS Publishing, Boston, MA, 1996, pp. 12-19 – 12-21.

[2.35] L. Prechelt, Early stopping--But when?, in Orr and Mueller (1998), 55-69.

[2.36] D. Beriault, Run-Around membrane energy exchanger prototype 4 design and laboratory testing, M.Sc. Thesis, University of Saskatchewan, Saskatoon, SK, 2011, in preparation.

[2.37] M.D. Larson, R.W. Besant, C.J. Simonson, The effect of membrane deflections on flow rate in cross flow air-to-air exchangers, HVAC&R Research 14 (2008) 275-288.

[2.38] W. Shang, R.W. Besant, Effects of pore size variations on regenerative wheel performance, Journal of Engineering for Gas Turbines and Power 127 (2005) 1-15.

[2.39] M. Rasouli, S. Akbari, H. Hemingson, R.W. Besant, and C.J. Simonson, Application of a run-around membrane energy exchanger in an office building HVAC system, ASHRAE Transactions, 117(2), (2011), 686-703.

[2.40] M. Rasouli, S. Akbari, C. J. Simonson, R. W. Besant, Energetic, Economics and environmental analysis of a health-care facility HVAC system equipped with a run-around membrane energy exchanger, Manuscript submitted for publication (2010).

CHAPTER 3

TRANSIENT PERFORMANCE OF RAMEE SYSTEM

3.1. Overview of Chapter 3

After developing the steady-state model described in Chapter 2, it was decided to modify the NN model to predict the transient performance of RAMEE. In addition to all the parameters that affect the steady-state performance of the RAMEE, the effects of parameters that might play a role in transient behavior of the system were studied individually. Sensitivity studies showed that the problem can be simplified to achieve a very fast model to predict the transient performance of a given design of RAMEE with an acceptable accuracy. The general approach to model the transient behavior of a RAMEE system in this chapter is very similar to the previous chapter.

Version 1.3.1 of the EPS code was used to provide the required training data set. This data was processed using the Neural Network Toolbox of MATLAB® version 7.10.0.

The contributions of each author to this research work are as follows:

Soheil Akbari, M.Sc. student and main author, generated and processed the data, trained the networks, developed the figures and tables, and wrote the paper.

Carey J. Simonson, and **Robert W. Besant**, the research group supervisors, conceived the research study, read and edited the paper and improved this study with their valuable comments.

MANUSCRIPT #2

Application of neural networks to predict the transient performance of a Run-Around Membrane Energy Exchanger for yearly non-stop operation

Soheil Akbari, Carey J. Simonson, Robert W. Besant

3.2. Abstract

Application of soft computing methods (i.e. neural networks and genetic algorithms) for modeling and controlling the dynamic and transient behavior of systems has been increasing during the last decade. In this study, a Neural Network (NN) model is developed to predict the transient heat and moisture transfer performances (i.e., the sensible and latent effectivenesses) of a novel HVAC energy exchanger, called the Run-Around Membrane Energy Exchanger (RAMEE), which is able to transfer both heat and moisture between exhaust and supply air streams. The training data set for the NN model covers a wide range of outdoor conditions and system parameters and is produced using a Transient Numerical Model (TNM) that has been experimentally validated for some transient applications. Two separate NNs (one for sensible and one for latent energy transfer) each with 12 inputs and 1 output, are selected to represent the RAMEE. The ability of NN models to predict the performance of a given RAMEE design in different climates is numerically validated. The mean absolute difference (MAD) between the results of TNM and NN models for different locations are 0.5 °C for the sensible model and 0.2 g_v/kg_a for the latent model, which indicates satisfactory agreement for energy exchange calculations. These NN models are very fast and easy to use therefore, they might be used for design purposes or estimating the annual energy savings in different buildings with continuous operation and a RAMEE in their HVAC system.

3.3. Introduction

The use of computational intelligence techniques like neural networks (NNs), instead of conventional simulation methods, is increasing since they have many interesting advantages [3.1]. NNs are easy to implement and use. Also a correctly designed NN can approximate any complex, continuous, and nonlinear function to a pre-specified accuracy and can generalize underlying functions describing a physical phenomenon (e.g. the performance function of a heat and/or moisture transfer system). Kalogirou [3.1] discuses various applications of neural networks in energy analysis problems. Tan et al. [3.2] studied the thermal performance of a compact fin-tube heat exchanger using a neural network model. Xie et al. [3.3] developed a neural network with experimental data to model heat transfer from shell-and-tube heat exchangers. Many other researchers have used neural networks to predict the performance of thermal systems using experimental or numerical data [3.4-3.8].

Beside modeling different thermal systems using NNs, extensive research has been conducted to model heat and moisture exchanger systems. Simonson et al. developed the dimensionless parameters for air to air regenerative energy wheels to find the performance correlations [3.9-3.11]. Zhang [3.12] studied heat and mass transfer in hollow fiber membrane contactors for liquid desiccant air dehumidifiers analytically. Bergero et al. [3.13] numerically investigated the steady state performance of a hybrid air conditioning system working with a vapour compression inverse cycle combined with an air dehumidification system. Using numerical simulation methods, Vali et al. [3.14] studied the effectiveness of a Run-Around Heat Recovery Exchanger system with combined counter and cross flow exchangers. They also developed a new effectiveness correlation for counter/cross flow configuration. Fan et al. [3.16] developed a finite difference (FD) model to predict

the performance of a Run-Around Membrane Energy Exchanger (RAMEE) system using cross flow exchangers for simultaneous heat and moisture transfer for air-to-air energy recovery. The transient performance of the RAMEE was numerically modeled by Seyed Ahmadi et al. [3.16,3.17] and it was experimentally investigated by Erb et al. [3.18]. A comprehensive numerical study on the *steady state* performance under different outdoor air conditions was presented by Hemingson et al. [3.19,3.20]. Akbari et al. [3.21] developed a neural network to predict the *steady state* performance of a RAMEE system under different design and operating parameters.

Although a numerical model for the transient performance prediction of counter flow RAMEE system exists, it is computationally too intensive to be used for some applications. For example, in order to estimate annual energy savings in a building using the RAMEE system, the transient performance of the system during every operational hour through the year is required. Therefore, having a correlation or a computationally fast model that relates the operating conditions to performance of RAMEE would be necessary.

The purpose of this study is to present a new mathematical model to correlate the transient performance (i.e. sensible and latent effectivenesses) of a counter flow RAMEE system for a practical range of independent parameters. For this purpose, a Multi-Layer Perceptron (MLP) neural network [3.22] was trained with a back-propagation (BP) algorithm [3.23].

3.4. Description of RAMEE

3.4.1. Main Components

As can be seen in Figure 3.1A, the RAMEE is composed of two exchangers, which simultaneously transfer heat and moisture between two air streams using an

aqueous salt solution as a coupling liquid. An example to show how the RAMEE can be beneficial in HVAC applications during winter operating condition which the outdoor air (inlet of supply exchanger) is usually cooler and dryer than the indoor air (inlet of exhaust exchanger). During such conditions, the RAMEE recovers heat and moisture from the exhaust air and transfers this recovered heat and moisture to the supply air. Therefore it saves energy and increases the indoor comfort for occupants. Similarly, the RAMEE reduces energy consumption in the summer by cooling and drying the hot and humid outdoor ventilation air being supplied to a building by rejecting heat and moisture to the cool and dry exhaust air leaving the building.

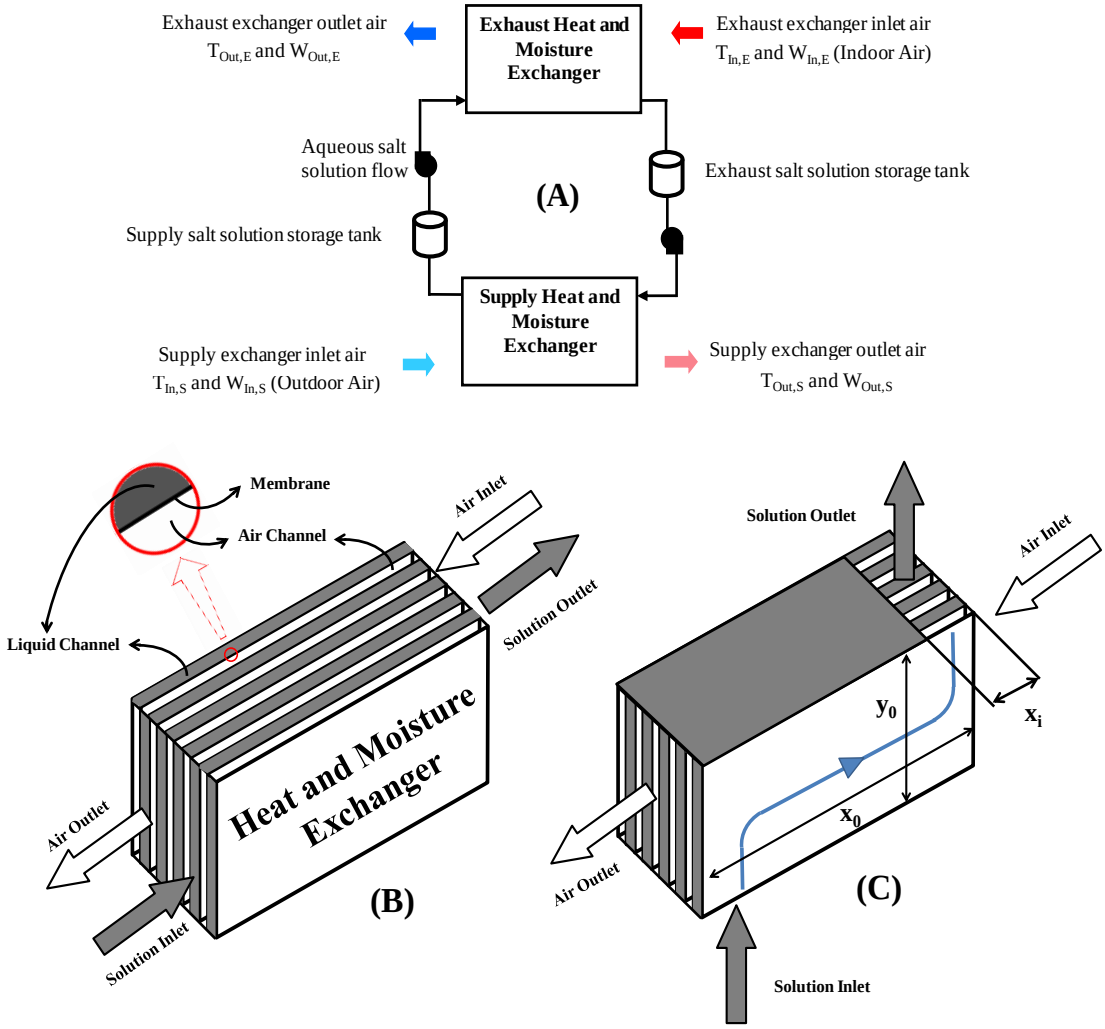

Figure 3.1. A) Schematic view of RAMEE components and inlet and outlet air conditions. More details for structure and operation of B) counter flow LAMEE C) cross-counter flow LAMEE.

Each exchanger is made up of many air and liquid flow channels, each separated by a semi-permeable membrane (Figure 3.1B). These membranes allow water vapor to transfer between the fluid streams (i.e. air and liquid) but they prevent liquid transfer [3.24]. Such a heat and moisture exchanger is called a Liquid-to-Air Membrane Energy Exchanger (LAMEE). An individual LAMEE can have different flow configurations. Figure 3.1B and 3.1C show counter and cross-counter flow configurations respectively. The mass flow rate of air in the supply and exhaust LAMEEs are equal or nearly equal. After each exchanger there is a storage tank (of the same volume) and a pump which provides a continuous salt solution circulation through the system.

3.4.2. Numerical Model

A numerical model which solves the physical governing equations for transient coupled heat and mass transfer through the RAMEE system was presented by Seyed Ahmadi et al. [3.16]. This model was modified and expanded by Hemingson [3.20] which predicts the transient sensible and latent effectivenesses of the RAMEE system under different initial and operating conditions. For the case of balanced exhaust and supply air mass flow rates, Equations 3.1 and 3.2 define sensible and latent effectivenesses of the RAMEE.

$$\varepsilon_s = \frac{\Delta T_S}{\Delta T} = \frac{T_{In,S} - T_{Out,S}}{T_{In,S} - T_{In,E}} \tag{3.1}$$

$$\varepsilon_l = \frac{\Delta W_S}{\Delta W} = \frac{W_{In,S} - W_{Out,S}}{W_{In,S} - W_{In,E}} \tag{3.2}$$

where ΔT_S and ΔW_S are the temperature and humidity ratio difference of air between the inlet and outlet of supply LAMEE, and ΔT and ΔW are the temperature and humidity ratio difference of air between the inlets of supply and exhaust LAMEEs.

ΔT and ΔW can be considered as the driving potentials for heat and moisture transfer in a RAMEE. In this study, the results from the transient numerical model (TNM) are used to develop the NN models.

3.4.3. Parameters Affecting the Transient Performance of RAMEE

Seyed Ahmadi et al. [3.17] identified the important parameters affecting the transient performance of the RAMEE. He studied the transient response of RAMEEs with changing parameters including: the number of heat transfer units (*NTU*), thermal capacity rate ratio (*Cr**), salt solution storage volume, and the initial salt solution concentration.

In this paper the effect of affecting parameters was studied more specifically. The purpose of studying the effect of these parameters is to determine the importance of each parameter. It helps us to simplify the predicting model by eliminating the parameters that are less important or practically unnecessary to be included in the NN models. Here the parameters are organized into three groups, first *outdoor and initial conditions*, second *system parameters*, and third *geometrical parameters and salt solution storage tank volume*.

3.4.3.1 Outdoor and Initial Conditions

The purpose of having a predicting model for the transient performance of the RAMEE system under *non-stop yearly operating condition*s, is to find the sensible and latent effectiveness of the RAMEE for each hour of operation since they are needed for annual energy consumption calculations. Figure 3.2 shows the transient sensible and latent effectiveness for first two weeks (January 1st to January 14th) of the typical meteorological year [3.25] in Calgary, AB, predicted by Seyed Ahmadi's model [3.16].

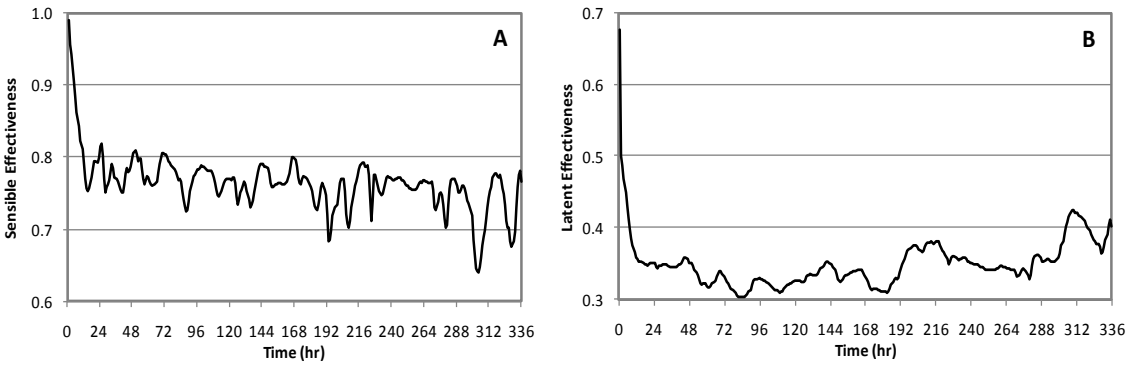

Figure 3.2. A) Sensible and B) latent transient effectivenesses for the first 336 hours (two weeks) of the RAMEE operation in Calgary, AB. (*NTU*=9, *Cr=2)**

As can be seen in Figure 3.2, sensible and latent effectivenesses are sharply decreasing during first a few hours then keep fluctuating with the time. The sharp initial drop of the RAMEE effectivenesses is mainly caused by the initial conditions (initial salt solution temperature and concentration in exchangers and reservoir tanks) while, the fluctuations that happen after are the result of variable outdoor conditions (variable supply exchanger inlet temperature and humidity ratio). Figure 3.3 is presented to show how the variation of outdoor condition changes the performance of RAMEE.

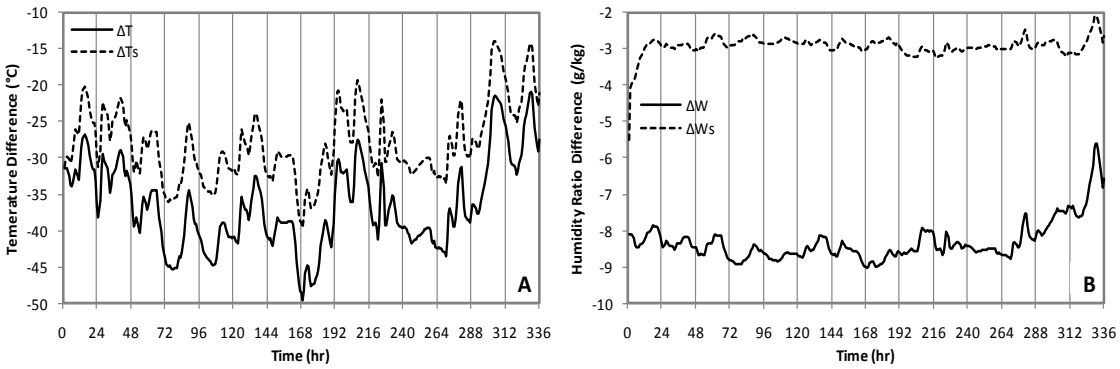

Figure 3.3. A) Supply side temperature difference (ΔT_s) compared to temperature difference between supply and exhaust inlets (ΔT) B) Supply side humidity ratio difference (ΔW_s) compared to humidity ratio difference between supply and exhaust inlets (ΔW) for the first 336 hours (two weeks) of the RAMEE operation in Calgary, AB, (*NTU*=9, *Cr=2).**

In Figure 3.3A, the supply side air temperature difference (ΔT_S) is compared to the air temperature difference between supply and exhaust inlets (ΔT). As is shown ΔT and ΔT_S are chosen to be equal at the initial point while they deviate as

soon as the system starts to operate. Both ΔT and ΔT_S have a similar trend although ΔT_S values are a portion of ΔT at any time, since ΔT is considered as the driving potential for sensible heat transfer. Seyed Ahmadi's numerical model does not show a significant lag between ΔT and ΔT_S values since the thermal mass effect of the materials of the exchangers and also heat losses to the environment from exchangers, reservoir tanks, and connecting tube lines are not included in this model. The same trend for latent performance of system can be seen in Figure 3.3B.

Figures 3.2 and 3.3 are only a sample of system behavior under variable outdoor condition and cannot be used for generalizing the behavior of system. For example for a different initial temperature and concentration of salt solution, the effect of initial condition might be longer or shorter than what is shown in Figure 3.2.

According to Figure 3.2 and 3.3, the effect of outdoor condition must be included in the neural models since the outdoor condition has a major and continuous effect on system transience. While the effect of salt solution initial condition on transient performance can be neglected for two main reasons. First, the aim in this study is to develop a model to predict the *non-stop yearly transient performance* of RAMEE and a discrepancy for the first a few hours or days does not change the accuracy of yearly results significantly. Second, a reasonable and practical assumption for initial condition is selected that is close to real operation of the RAMEE system. It is assumed that at $t = 0$ the only air in the supply exchanger is the only part of the system that is in equilibrium with the outdoor air and the rest of the system, including the air in the exhaust system and salt solution temperature and concentration in the storage tanks, is in equilibrium with the indoor air. This implies that the RAMEE is located inside the building.

3.4.3.2 System Parameters

System parameters are parameters that may change during the design or operation of a RAMEE. These parameters include the number of heat transfer units, *NTU*, number of mass transfer units, NTU_m, which are both design and operating parameters, and the heat capacity rate ratio, *Cr** which is only an operating parameter, as are defined in Equations 3.3 to 3.5.

$$NTU = \frac{UA}{C_{Air}} = \frac{UA}{\dot{m}_{Air} C_{P,Air}} \tag{3.3}$$

$$NTU_m = \frac{U_m A}{\dot{m}_{Air}} \tag{3.4}$$

$$Cr^* = \frac{C_{Sol}}{C_{Air}} \tag{3.5}$$

According to Equations 3.3 and 3.4, the ratio of NTU_m to *NTU* would be:

$$\frac{NTU_m}{NTU} = C_{p,air} \frac{U_m}{U} \tag{3.6}$$

where $C_{p,air}$ is the thermal capacity of air and can be assumed as a constant value. The ratio of U_m to *U* is equal to

$$\frac{U_m}{U} = \frac{\left[\frac{1}{h_{m,air}} + \frac{\delta}{k_m}\right]^{-1}}{\left[\frac{1}{h_{air}} + \frac{\delta}{k}\right]^{-1}} \tag{3.7}$$

where h_{air} and $h_{m,air}$ are air-side convective heat and moisture transfer coefficients respectively. The air and salt solution flows are assumed to be laminar and fully developed for the practical operating range of RAMEEs, therefore the convective heat and mass transfer coefficients for a *given design* are constant since the Nusselt number for a fully developed laminar flow is constant and is equal to 8.24 for a uniform heat flux in a parallel plate channel [3.26].Thus, U_m/U is only a function of air channel thickness, *th*, (since for a constant Nusselt number, the convective heat and mass transfer coefficients change with *th*) the thickness of membrane, δ, and the

heat conductivity and mass conductivity of the membrane, k and k_m. Therefore, for a given membrane and air channel thickness the ratio of U_m to U is constant provided that analogy between heat and mass transfer applies in the airstream and the flow configuration (counterflow in this paper) remains constant [3.27, 3.28]. For other conditions and designs, the heat and mass transfer coefficients and the ratio of Um to U may change [3.27-3.32]. Since this paper focus on a given LAMEE design, where NTUm and NTU are nearly proportional, only one of these design parameters needs to be known or used as input to the NN model. In this paper, *NTU* will be used as an input parameter for the NN model and NTU_m/NTU will be constant and equal to 0.26 based on the specifications of the LAMEEs presented in Table 3.1.

Table 3.1. Dimensions and membrane properties of each LAMEE.

Property	Value
LAMEE Dimensions	
Length	1800 [mm]
Height	200 [mm]
Entrance Length	76 [mm]
Channel Thickness	
Air	4.4 [mm]
Solution	2.7 [mm]
Membrane Properties	
Thickness	0.2 [mm]
Thermal Conductivity	0.334 [W/(m·K)]
Water Vapour Permeability	1.66×10^{-6} [kg/(m·s)]

The physical dimensions of the LAMEEs in Table 3.1 are based on physical LAMEEs that have been built and tested under steady-state operating conditions in a test laboratory [3.33, 3.34]. Other LAMEE physical dimensions (e.g., airflow gaps) and combinatios of NTUm/NTU have been studied by other researchers to determine the steady-state heat and moisture transfer performance and pressure drop [3.34-3.36, 3.14, 3.19] and are not considering in this study. Rather this study focuses on the transient NN modeling of a RAMEE during continuous operation in a building HVAC system. Figure 3.4 (A and B) shows the effect of *NTU* on the sensible and

latent effectiveness of RAMEE. The effectivnesses increase with *NTU* as expected. Therefore, the effect of *NTU* on the RAMEE performance must be included in the NN models.

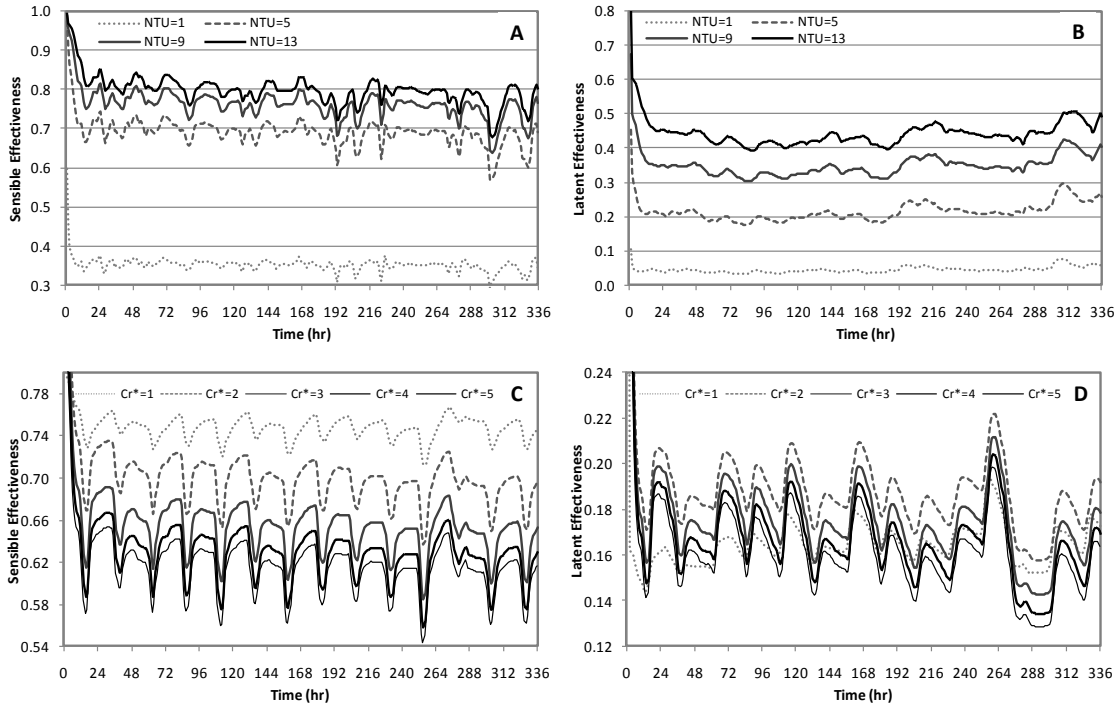

Figure 3.4. A) Sensible and B) latent effectivenesses, for different *NTU* values, C) Sensible and D) latent effectivenesses, for different *Cr values for the first 336 hours (two weeks) of the RAMEE operation in Calgary, AB.**

The next parameter that has to be included in the NN models is the heat capacity rate ratio, *Cr**, which is defined as the ratio of salt solution heat capacity rate, C_{Sol}, to air heat capacity rate, C_{air}. *Cr** is a pure operating parameter and is typically adjusted by changing the salt solution flow rate since the air flow rate is often determined by building needs. Figure 3.4 (C and D) presents the variation of sensible and latent effectivenesses for different *Cr** values. For the case presented in Figure 3.4 (C and D) the sensible effectiveness decreases with *Cr** while latent effectiveness is maximum for *Cr**=2. The optimal *Cr** is case sensitive due to the coupled effect of heat and moisture transfer in the RAMEE, therefore *Cr** can be

changed to optimize annual energy transfer in different climates. Rasouli et al. showed the optimal operation of RAMEE for an office building [3.37] and a health care facility [3.38] using optimized hourly *Cr** values. In these studies, the steady-state neural network model developed by Akbari et al. [3.21] was subjected to an optimization algorithm to predict the optimum sensible and latent effectivenesses in each hour of RAMEE operation that results in a maximum annual savings for a building. According to the discussion above *Cr**, like *NTU,* is a very important operating parameter which must be included in the NN models.

3.4.3.3. Effect of Geometrical Parameters and Salt Solution Storage Tanks Volume

The third group of parameters that effect RAMEE performance is the geometrical parameters (i.e. aspect and entrance ratios as defined in Equations 3.8 and 3.9) and the volume of salt solution in the storage tanks.

$$Aspect\ Ratio = \frac{Y_0}{X_0} \tag{3.8}$$

$$Entrance\ Ratio = \frac{X_i}{X_0} \tag{3.9}$$

Akbari et al. [3.21] showed that the *steady state* sensible and latent effectivenesses for counter flow RAMEE can be used to predict the performance of cross-counter flow RAMEE systems of sufficiently small aspect and entrance ratios. Where the entrance ratio is less than 0.1 (and the aspect ratio is less than 0.1), the difference between cross-counter and counter flow RAMEEs for both sensible and latent effectivenesses is smaller than 5%. Also for aspect ratios less than 0.2 (when the entrance ratio is less than 0.05), this difference is not more than 1%.

In this study, we are interested to model the *transient* behavior of the cross-counter flow RAMEE of Mahmud [3.34, 3.34] where the physical dimensions of the

LAMEEs are presented in Table 3.1. Therefore, the results of a sensitivity study that compares the transient performance of this specific design (Table 3.1) to a counter flow RAMEE is presented in Table 3.2. The supply side outlet air temperature and humidity ratio from the counter flow RAMEE ($T_{S,Out,C}$ and $W_{S,Out,C}$) is compared to the corresponding values from cross-counter flow RAMEE ($T_{S,Out,CC}$ and $W_{S,Out,CC}$) in terms of Root Mean Squared Error (RMSE).

Table 3.2. The RMSE between counter flow and cross-counter flow yearly simulations for different locations. (*NTU*=5, *Cr=2, AHRI summer indoor condition)**

	RMSE between $T_{S,Out,C}$ and $T_{S,Out,CC}$ (°C)	**RMSE between** $W_{S,Out,C}$ and $W_{S,Out,CC}$ (g/kg)
Saskatoon, SK	0.08	0.016
Chicago, IL	0.06	0.011
Miami, FL	0.03	0.005
Phoenix, AZ	0.04	0.008

The yearly simulations using typical meteorological year [3.25] for different locations of different climates are performed. The results from Table 3.2 shows almost identical supply side outlet temperature and humidity ratio for a counter flow RAMEE and a cross-counter flow RAMEE as described in Table 3.1 (*Aspect Ratio = 0.111* and *Entrance Ratio = 0.042*). Therefore all required data in this study is produced using the counter flow model since it uses less computational nodes (by a factor of 25) and is much faster than the cross-counter flow model.

Seyed Ahmadi [3.39] showed that the volume of the salt solution in the storage tanks has a significant effect on the required time for the RAMEE to reach a *quasi-steady state* condition. He showed that a 5.5 times reduction in the size of storage tanks, results in a 75% lower transient time for standard AHRI operating conditions [3.39]. So it is very important to determine the effect of the storage tank volume on the specific application that we are studying in this paper which is *yearly dynamic and transient performance* of the RAMEE. Therefore, different simulations with different storage tank volumes were performed and the results were compared

to each other. Parameter 'x' is defined as the volume of the salt solution in each exchanger that is 9.72 liters for an exchanger with 10 solution channels. Figure 3.5 compares the response of a system with storage tank volume of 1x to the same system with a bigger storage tank (20x) during a step change in the outdoor condition at hour 1300.

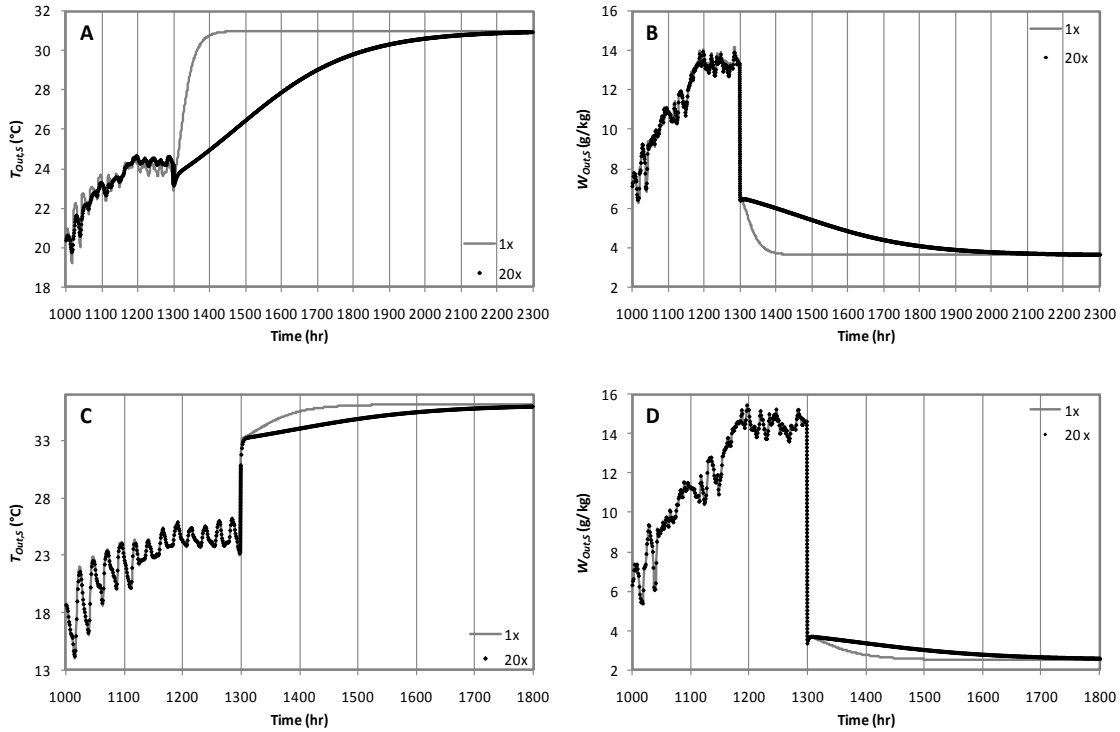

Figure 3.5. Sensible and latent responses of systems with different storage tank volumes (1x vs. 20x) for A and B) *NTU=5, Cr*=2*. C and D) *NTU=1, Cr*=10* before, during, and after the step change of the outdoor condition at hour 1300 in Miami, FL.

In this figure at hour 1300 the outdoor air jumps to 42 °C and 2g/kg and is kept constant since then. Before hour 1300, which shows the transient operation of the system under variable outdoor condition, a close agreement between the responses of 1x and 20x systems is shown although after the step change in the operating condition, which represents the transient operation of the system under *constant operating condition* (similar to Seyed Ahmadi's study [3.39]), 1x system shows a quicker response to the change in operating condition. In Figures 3.5A and

3.5B the response of the system for *NTU=5* and *Cr*=2* is shown and can be compared to Figures 3.5C and 3.5D with *NTU=1*and *Cr*=10*. For *NTU=1*and *Cr*=10*, which has a higher mass flow rate of air and salt solution, the system shows a better agreement before the step change, quicker response during the step change hour (from hour 1299 to 1300), and shorter transient time after step change. Therefore it seems necessary to study the effect of *NTU* and *Cr** on the response of the systems with different storage tank sizes.

As shown in Figure 5, there is a difference between continuous operation of the RAMEE where the outdoor weather conditions change gradually with time compared to the case where the outdoor conditions change drastically (such as the large step change introduced in Figure 3.5). A step change in outdoor conditions might be experienced if the RAMEE is used intermittently such that it turned off for many days or even months and then turned back on. During continuous operation, the effect of the mass of the storage tank is quite small, but during intermittent operation (a step change in outdoor conditions here), the size of the storage tank plays a large role. In some cases, it would be beneficial to have a small storage tank so that the time constants of the RAMEE are small, while in other cases, it would be advantageous to have a large storage tank and large time constants as discussed by Erb [3.41] for the RAMEE and by other researchers for thermal storage systems [3.42, 3.43].

In real applications of The RAMEE in HVAC systems with continuous operation as studied in this paper, “There will be a minimum allowable storage volume for a range of ambient weather conditions. This minimum storage volume depends on several parameters which cannot be selected arbitrarily. The operating condition of the system, including inlet air conditions, has a significant impact on the appropriate

size of the storage volume. In practice, the operating condition may change on a daily or even an hourly basis. This suggests that the appropriate liquid desiccant storage volume must be chosen to cover a range of humidity conditions from dry to humid during which the desiccant volume will change significantly" [3.39]. During many simulations with the TNM it was observed that the minimum allowable storage volume for different *NTU* and *Cr** values in most climates is around 10x or more. Therefore the difference between hourly results from two systems with different salt solution volumes (10x and 20x) in different locations with extreme climates in North America was found. Extreme climatic condition causes a large amount of heat and mass transfer between the exchangers and helps us to notice the possible difference between 10x and 20x systems easier. Miami, FL, is the representative of hot and humid climate, Calgary, AB, represents cold and dry climate with sharp variations in temperature and humidity, and Tucson, AZ, is the representative of hot and dry climate with drastic changes in temperature and humidity during the Monsoon season. In order to include the effect of *NTU* and *Cr**, different simulations for *NTU=7*and *Cr*=1, 3, 5* and also *Cr*=3* and *NTU=1, 7, 13* was performed and in each case the supply side outlet temperature and humidity ratio from 10x system were compared to the corresponding value from 20x system in terms of MAD (Figure 3.6).

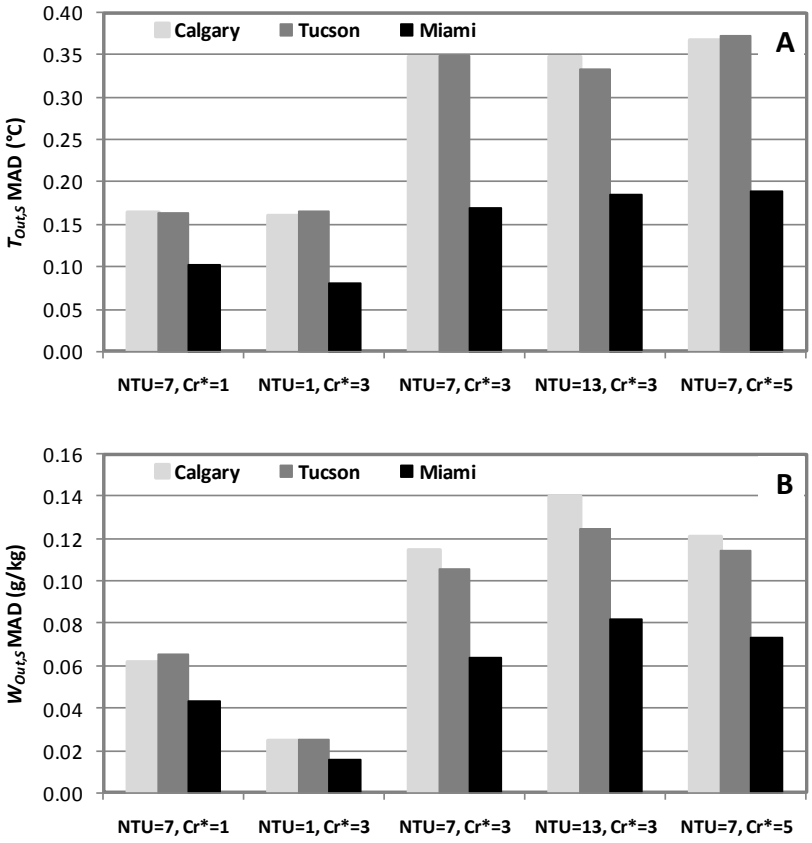

Figure 3.6. MAD values for supply side outlet A) temperature and B) humidity ratio between the outlet air condition of two systems with storage tank volume of 10x and 20x for different *NTU* and *Cr values in different locations of different climates.**

Figure 3.6 shows a negligible difference between the TNM results for storage volume of 10x and 20x. At first glance, the very minor effect of storage tank volume on the dynamic and transient performance of the system seems unreasonable. Since Seyed Ahmadi's [3.39] results show a major dependency between the storage volume and the system time response. The key difference is that his study is based on the *transient performance of the system under constant operating condition* which requires a long time for salt solution in storage tanks to reach a stable temperature and concentration, while the current study, considers the *transient performance of the RAMEE under variable operating conditions* in which the outdoor temperature and humidity ratio are changing on an hourly basis.

Therefore the effect of storage tank volume is not included in the NN models. All the TNM simulations in this study for developing the NN model is done using the tank volume equal to 10x.

3.5. Back-Propagation Algorithm

Neural networks are a non-algorithmic modeling method and can learn based on examples. Among various types of NNs, Multi Layer Perceptrons [3.22], using back-propagation (BP) [3.23] method, are being widely used to solve many engineering modeling problems [3.4-3.7]. The main idea of the back-propagation method is to update the matrices of weights and biases based on the error between desired output values (targets) and NN output. Different error functions can be applied to achieve a neural model of desired accuracy. In order to simply implement the back-propagation algorithm, Equation 3.10 can be considered.

$$F_{n+1} = F_n + \Delta F \tag{3.10}$$

Where F_n is the current weights and biases matrix and ΔF is the update matrix which mainly depends on the error gradient vector and the type of training and performance functions. Reference [3.23] provides a more detailed description about the BP method.

One of the most popular applications of NNs in engineering is called *function approximation.* In this study the BP algorithm will be applied to approximate the underlying function describing the transient performance of the RAMEE system. To achieve this, the inputs and outputs of the neural model have to be selected then a training data set including inputs and corresponding outputs is required.

3.6. Neural Model Inputs and Outputs and Data Generation

3.6.1. Neural Model Inputs and Outputs

The results of the sensitivity studies presented in section 3.4.3.1 showed that the effect of outdoor condition has to be included in the transient NN model while initial conditions effects can be neglected. In order to cover a wide range of outdoor conditions real hourly meteorological data [3.25] (i.e. hourly outdoor temperature and humidity ratio for a year) in Saskatoon, SK, Chicago, IL, Miami, FL, and Phoenix, AZ, are selected as the representative of cold and dry, cold and humid, hot and dry, and hot and humid climates respectively [3.44].

Section 3.4.3.2 showed the important effect of *NTU* and *Cr** on the transient behavior of the RAMEE system. Akbari et al. [3.21] presented a sensitivity study which shows the effective and practical range of *NTU* and *Cr**. According to this sensitivity study, the variations in sensible and latent effectivenesses are very slight for *NTUs* larger than 14 or *Cr*s* higher than 5. Therefore the inputs of the NN models for *NTU* and *Cr** were limited to these values.

In section 3.4.3.3 the difference between the performance of counter flow RAMEE and cross-counter flow RAMEE (i.e. Table 3.1) is investigated. Aspect and entrance ratio which describe the geometry of cross-counter flow LAMEEs are not included in neural models since the difference between the performance of a counter flow RAMEE and the cross-counter flow RAMEE, studied in this paper, is negligible. Therefore, the neural model was developed based on counter flow numerical model. Also the results of section 3.4.3.3 showed that effects of storage tank volume are negligible for the case of continuous RAMEE operation.

Figure 3.7 depicts a black box illustration of the neural model and its inputs and outputs. A model with 12 inputs and one output is presented to predict the transient performance of RAMEE system.

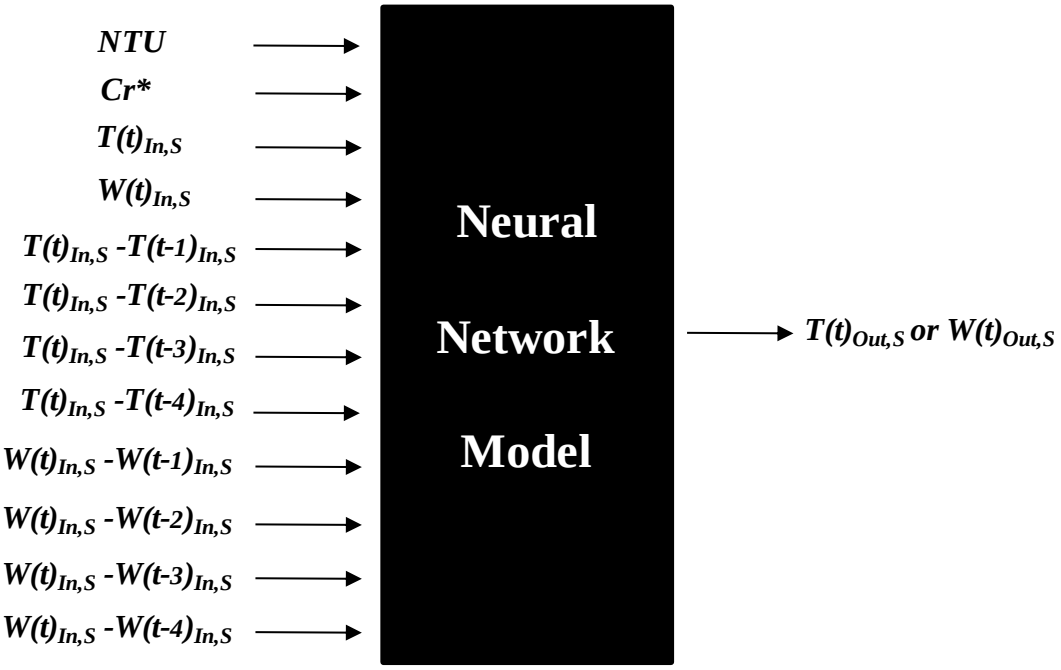

Figure 3.7. Black box illustration of the NN model and its inputs and output.

NTU, *Cr**, outdoor temperature and humidity ratio at the current time, and their difference with the outdoor temperature and humidity ratio during past four hours of system operation are the inputs of the neural networks. Using the previous outdoor conditions for more than four hours may improve the results, while it significantly increases the complexity of the models and the training time. Also some models with less hours of the history of system operation were tried that could not achieve the desired accuracy and were mainly unstable models that would generate unacceptable (extremely big) outputs.

Outlet temperature and humidity ratio of the supply side exchanger ($T_{Out,S}$ and $W_{Out,S}$) are respectively the output for sensible and latent NN models which can be easily substituted in Equations 3.1 and 3.2 to calculate sensible and latent effectivenesses.

3.6.2. Data Generation

The training data set used in this study is provided using the TNM developed by Seyed Ahmadi [3.16]. Training set has a key role in the training process and should cover a practical range of the input parameters. Therefore a training set of various *NTU*, *Cr**, $T_{In,S}$, and $W_{In,S}$ and the corresponding outputs (i.e. $T_{Out,S}$ and $W_{Out,S}$) is required.

For each *NTU* and *Cr** a yearly simulation for 8760 hourly meteorological data ($T_{In,S}$ and $W_{In,S}$) from four different climatic representative locations, listed in section 3.6.1, was done. The indoor condition was assumed as constant and equal to AHRI summer condition ($T_{In,E}$=24 °C and $W_{In,E}$ =9.3 g/kg).

Seven values of *NTU* (ranging from 1 to 13 in increments of 2), nine values of *Cr**, (ranging from 1 to 5 in increments of 0.5), and 4×8760 sets of ($T(t)_{In,S}$, $W(t)_{In,S}$) were applied to get approximately 2.2 million data points. This test set is extremely large and it causes computational difficulty in training the NN models. Also the authors realized that such a huge training set is not required for developing the neural networks, since the real outdoor data is highly redundant (the weather patterns in many days of year are very similar and the temperatures and humidity values are almost the same). In order to shrink this data set, smaller data sets (e.g. 50000, 100000, 150000, etc.) were randomly picked from the 2.2 million points then some neural networks were trained using these smaller data sets. The trained neural networks were tested for both the full 2.2 million-point data set and the smaller ones. The errors were identical which shows that even the smallest data set includes all the

patterns in the 2.2 million-point data set. Therefore, for simplicity of computations the 50,000 point data set was used for training purposes.

3.7. NN Architecture and Training Process

Generally speaking, there is no proven method to find the optimum neural model (the simplest model with the highest accuracy) for different problems. Thus, for every specific problem a pre-defined desired accuracy would be a reasonable stopping criterion. Finding a neural model to represent a real and unique problem is basically a trial and error process and depends on the type and complexity of the problem as well as the experience of the trainer.

Two separate Multi Layer Perceptron feed-forward networks using the well-known Levenberg-Marquardt [3.45, 3.46] training algorithm were used to map the inputs of the network to the corresponding targets. The network with an output of $T_{Out,S}$ is called the sensible network and the other network (with $W_{Out,S}$ as output) is called the latent network. It would be possible to develop a single neural model to predict both $T_{Out,S}$ and $W_{Out,S}$ at once. But defining a network with multiple outputs usually decreases the accuracy of the results because the hidden neurons would have difficulty to model two complicated functions at the same time. Therefore it is very common to train separate networks for each output, then combine them into a package and run them as a unit. This is the method used in this study.

To improve the generalization of the neural model, the early stopping method [3.47] was applied. In this method, the generated data set is divided into three subsets. The first subset is called the training subset, which is used for back-propagating the errors and updating weights and biases during the training session. The second subset is called the validating set which is monitored during the training session by the early stopping method to prevent the network from over-fitting the

training subset. The third subset is called the test set. The test set is “unseen” by the NN because it is not used for either updating weights or stopping the training. The error of the test set is very important because it is monitored by the trainer to make sure that the accuracy of network is acceptable for unseen data. This error facilitates the comparison of different neural models for a specific problem and allows the researcher to choose the most accurate one.

In this paper, the generated data set was divided into three subsets (training, validating, and testing). Different dividing ratios were applied to the data set to get the best results. The lowest errors were reached using training subset, 60%, validating, 25 %, and testing, 15% of the 50,000-point data set.

Different topologies for the neural models of one to three hidden layers with combinations of linear and non-linear neurons in output and hidden layers were tried to get the model of highest accuracy. In order to make the computations easier all input and corresponding outputs were normalized using a standard deviation based function which, for every parameter, sets the min value as zero and deviations as one. After dividing and normalizing the training data set, the Levenberg-Marquardt [3.45, 3.46] algorithm was applied to minimize the error between the targets (TNM outputs) and the NN outputs for various architectures. Table 3.3 presents the results of linear regression analysis for training, validating, and testing sets for some of the best architectures that were tried to achieve a sensible NN of satisfactory accuracy.

Table 3.3. Result of linear regression along with MSE for different architectures on training, validating, and test sets. M and B are the slope and intercept of the linear trend line respectively. 'r' and MSE are the correlation coefficient and Mean Squared Error between the NN and TNM outputs respectively.

#	Architecture For The Sensible Network	Training Set Error				Validating Set Error				Test Set Error			
		M	B	r	MSE $(°C)^2$	M	B	r	MSE $(°C)^2$	M	B	r	MSE $(°C)^2$
1	12-10-8-8-1	0.992	0.21	0.994	0.3613	0.991	0.23	0.994	0.3703	0.991	0.22	0.994	0.3638
2	12-8-6-1	0.994	0.19	0.996	0.2916	0.992	0.19	0.995	0.3100	0.994	0.16	0.944	0.3095
3	12-20-20-1	0.997	0.25	0.995	0.4055	0.996	0.28	0.994	0.4185	0.996	0.24	0.994	0.4147
4	12-16-16-1	0.996	0.24	0.994	0.3884	0.995	0.29	0.994	0.4075	0.996	0.27	0.994	0.3987

As can be seen in Table 3.3, the errors are very close. Network number 2 gives the lowest errors and is the simplest (smallest) model that was trained. Although further investigation shows that it is not the best NN. The accuracy and the ability of the models, listed in Table 3.3, to predict transient performance of the system for new locations (locations that are different from the training cities) with different climates were double checked. Finally it was concluded that the 12-16-16-1 model has the best performance over all unseen locations for both sensible and latent models. Further explanation and verification for model number 3 is presented in the next section. Table 3.4 shows the architecture and properties of the selected NN and Appendix B presents the weights and biases of the trained NN.

Table 3.4. Architecture and configuration of the NN models.

Number Of Inputs	12
Number Of Outputs	1
Number Of Hidden Layers	2
Number Of Neurons In each Hidden Layer	16
Number Of Neurons In Output Layer	1
Network Type	Fully Connected With Biases For All Neurons
Hidden Layers Transfer Function	Tangent Hyperbolic (Tangent Sigmoid)
Output Layer Transfer Function	Linear

3.8. Verification and Application of the NN Models

3.8.1. Verification of the NN Models for Different Locations

To verify the ability of selected NN models to predict the performance of the RAMEE system under different climates, the yearly results from NN models for six

different unseen locations (Vancouver, BC, Halifax, NS, Boston, MA, Calgary, AB, Albuquerque, NM, and Tucson, AZ) were compared to the values from the TNM. None of the locations listed above were used for training purpose that is why these are called 'unseen'. Table 3.5 briefly describes the climate types and weather patterns in these test locations.

Table 3.5. Climate description of the unseen test locations.

Location	Climate Type	Brief Climate Description
Vancouver, BC	Oceanic	Mild climate. Minor and slow variations in temperature and humidity. Cool summers and warm winters compared to central Canada.
Halifax, NS	Humid Continental	Mild climate compared to the central Canada with temperature mostly changing between −15 °C and 25 °C. Tropical storms often from August to October.
Boston, MA	Humid Continental	Warm, rainy and humid summers with cold, snowy, and windy winters. Unstable weather with sharp variation in temperature and humidity due to winds.
Calgary, AB	Dry Humid Continental	Generally cold, long, and dry winters that may be occasionally warm due to Chinook winds blowing from Canadian Rocky mountains during the winter months. Chinook can raise the winter temperature by up to 15 °C in a few hours.
Albuquerque, NM	Arid	All monthly average temperatures are above freezing (0 °C). Sunny with four seasons. Due to a dry weather, sunshine, and very high elevation (~1620 m above sea level), temperature fluctuates between day and night (e.g. warm summer days and cool nights).
Tucson, AZ	Desert	Two main seasons. Hot summers and warm winters. Three minor seasons: spring, fall, and monsoon. Monsoon causes serious thunderstorms that drastically change the air humidity.

As can be seen Vancouver and Halifax are two locations with moderate climate and smoother variations in outdoor temperature and humidity, while the rest of locations have different extreme climates with drastic changes in outdoor condition in a short period of time. For each location the TNM was run to simulate 8760 hourly performances over a wide range of *NTU* and *Cr** values (*NTU* =2, 4, 6, 8, 10 and *Cr**=1.75, 2.75, 3.75, 4.75) and the results were compared to the predicted

values by the NN models. The mean absolute difference (MAD), standard deviation, mean difference values (μ), and the distribution of ΔT and ΔW are listed in Table 3.6.

Table 3.6A. Mean Absolute Difference, Standard deviation, mean value of the difference between TNM and NN results, and percent of data falling in 1, 2, and 3 standard deviations for the sensible network outputs compared to transient simulations in different test locations (*NTU*=2, 4, 6, 8, 10 and *Cr=1.75, 2.75, 3.75, 4.75. The errors were calculated for over 200,000 points per location).**

Location	Mean Absolute Difference [K]	σ_T (Std. Dev. ΔT [K])	μ_T (Ave. ΔT [K])	% Falling In $\mu_T \pm 1\sigma_T$	% Falling In $\mu_T \pm 2\sigma_T$	% Falling In $\mu_T \pm 3\sigma_T$
Vancouver, BC	0.34	0.36	0.21	77.1	94.5	98.1
Halifax, NS	0.42	0.52	0.18	76.0	96.0	99.0
Boston, MA	0.37	0.54	0.03	78.8	94.6	98.5
Calgary, AB	0.52	0.71	0.04	75.1	94.6	98.8
Albuquerque,	0.71	0.81	-0.32	70.9	94.8	99.6
Tucson, AZ	0.79	0.91	-0.43	70.6	94.8	99.3

Table 3.6B. Mean Absolute Difference, Standard deviation, mean value of the difference between TNM and NN results, and percent of data falling in 1, 2, and 3 standard deviations for the latent network outputs compared to transient simulations in different test locations (*NTU*=2,4,6,8,10 and *Cr=1.75,2.75,3.75,4.75. The errors were calculated for over 200,000 points per location).**

Location	Mean Absolute Difference [g/kg]	σ_W (Std. Dev. ΔW [g/kg])	μ_W (Ave. ΔW [g/kg]	% Falling In $\mu_W \pm 1\sigma_W$	% Falling In $\mu_W \pm 2\sigma_W$	% Falling In $\mu_W \pm 3\sigma_W$
Vancouver, BC	0.09	0.14	-0.021	82.9	95.5	97.3
Halifax, NS	0.13	0.17	-0.042	78.2	95.4	97.8
Boston, MA	0.14	0.20	-0.006	77.0	94.0	98.4
Calgary, AB	0.19	0.25	-0.019	72.8	94.9	99.1
Albuquerque,	0.27	0.31	0.15	71.0	94.6	99.4
Tucson, AZ	0.33	0.36	0.220	72.2	94.7	99.1

In all locations around 75% of ΔT and ΔW values fall in the range of one standard deviations ($\mu_T \pm 1\sigma_T$), 95% fall in two standard deviations, and 98% in three standard deviations that shows a normal distribution. The results show a better agreement for locations with smoother variations in the outdoor condition (Vancouver and Halifax) while larger errors happen in extreme climatic conditions. This trend is expected since the presented NN models produce the output not only based on the current hour outdoor condition but also include the effect of previous hours. For the conditions that a sharp change in the outdoor condition happens the

NN response will be different from TNM results while for smooth variations in the outdoor condition the TNM and NN outputs are closer.

The most important error for energy calculation purposes, which is one of the main applications of NN models, is the mean absolute difference (MAD). The average MAD for all six unseen locations is 0.52 °C for sensible NN and 0.2 g_v/kg_a for the latent one which shows satisfactory accuracy for energy calculations for the buildings with RAMEE in their HVAC system.

3.8.2. Applications

Generally speaking, NNs can simply interpolate any new pattern that falls in the domain of input parameters. Unlike the TNM model, the NN models predict the sensible and latent performance of the RAMEE system at a very high speed due to their non-iterative data processing (The NN models are approximately 10^5 times faster than the TNM). For example the NNs presented in this paper take less than 1 second to produce the results for 8760 points (i.e. hourly transient effectiveness values for 1 year) using a common desktop, while the TNM takes up to several days to produce the same data for a cross-counter flow configuration and up to 1 hour for counter flow system.

One of the most important applications of the NN models is to use their outputs to predict annual energy savings by the RAMEE. The definition of the optimal system performance for the RAMEE, operating under different outdoor and indoor conditions, is developed by Rasouli et al. [3.37]. This definition can vary depending on building demand. For example in the hours that the building needs sensible heating (i.e. only heat transfer from exhaust air to supply air is important and moisture transfer does not matter) the optimum performance is to maximize the sensible effectiveness of the RAMEE. As is discussed in previous sections the

sensible or latent effectiveness of the system can be maximized or minimized changing the Cr^* (or salt solution flow rate). Using an optimization algorithm applied to the neural network models, the optimum effectiveness values for RAMEE under different operating conditions are obtained. These optimum values are used for TRNSYS computer simulation of the RAMEE system when operating in an office building in four different climates to estimate the annual savings by RAMEE [3.37]. The results show up to 43% heating energy saving in cold climates, and up to 15% cooling energy saving in hot climates. The same analysis for the application of a RAMEE system in the HVAC system of a hospital shows even more energy savings. The optimized RAMEE saves the annual heating energy by 58 - 66% in cold climates, and the annual cooling energy by 10 - 18% in hot climates. The RAMEE can also downsize the heating system by 45% in cold climates, and the cooling system by 25% in hot climates [3.38].

3.9. Conclusions

In this study, the sensible and latent effectivenesses for the non-stop yearly transient operation of Run-Around Membrane Energy Exchanger (RAMEE) were predicted using two separate neural network (NN) models. A training data set of approximately 50,000 points, provided using a transient numerical model (TNM), was subjected to a back-propagation algorithm to minimize the error between the outputs of the simulations and the NN models. Finally, a 12-16-16-1 configuration was concluded to result in a NN model of satisfactory accuracy for either sensible or latent energy transfer in the RAMEE.

The ability of the trained NN models to predict the effectiveness of the RAMEE was double checked numerically. The TNM was used to provide a completely unseen test set for six new locations (with two location of moderate

climate and four location of different extreme climatic conditions) over a wide range of *NTU* and *Cr** and the results were compared to the corresponding values from NN models. The mean absolute difference (MAD) between the results from TNM and NN models were around 0.5 °C for the sensible NN and 0.2 g_v/kg_a for the latent neural network.

Such a fast and non-iterative mathematical model can be used as a computational component in commercial building energy simulation packages to estimate the annual energy savings that are possible using a RAMEE [3.38]. Also the NN models can be used to find the optimum design or operating parameters (*NTU and Cr**) of RAMEE for various outdoor air conditions.

The application of this model is not only limited to non-stop yearly operation. For the applications that the effect of initial condition is not important or for the cases that the performance of the system after initial hours is requested, NN model will provide a fast and sufficiently accurate response.

3.10. References of chapter 3

[3.1] S.A. Kalogirou, Applications of artificial neural networks in energy systems, Energy Con. & Mgmt. 40 (1999) 1073–1087.

[3.2] C.K. Tan *, J. Ward, S.J. Wilcox, R. Payne, Artificial neural network modelling of the thermal performance of a compact heat exchanger, Appl. Therm. Eng. 29 (2009) 3609–3617.

[3.3] G.N. Xie, Q.W. Wang , M. Zeng, L.Q. Luo, Heat transfer analysis for shell-and-tube heat exchangers with experimental data by artificial neural networks approach, Appl. Therm. Eng. 27 (2007) 1096–1104.

[3.4] G. Xie, B. Sunden, Q. Wang, L. Tang, Performance predictions of laminar and turbulent heat transfer and fluid flow of heat exchangers having large tube-diameter and large tube-row by artificial neural networks, Int. J. Heat Mass Transfer 52 (2009) 2484–2497.

[3.5] H. Peng, X. Ling, Neural networks analysis of thermal characteristics on plate-fin heat exchangers with limited experimental data, Appl. Therm. Eng. 29 (2009) 2251–2256.

[3.6] G. Diaz, M. Sen, K.T. Yang, R.T. McClain, Simulation of heat exchanger performance by artificial neural networks, Int. J. of HVAC&R Research 5 (1999) 195–208.

[3.7] A. Pacheco-Vega, G. Diaz, M. Sen, K.T. Yang, R.T. McClain, Heat rate predictions in humid air–water heat exchangers using correlations and neural networks, ASME J. Heat Transfer 123 (2001) 348–354.

[3.8] Y. Islamoglu, A. Kurt, Heat transfer analysis using ANNs with experimental data with air flow in corrugated channels, Int. J. Heat Mass Transfer 47 (2004) 1361–1365.

[3.9] E.M. Sparrow, J.C.K. Tong, M.R. Johnson, G.P. Martin, Heat and mass transfer characteristics of a rotating regenerative total energy wheel, Int. J. Heat Mass Transfer 50 (2007) 1631–1636.

[3.10] C.J. Simonson, R.W. Besant, Energy wheel effectiveness: part i – development of dimensionless groups, Int. J. Heat Mass Transfer 42 (1999) 2161–2170.

[3.11] C.J. Simonson, R.W. Besant, Energy wheel effectiveness: part ii – correlations, Int. J. Heat Mass Transfer 42 (1999) 2171–2185.

[3.12] L.Z. Zhang, An analytical solution to heat and mass transfer in hollow fiber membrane contactors for liquid desiccant air dehumidification, ASME J. Heat Transfer 133 (2011) 092001-1–092001-8**.**

[3.13] S. Bergero, A. Chiari, Performance analysis of a liquid desiccant and membrane contactor hybrid air-conditioning system, Energy and Buildings 42 (2010) 1976-1986.

[3.14] A. Vali, C. J. Simonson, R. W. Besant, G. Mahmood, Numerical model and effectiveness correlations for a run-around heat recovery system with combined counter and cross flow exchangers, Int. J. Heat Mass Transfer 52 (2009) 5827–5840.

[3.15] H. Fan, C.J. Simonson, R.W. Besant, W. Shang, Performance of a run-around system for HVAC heat and moisture transfer applications using cross-flow plate exchangers coupled with aqueous lithium bromide, HVAC&R Res. 12 (2006) 313–336.

[3.16] M. Seyed Ahmadi, B. Erb, C.J. Simonson, R.W. Besant, Transient behavior of run-around heat and moisture exchanger system, Part I: Model formulation and verification, Int. J. Heat Mass Transfer 52 (2009) 6000-6011.

[3.17] M. Seyed Ahmadi, B. Erb, C.J. Simonson, R.W. Besant, Transient behavior of run-around heat and moisture exchanger system, Part II: Sensitivity studies for a range of initial conditions, Int. J. Heat Mass Transfer 52 (2009) 6012-6020.

[3.18] B. Erb, M. Seyed Ahmadi, C.J. Simonson, R.W. Besant, Experimental measurements of a Run-Around Membrane Energy Exchanger (RAMEE) with comparison to a numerical model, ASHRAE Trans. 115 (2009) 689-705.

[3.19] H.B. Hemingson, C.J. Simonson, R.W. Besant, Steady-state performance of a run-around membrane energy exchanger for a range of outdoor air conditions, Int. J. Heat Mass Transfer 54 (2011) 1814–1824.

[3.20] H.B. Hemingson, The impacts of outdoor air conditions and non-uniform exchanger channels on a run-around membrane energy exchanger, M.Sc. thesis, University of Saskatchewan, Saskatoon, SK, 2010.

[3.21] S. Akbari, H.B. Hemingson, D. Beriault, C.J. Simonson, R.W. Besant, Application of neural networks to predict the steady state performance of a Run-Around Membrane Energy Exchanger, Int. J. Heat Mass Transfer 55 (2012) 1628–1641.

[3.22] Y. Wang, A neural network adaptive control based on rapid learning method and its application, Advances in Modeling and Analysis 46 (1994) 27–34.

[3.23] M.T. Hagan, H.B. Demuth, M.H. Beale, Neural Network Design, PWS Publishing, Boston, MA, 1996, pp. 11-2 -12-52.

[3.24] M.D. Larson, C.J. Simonson , R.W. Besant, P.W. Gibson, The elastic and moisture transfer properties of polyethylene and polypropylene membranes for use in liquid-to-air energy exchangers, Journal of Membrane Science 302 (2007) 136-149.

[3.25] W. Marion, K. Urban, User's Manual for TMY2s, 1995, National Renewable Energy Laboratory.

[3.26] F.P. Incropera, D.P. DeWitt, Fundamentals of Heat and Mass Transfer, Sixth ed., John Wiley & Sons, New York, 2007, pp. 518-521.

[3.27] H.J. Steeman, C. T'Joen, M. Van Belleghem, A. Janssens, M. De Paepe, Evaluation of the different definitions of the convective mass transfer coefficientfor water evaporation into air, International Journal of Heat and Mass Transfer 52 (2009) 3757-3766.

[3.28] L.Z. Zhang, C.H. Liang, L-X Pei, Conjugate heat and mass transfer in membrane-formed channels in all entry regions. International Journal of Heat Mass Transfer 53 (2010) 815-824.

[3.29] L.Z. Zhang, Heat and mass transfer in a cross flow membrane-based enthalpy exchanger under naturally formed boundary conditions. International Journal of Heat Mass Transfer 50 (2007) 151-162.

[3.30] S.M. Huang, L.Z. Zhang, K. Tang, L-X Pei, Fluid flow and heat mass transfer in membrane parallel-plates channels used for liquid desiccant air dehumidification, International Journal of Heat Mass Transfer 55 (2012) 2571-2580.

[3.31] L.Z. Zhang, S.M. Huang, Coupled heat and mass transfer in a counter flow hollow fiber membrane module for air humidification, International Journal of Heat Mass Transfer, 54 (2011) 1055-1063.

[3.32] C.R. Iskra, C.J. Simonson, Convective mass transfer coefficient for a hydrodynamically developed airflow in a short rectangular duct, International Journal of Heat and Mass Transfer 50 (2007) 2376-2393.

[3.33] K. Mahmud, G.I. Mahmood, C.J. Simonson, R.W. Besant, Performance testing of a counter-cross-flow run-around membrane energy exchanger (RAMEE) system for HVAC applications, Energy and Buildings 42 (2010) 1139-1147.

[3.34] K. Mahmud, Design and performance testing of counter-cross-flow run-around membrane energy exchanger system, M.Sc. thesis, University of Saskatchewan, Saskatoon, SK, 2009.

[3.35] H.B. Hemingson, C.J. Simonson, R.W. Besant, Effects of non-uniform channels on the performance of a run-around membrane energy exchanger (RAMEE), Proceedings of the 12th International Conference on Air Distributions in Rooms (Roomvent 2011), Trondheim, Norway, June 19-22, 2011 (8 pages).

[3.36] P.P. LePoudre, C.J. Simonson, R.W. Besant, Channel flow with sinusoidal screen insert, Proceedings of the 19th Annual Conference of the CFD Society of Canada (CFDSC 2011), Montreal, April 27-29, 2011 (6 pages).

[3.37] M. Rasouli, S. Akbari, H. Hemingson, R.W. Besant, and C.J. Simonson, Application of a run-around membrane energy exchanger in an office building HVAC system, ASHRAE Transactions, 117(2), (2011), 686-703.

[3.38] M. Rasouli, S. Akbari, C. J. Simonson, R. W. Besant, Energetic, Economics and environmental analysis of a health-care facility HVAC system equipped with a run-around membrane energy exchanger, Manuscript submitted for publication (2010).

[3.39] M. Seyed Ahmadi, Modeling the Transient Behaviour of a Run-around Heat and Moisture Exchanger System, M.Sc. thesis, University of Saskatchewan, Saskatoon, SK, 2008.

[3.40] AHRI. 2005. ANSI/ARI Standard 1060, Standard for Rating Air-to-Air Exchangers for Energy Recovery Ventilation Equipment. Arlington, VA: Air-Conditioning & Refrigeration Institute.

[3.41] B. Erb, Run-around membrane energy exchanger performance and operational control strategies, M.Sc. thesis, University of Saskatchewan, Saskatoon, SK, 2009.

[3.42] I. Dincer, M.A Rosen, Thermal energy storage systems and applications, 2nd edition, John Wiley, New York, 2011.

[3.43] B. Zalba, J.M. Marín, L.F. Cabeza, H. Mehling, Review on thermal energy storage with phase change: materials, heat transfer analysis and applications, Applied Thermal Engineering 23 (2003) 251-283

[3.44] R.S. Briggs, R.G. Lucas, T.Z. Todd, Climate classification for building energy codes and standards: Part 2 - Zone definitions, maps, and comparisons, ASHRAE Transactions 109 (2003) 122-130.

[3.45] K. Levenberg, A method for the solution of certain problems in least squares, Quarterly of Applied Mathematics 2 (1944) 164-168.

[3.46] D. Marquardt, An algorithm for least-squares estimation of nonlinear parameters, SIAM Journal of Applied Mathematics 11 (1963) 431-441.

[3.47] L. Prechelt, Early stopping--But when?, in Orr and Mueller (1998), 55-69.

CHAPTER 4

APPLICATION OF A RAMEE IN A HEALTH-CARE FACILITY HVAC SYSTEM

4.1. Overview of Chapter 4

This chapter shows an example of a practical application of the neural network (NN) model presented in chapter 2. A health-care facility HVAC system which benefits from a RAMEE is investigated. After an overview of previous research on RAMEE (sections 4.3 and 4.5.1 and 4.5.2), a summary of the strategies to control the RAMEE in different conditions (section 4.5.2) is presented. Then using the optimal control of ERV (presented in Appendix A), a definition for the optimal effectiveness of RAMEE for each hour is provided. These hourly optimal effectiveness definitions are met using an optimization algorithm (implemented in MATLAB® version 7.10.0) which runs the NN models as the function that needs to be optimized to obtain the optimal effectiveness values for each hour. A hospital building, the RAMEE and the HVAC system are simulated in TRNSYS and then the optimal effectiveness values are used to calculate the effect of an optimally controlled RAMEE on:

1. Cooling and heating energy consumption,
2. HVAC equipment capacity,
3. Life-cycle cost of the HVAC system, and
4. Greenhouse gas emissions

The results from a similar study for an office building (Appendix A) and the hospital described in this chapter are compared in section 4.6.5.

The contributions of each author to this research work are as follows:

Mohammad Rasouli, M.Sc. student and main author, simulated the hospital building and the HVAC system in TRNSYS, post-processed the results to provide most of the figures and data in the article, and wrote the first draft of manuscript # 3.

Soheil Akbari, M.Sc. student, developed steady-state NN models, determined the optimum effectiveness of the RAMME for different operating conditions by implementing the definitions of the RAMEE optimum operation (provided by the main author) on NN outputs. This optimal effectiveness values were needed for TRNSYS simulations and energy calculation purposes (Figures 4.4 and 4.5).

Carey J. Simonson, and **Robert W. Besant**, the research group supervisors, conceived the research study, read and edited the paper and improved this study with their valuable comments.

MANUSCRIPT #3

Energetic, economics and environmental analysis of a health-care facility hvac system equipped with a run-around membrane energy exchanger

M. Rasouli, S. Akbari, C.J. Simonson and R.W. Besant

4.2. Abstract

Run-Around Membrane Energy Exchanger (RAMEE) is a novel heat and moisture recovery system that consists of two separate supply and exhaust exchangers coupled with an aqueous salt solution flow. The salt solution transfers energy (heat and moisture) in a closed loop between outdoor ventilation air and the exhaust air from buildings. The system performance is a function of the flow rate of the salt solution and ventilation air and the outdoor air conditions. The dependency of system performance on the solution flow rate and the outdoor conditions requires adjustment of the appropriate flow rate which gives the optimal system performance at any specific outdoor condition. In this paper, the RAMEE is simulated for a hospital building in four different climates using TRNSYS and MATLAB computer programs. The steady-state RAMEE can reduce the annual heating energy by 60% in cold climates and annual cooling energy by 15% to 20% in hot climates. The RAMEE has an immediate payback in cold climates and a 1 to 3-year payback in hot climates depending on the pressure drop across the exchangers. Finally, the RAMEE reduces greenhouse gas emission (CO_2- equivalent) by 25% and 10% in cold climates and hot climates, respectively.

4.3. Introduction

Energy Recovery Ventilators (ERVs) have been widely used to reduce the energy required to condition the ventilation air. ERVs transfer heat (heat recovery systems) or heat and moisture (energy recovery systems) between conditioned

exhaust air and outdoor ventilation air. Heat pipes, fixed-plate heat exchangers and heat wheels are examples of the heat recovery systems, and energy wheels coated with desiccant [4.1] and flat-plate exchangers made of water permeable membranes [4.2] are examples of energy recovery systems. The main disadvantage of present ERVs is that some are unable to transfer moisture. Also, they all require a side-by-side installation of the supply and exhaust ducts. This may impose a higher ducting cost for adjacent installation of the supply and exhaust ducts. Adjacent air inlet and exhaust increases the probability of contaminant transfer from exhaust air to the supply air, especially for polluted spaces (e.g., some laboratories) and highly-sensitive areas (e.g., surgery room).

A novel Run-Around Membrane Energy Exchanger (RAMEE) that consists of two separate supply and exhaust exchangers was presented by Fan et al. [4.3]. For this system, each exchanger is a flat-plate energy exchanger constructed with water vapor permeable membranes that allow the transfer of heat and water vapor. Such a system is suitable for retrofitting buildings even where the supply and exhaust ducts are not adjacent. Research has been done on (a) developing numerical models of the RAMEE [4.4-4.8] (b) predicting the system performance at different conditions using an artificial neural network [4.9] (c) investigating the crystallization risk of the salt solution [4.10] and (d) obtaining experimental data on RAMEE performance for two prototypes [4.11-4.12].

ASHRAE Standard 170-2008 [4.13], ventilation of health-care facilities, has recommended much higher rates of outdoor air flow compared to ASHRAE 62-2010 [4.14] for ventilation rates of other types of buildings. For example, a typical office building may require about 0.5 ACH ventilation air [4.15], while a minimum outdoor air change of 2 to 6 ACH is recommended for health-care facilities. The energy

consumption due to conditioning of ventilation air increases as the ventilation rate increases [4.16-4.18]. For instance, McDowell et al. [4.16] showed that, without energy recovery, increasing the ventilation rate of a building in Washington D.C. from 0 to 10 l/s.person (corresponding to about 0.37 ACH) increases the annual energy consumption of the HVAC system by 14%. This result is in a good agreement with Commercial Building Energy Consumption Survey (CBECS) in 2003 [4.19] that reported that health-care facilities were the second highest energy-intense commercial buildings with 1472 MJ/ m^2.year HVAC system energy consumption. This is 2.8 times higher than the average HVAC energy consumption in US office buildings (i.e., 533 MJ/m^2.year) [4.19]. Although the ventilation energy is very significant in hospitals, most of the recent research has focused on energy-saving technologies in office spaces, residential buildings and educational facilities. Rasouli et al. [4.20] studied the application of a RAMEE in an office building HVAC system. The TRNSYS simulation of the RAMEE showed savings of about 30 to 40% for heating energy in cold climates (Saskatoon and Chicago) and 8 to 15% for cooling energy in hot climates (Miami and Phoenix). This paper presents the energy saving with a RAMEE for a hospital building (as the second case study of the RAMEE). An overview of the RAMEE is presented and the findings of Rasouli et al. [4.20] regarding the control and operation of the RAMEE are implemented when it operates in a hospital building. This paper presents the energy savings, Life-Cycle Cost (LCC) analysis and Life Cycle Environmental Assessment (LCEA) of the RAMEE in the hospital over a 15-year life-cycle for four different climates.

4.4. Model Description

A 3-storey hospital with total floor area of 3150 m^2 is chosen for this study. The thermal resistances of walls, roof and the floor are 2.72, 3.64 and 3.45

(m^2.K/W), respectively. The building has double-glazed windows, about 31 (W/m^2) of internal heat gains (includes lighting, cooking and equipment loads based on CBECS data, [4.19]) and an occupant density of 5 People/100 m^2. A variable air volume HVAC system is considered for the building that maintains the indoor temperature within ASHRAE comfort zone (i.e., 24°C in summer and 22°C in winter [4.21]), and the indoor humidity below 60% RH. The day-time (6:00-22:00) ventilation rate is set at 2 ACH as an average rate recommended by ASHRAE ventilation standard for different spaces in health-care facilities [4.13] and is reduced to 1.3 ACH for the rest of the day (22:00-6:00) when a lower occupancy is expected. A total air change rate of 3 times the ventilation rate is always maintained for the space (as recommended by ASHRAE for most of health-care spaces [4.13]).

The building is simulated in Saskatoon (Saskatchewan, Canada), Chicago (Illinois), Miami (Florida) and Phoenix (Arizona) as the four North American cities which represent different climatic conditions. Chicago, Miami and Phoenix are chosen as representatives of cool-humid, hot-humid and hot-dry climates, respectively, based on Briggs et al. [4.22] climatic classifications for building energy analysis. Saskatoon is chosen to represent a cold climate because heating is required for a large fraction of a year [4.20].

4.5. Run-Around Membrane Energy Exchanger (RAMEE)

4.5.1. Overview

Figure 4.1 schematically presents a HVAC system equipped with a RAMEE. The RAMEE shown in Figure 4.1 consists of two separate exchangers located in supply and exhaust ducts. Each exchanger is a flat-plate, liquid-to-air membrane energy exchanger (LAMEE) that is made using water vapor permeable membranes.

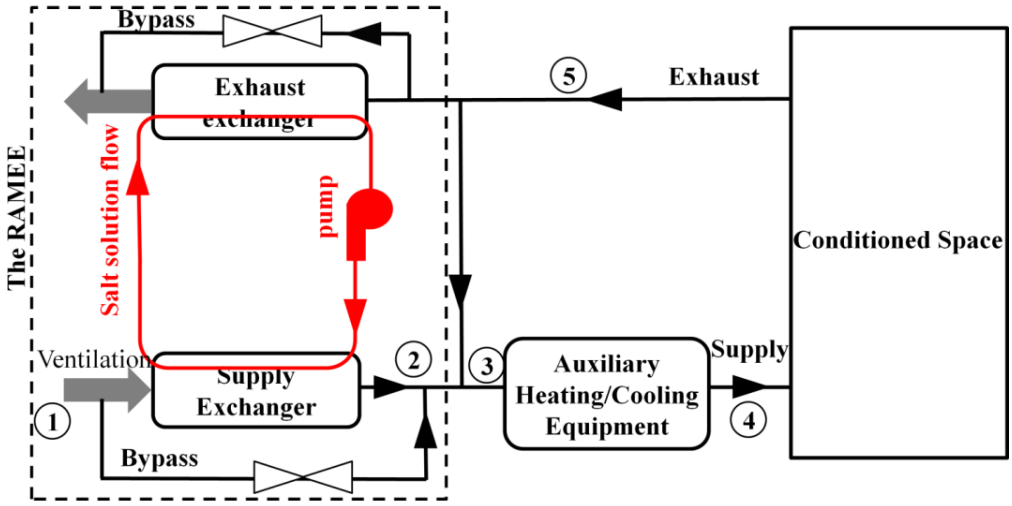

Figure 4.1. Schematic view of a HVAC system equipped with a RAMEE.

The LAMEEs are coupled with an aqueous salt solution that is pumped in a closed loop and transfers both heat and moisture between the exhaust and ventilation airstreams. Such a design has the capability of transferring both heat and moisture in new and retrofit applications where the ducts are not adjacent.

During the winter, the mixture of outdoor ventilation air and the return air is heated by the heating system up to the desired supply temperature. In the absence of the RAMEE, the ventilation air temperature is equal to the outdoor temperature. But, the RAMEE transfers energy (heat and moisture) from the exhaust air to the supply air. Such an energy transfer increases the ventilation air temperature and consequently lowers the energy consumption of the heating system. During the summer, the mixture of outdoor ventilation air and the return is cooled and also dehumidified if the humidity of the mixture (state 3) is unable to maintain the indoor humidity within comfort zone (i.e., below 60% RH; [4.21]). The operation of the RAMEE in summer transfers heat and moisture from warm-humid outdoor air to the cool-dry exhaust air. This reduces the enthalpy of the ventilation air and consequently decreases the cooling energy for the auxiliary cooling system. The air and salt solution can flow in counter flow, cross flow or counter/cross flow

arrangements through each LAMEE. A counter flow RAMEE is studied in this paper.

4.5.2. System Performance, Controls and Operation

The effectiveness of a RAMEE for transferring heat (ε_s), moisture (ε_l) and enthalpy (ε_t) is mainly a function of three dimensionless groups defined in Equations 4.4 to 4.6, indoor and outdoor air conditions and the air/salt solution flow arrangement. Figure 4.2 illustrates the dependency of RAMEE effectiveness on *NTU*, *Cr** and outdoor conditions for some specific conditions.

$$\varepsilon_s = \frac{T_1 - T_2}{T_1 - T_5} \tag{4.1}$$

$$\varepsilon_l = \frac{W_1 - W_2}{W_1 - W_5} \tag{4.2}$$

$$\varepsilon_t = \frac{h_1 - h_2}{h_1 - h_5} \tag{4.3}$$

$$NTU = \frac{UA}{\dot{m}_{air} C_{p,air}} \tag{4.4}$$

$$NTU_m = \frac{U^{'} A}{\dot{m}_{air}} \tag{4.5}$$

$$Cr^* = \frac{\dot{m}_{sol} C_{p,sol}}{\dot{m}_{air} C_{p,air}} \tag{4.6}$$

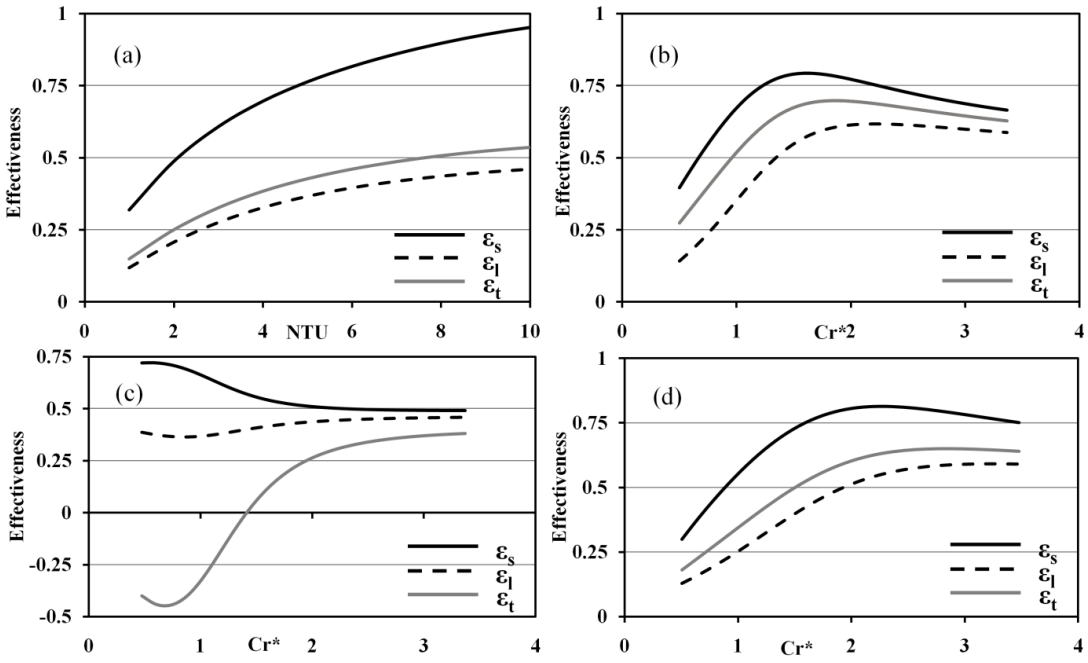

Figure 4.2. RAMEE effectiveness (a) as a function of *NTU* at Cr*=2, and as a function of *Cr and outdoor air conditions at (b) cold, (c) hot-low enthalpy and (d) hot-high enthalpy outdoor conditions with *NTU*=10.**

Similar to the other types of ERVs, *NTU* is directly proportional to the surface area or the size of the RAMEE. Hemingson et al. [4.8] showed that RAMEE effectiveness increases with *NTU* (as shown in Figure 4.2a) and follows a similar trend expected by other references [4.23-4.24]. By increasing *NTU*, the sensible effectiveness increases significantly and the latent effectiveness increases slightly. Also, a considerable increase in latent effectiveness may be obtained by increasing NTU_m to a larger value. A design *NTU* of 10 may be feasible for ERVs [4.25] therefore, it is used for this study. As well, *NTU* will increase when the night-time ventilation rate is lower than the day-time.

Hemingson [4.7] found that the variation of indoor conditions between the heating and cooling indoor set-points has a minimal impact on the RAMEE effectiveness, and may change the total effectiveness by 0.3%. But, the dependency of RAMEE effectiveness on outdoor air conditions is more significant which is due to the impact that the outdoor temperature and humidity have on the liquid desiccant

and the fact that heat and moisture transfer are coupled in the RAMEE [4.8]. A greater temperature difference between outdoor and indoor air (either summer or winter) improves the RAMEE moisture transfer. Also, the RAMEE heat transfer increases as the humidity ratio difference between indoor and outdoor air increases. Figures 4.2b, 4.2c and 4.2d present the RAMEE effectiveness as a function of Cr* in different outdoor conditions and *NTU*=10. As shown in these figures, the *Cr** at which the peak effectiveness is achieved (Cr^*_{opt}) varies depending on the outdoor conditions. Therefore, at any given outdoor condition, the *Cr** should be controlled so that the maximum effectiveness is achieved. Rasouli et al. [4.20] studied the operation of the RAMEE in different outdoor conditions in an office building and showed that the strategy of controlling the Cr^*_{opt} depends on RAMEE's operating condition (heating, cooling and part-load operation). Figure 4.3 presents the TMY operating conditions of the RAMEE for one year in different locations.

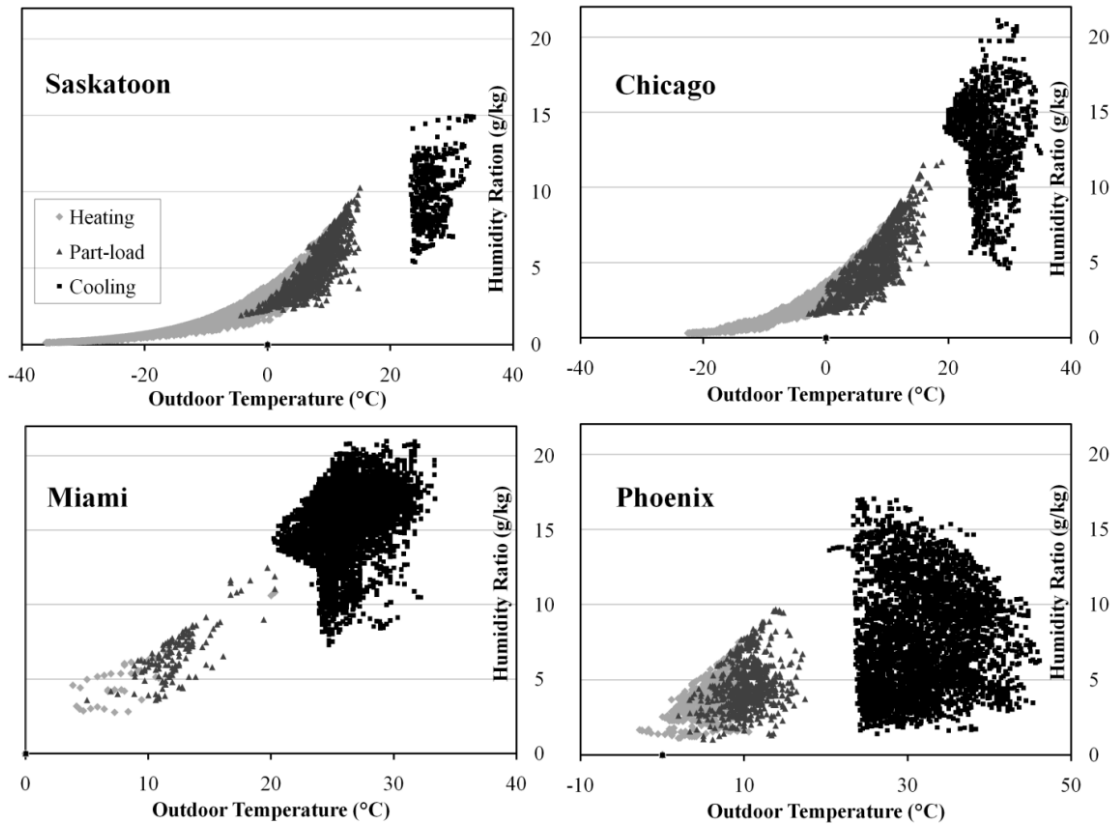

Figure 4.3. Operating conditions of the RAMEE for different locations for the hospital building in one year.

As an explanation of Figure 4.3, the RAMEE heats the ventilation air in a full-load or part-load operation for low outdoor temperatures. The RAMEE should be off or by-passed when the building needs cooling while both outdoor temperature and enthalpy are lower than that of the indoor air [4.26]. The operation of RAMEE in such conditions heats and humidifies the cool outdoor air and increases the cooling energy consumption. When either the outdoor temperature or the outdoor enthalpy is greater than that of the indoor air, the RAMEE should be operated to reduce the temperature or the enthalpy of the ventilation air. Rasouli et al. [4.20] found that in order to optimize the operation of the RAMEE, the Cr* needs to be controlled under a different strategy as the RAMEE's operating condition changes. Table 4.1 summarizes the required control strategy to achieve optimal performance of the RAMEE.

Table 4.1. *Cr control strategy and definitions of Cr^*_{opt} for optimal performance of the RAMEE for different steady-state operating conditions.**

RAMEE's operating condition	Heating	Cooling ($h_{out}>h_{in}$)	Cooling ($h_{out}<h_{in}$)	Part-load
Cr^*_{opt} is the Cr^* at which:	ε_s is maximum	ε_t is maximum and positive	ε_t is minimum and negative	ε_s is maximum and bypass fraction of : $R = \frac{\dot{m}_{bypass}}{\dot{m}_{ventilation}} = 1 - \frac{T_4 - T_1}{\varepsilon_s(T_5 - T_1)}$

The numerical solution of heat and mass transfer in the RAMEE for steady-state operation was developed in previous research [4.3], [4.6], and [4.8]. Based on the numerical solution of the counter flow RAMEE, Akbari et al. [4.9] developed an optimization Artificial Neural Network (ANN) using MATLAB 2010 neural network toolbox. For given RAMEE operating condition, *NTU* and indoor and outdoor conditions, the ANN is able to predict the Cr^*_{opt} and the associated effectivenesses. Figure 4.4 shows the variation of hourly Cr^*_{opt} during a TMY of operation of the RAMEE in each location. *Cr** of zero refers to RAMEE's being off operation that means the conditions specified in Table 4.1 are not satisfied.

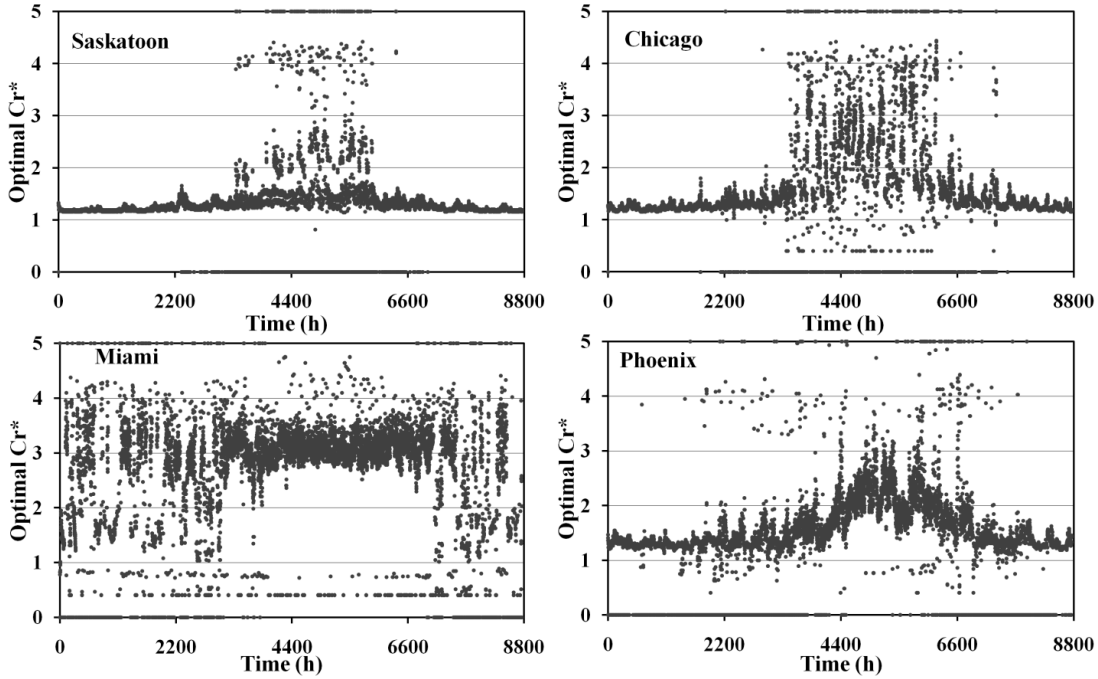

Figure 4.4 Yearly variation of the hourly *Cr for optimal operation of the RAMEE.**

Figure 4.4 shows less scatter variation of Cr^*_{opt} during the winter compared to the summer. For all climates (except for Miami), the Cr^*_{opt} varies between 1.2 and 1.3 during the heating season, and increases up to 4 during the summer. It should be noted that Cr^* is a function of ventilation rate and salt solution flow rate (Equation 4.6). Since the air flow rate is typically set based on minimum standard ventilation requirement, the solution flow rate remains the controllable variable to achieve Cr^*_{opt}.

As mentioned previously, the effectiveness of the RAMEE depends on the outdoor/indoor air conditions, the operating Cr^* and the ventilation air flow rate. All these variables (except for *NTU* that switches between day-time and night-time values) show scatter during a year which may results in a variation of the effectiveness. The ANN can determine the effectiveness of the RAMEE based on the specified outdoor conditions (Figure 4.3), indoor conditions (ASHRAE [4.21]) and operating Cr^* (Figure 4.4). Figure 4.5 shows the variation of sensible and latent effectiveness for different locations for one typical year. The effectiveness values are bounded between 0 and 1 in Figure 4.5. However, the effectiveness of RAMEE may exceed 100% at specific operating conditions. These mostly occur when the energy transfer via the RAMEE is not very significant [4.7].

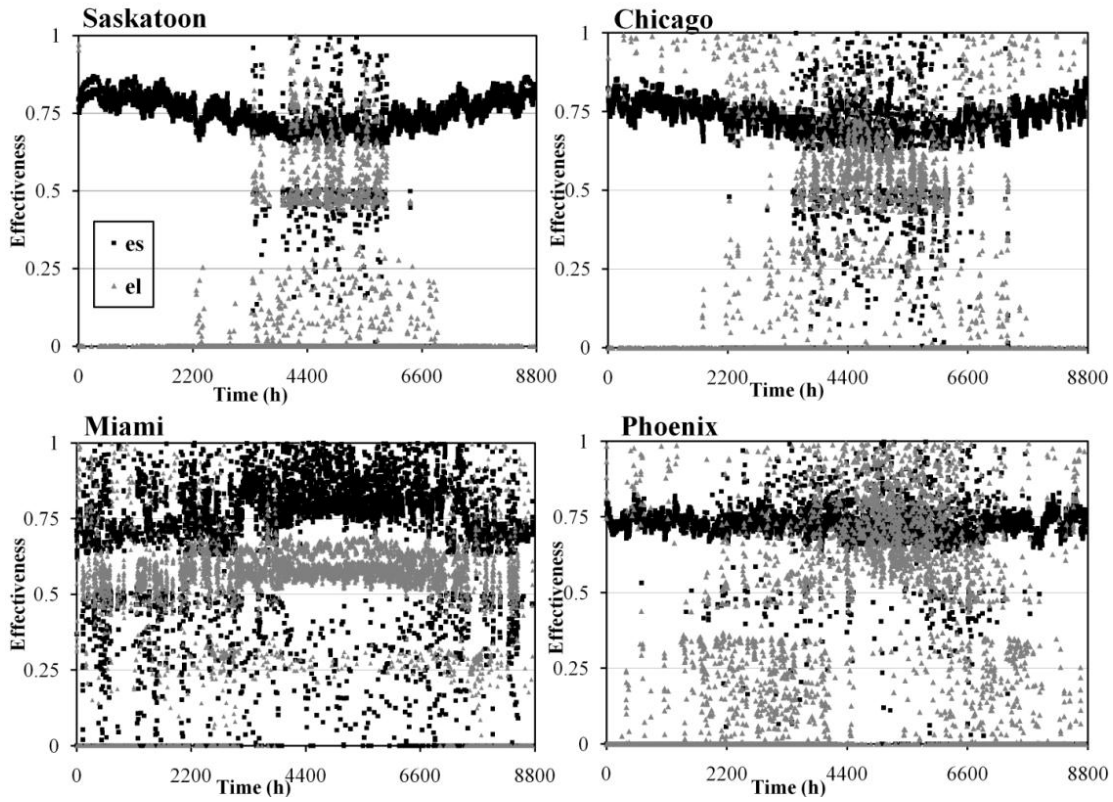

Figure 4.5 Variation of the RAMEE steady-state sensible and latent effectiveness for a TMY in different locations ($Cr^*=Cr^*_{opt}$).

The hourly effectiveness values are inputs to the TRNSYS [4.27] model of the RAMEE. The thermal system (including the HVAC system, RAMEE and the building) is simulated using the TRNSYS building energy simulation program equipped with TESS libraries (Thornton et al. [4.28]).

In order to quantify an average operating effectiveness for the RAMEE, the hourly effectiveness values are weighted by the associated hourly net energy transfer via the RAMEE. Table 4.2 presents the average sensible and latent effectiveness of the RAMEE throughout a year in different locations.

Table 4.2. Average sensible and latent effectiveness of the RAMEE.

Location	Saskatoon	Chicago	Miami	Phoenix
Average sensible effectiveness	0.78	0.76	0.86	0.73
Average latent effectiveness	0.70	0.59	0.59	0.58

4.6. Results

In this section, the following assumptions are made regarding the RAMEE and the HVAC system unless otherwise stated: The HVAC system consists of a gas-fired boiler with efficiency of 88% and a direct-expansion water chiller with a COP of 3 which satisfies ASHRAE Standard 90.1-2004 minimum boiler efficiency of 80% and chiller COP of 2.78 [4.29]. Fan efficiency is assumed to be 60% and air pressure drop of the HVAC system and each LAMEE are assumed to be 10 cm and 2 cm of water, respectively. The RAMEE operates under hourly Cr^*_{opt} and design *NTU* of 10.

4.6.1. Energy

Figure 4.6 shows the simulation results for the impact of RAMEE on annual heating and cooling energy consumption in the hospital compared to the case of no energy recovery. The RAMEE saves 58%, 66%, 90% and 83% of annual heating energy in Saskatoon, Chicago, Miami and Phoenix, respectively. Also, it saves 4%, 10%, 18% and 15% of the annual cooling energy in Saskatoon, Chicago, Miami and Phoenix, respectively. The cooling energy saved in cold climate (Saskatoon and Chicago) is not very significant since the internal loads (not the ventilation load) account for the larger portion of the cooling load.

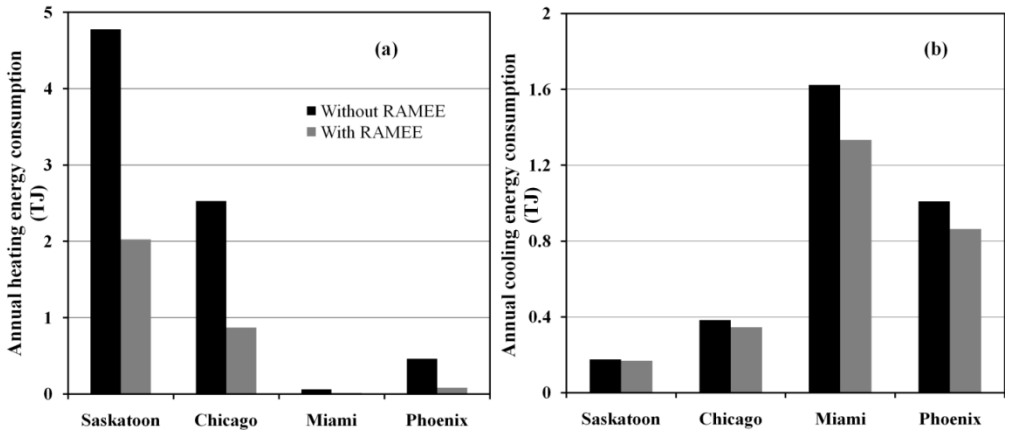

Figure 4.6. The impact of RAMEE on annual energy consumption for (a) heating and (b) cooling.

Figure 4.7 presents the impact of the RAMEE on the size of HVAC equipment compared to the case of no energy recovery. The size of heating equipment can be reduced by about 45% in cold climates and 65% in hot climates. Also, the cooling system can be downsized by about 25% in all climates.

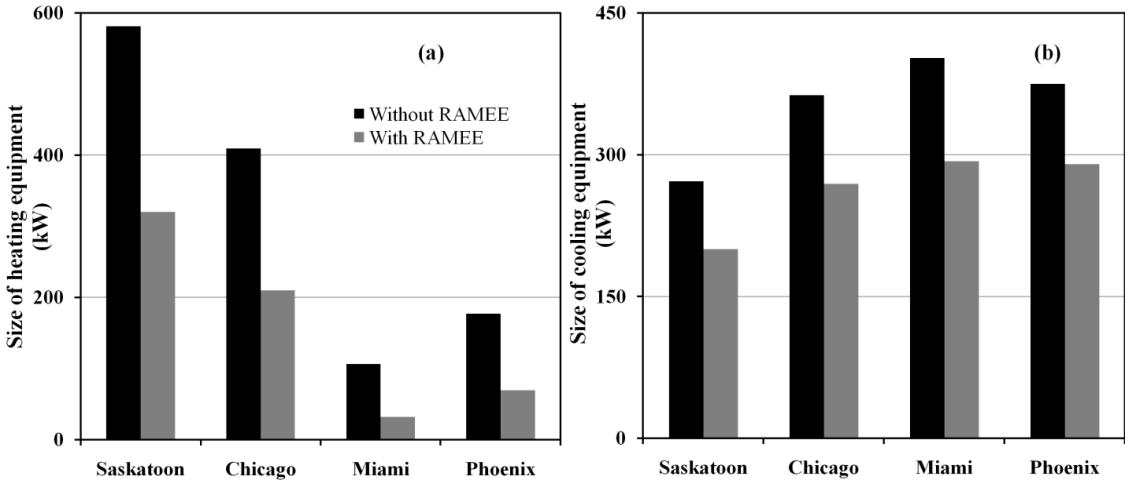

Figure 4.7. The impact of RAMEE on the capacity of HVAC equipment for (a) heating and (b) cooling.

CBECS reported inpatient health-care facilities to have the second highest energy intensity among US commercial buildings with an average total energy intensity of 2830 (MJ/m^2.year) in 2003. The HVAC system energy consumption accounted for 52% of the total energy use which gives an average HVAC energy intensity of 1472 MJ/m^2.year. Thus the HVAC energy intensity of inpatient health-care facilities was much higher than the total energy intensity of educational facilities (944 MJ/m^2.year) or office buildings (1055 MJ/m^2.year). In this research, the HVAC system for the studied hospital has an energy intensity of 1730, 1100, 739 and 672 MJ/m^2.year with no energy recovery in Saskatoon, Chicago, Miami and Phoenix, respectively (giving an average of 1060 MJ/m^2.year). By employing the RAMEE, the total energy intensities will be reduced by 48%, 45%, 8% and 17% in Saskatoon, Chicago, Miami and Phoenix, respectively.

It should be noted that the underestimating of annual energy consumption using the computer simulation (compared to CBECS reported values) might be mostly due to the energy-saving envelope (well-insulated walls and roofs and double-glazed windows) considered for the simulated building compared to the data obtained from the US office building categorization. In addition, the following assumptions are made for this research which may cause underestimation of energy consumption in computer simulation compared to real buildings: (1) high-efficiency heating and cooling systems (combustion efficiency of 88% and chiller COP of 3), (2) zero heat loss and leakage from equipment and ducting, and (3) running a VAV HVAC system in the building (instead of a less-efficient CAV system; Yao et al. [4.31]).

4.6.2. Control based on an Operating Averaged *Cr**

As discussed in section 4.5.2, the optimal operation of the RAMEE requires an accurate control of the salt solution flow rate (giving the Cr^*_{opt}). Rasouli et al. [4.20] showed that the RAMEE may be operated in an office building using an average seasonal or yearly *Cr** value with no significant impact on energy savings (i.e., less than 2% for most climates). The advantage of operating the RAMEE using an average *Cr** is that there is no need for an accurate control of salt solution flow rate for each slight change of outdoor condition. In this section, the impact of applying an average seasonal or yearly *Cr** value on energy saving with the RAMEE in the hospital is studied. Table 4.3 shows the seasonal and yearly averaged *Cr** weighted by hourly energy transfer via the RAMEE and the associated standard deviation. Table 4.4 presents the annual cooling and heating energy savings when the RAMEE system operates under specified average *Cr** values.

Table 4.3. Seasonal and yearly weighted average Cr* and associated standard deviation for the hospital building.

	Seasonal average *Cr**		Yearly average *Cr**
Location	**Winter (heating)**	**Summer (cooling)**	**Heating and cooling**
Saskatoon	1.21±0.09	2.25±0.35	1.22±0.53
Chicago	1.26±0.12	2.78±0.42	1.37±0.70
Miami	1.52±0.28	3.07±0.52	2.99±0.71
Phoenix	1.31±0.13	1.88±0.47	1.64±0.55

Table 4.4. Annual energy saved with the RAMEE system operating with selected *Cr values.**

	Annual heating energy saved			Annual cooling energy saved		
Location	**Optimal *Cr****	**Seasonal *Cr****	**Yearly *Cr****	**Optimal *Cr****	**Seasonal *Cr****	**Yearly *Cr****
Saskatoon	58%	58%	58%	4%	4%	3%
Chicago	66%	66%	65%	10%	9%	7%
Miami	90%	90%	83%	18%	18%	18%
Phoenix	83%	83%	81%	15%	14%	14%

Compared to using the optimal *Cr**, the results in Table 4.4 show that the energy savings slightly reduce by using a yearly average *Cr**, however the reduction in energy savings is negligible with the averaged seasonal *Cr** values. The RAMEE may operate under seasonal or yearly average *Cr** with no significant loss of energy.

4.6.3. Life Cycle Cost (LCC) Analysis

LCC analysis is known as a very good measure to evaluate and compare different available alternatives in terms of expenses associated with each system during the life-cycle. The life-cycle of a system includes its production, operation, demolition and disposal. The two alternative systems in this research are: (1) A VAV HVAC system that is not equipped with any energy recovery systems, and (2) A VAV HVAC system that is equipped with the RAMEE. The cost analysis is conducted over a 15-year life-cycle for both systems. For this LCC study, only those expenses that are not equal for the two alternatives need to be considered. These costs can be categorized as capital costs, that have to be invested before the project

begins to operate, and operational costs that include all the expenses during the operation of the system (i.e., maintenance and energy).

The capital costs include the cost of the HVAC system that consists of a cast-iron gas-fired boiler ($68.3/kW), a direct expansion water chiller ($227/kW) and Centrifugal type HVAC fans ($851/m^3/s). These costs are based on RSMeans Mechanical Cost Data 2010 (Mossman et al. [4.31]). The cost of the RAMEE, as an ERV, is considered to be $3/CFM ($6357/m^3/s) as recommended by technical papers in the field of air-to-air energy exchangers [4.32-4.33]. Also, a zero residual value is assumed as the worth of the HVAC system at the end of its life-cycle. The operational costs include the cost of the energy consumed by the heating/cooling equipment and the fans and the maintenance cost. Assuming equal maintenance costs for both alternatives, the operational cost will only include the cost of energy. The energy rates may vary depending on the location and the energy source. In this study, natural gas and electricity are assumed to be those for the energy sources for heating and cooling, respectively. The gas-fired boiler using natural gas produces combustion heat at 37.8 MJ/m^3 [4.34]. Figure 4.8 presents the comparison of capital costs and operational costs for the two alternatives.

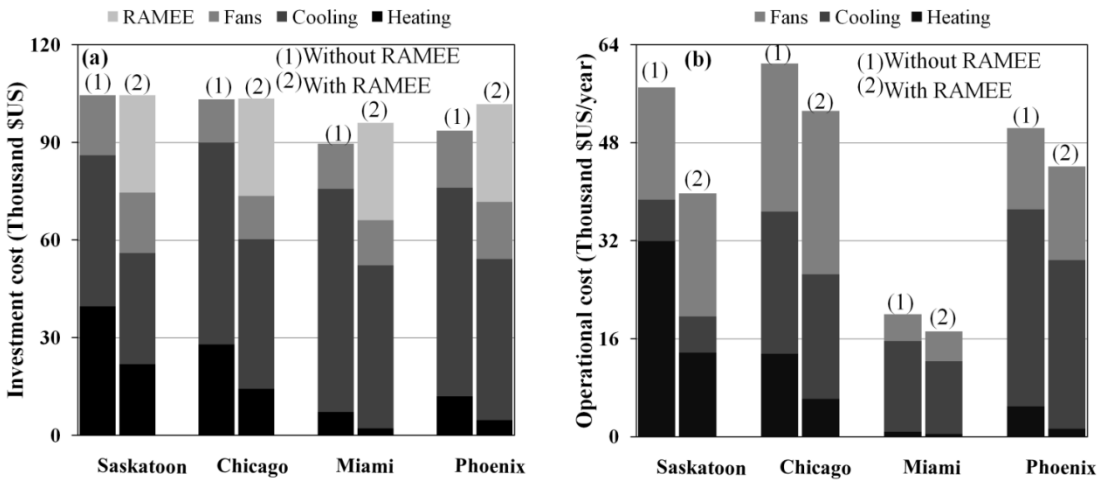

Figure 4.8 Life-cycle cost analysis results (a) capital costs and (b) operational costs for the HVAC system (1) without the RAMEE and (2) with the RAMEE.

It can be seen in Figure 4.8a that the RAMEE can be purchased at no net extra cost for cold climates (Saskatoon and Chicago) due to the money saved by downsizing the heating/cooling equipment. This means that the payback of the RAMEE in cold climate is instant (immediate payback) and the energy savings during the RAMEE's life-cycle are achieved with no extra investment. On the other hand, an HVAC system equipped with a RAMEE has a higher capital cost in hot climates (Miami and Phoenix shown in Figure 4.8a). The operational cost of the RAMEE depends on air pressure drop across each LAMEE. Figure 4.8b is plotted based on air pressure drop of 2 cm of water across each LAMEE. Increasing the RAMEE's pressure drop decreases the energy savings of the RAMEE due to higher fan energy. In cold climates (Saskatoon and Chicago), increasing the LAMEE's pressure drop reduces the energy saved, but the payback period will remain zero for air pressure drops within 0 to 5 cm of water across each LAMEE (expected range by manufacturer). On the other hand, increasing the LAMEE's pressure drop increases the payback period in hot climates (Miami and Phoenix). Figure 4.9 presents the payback period of the RAMEE in Miami and Phoenix as a function of the pressure drop across each LAMEE.

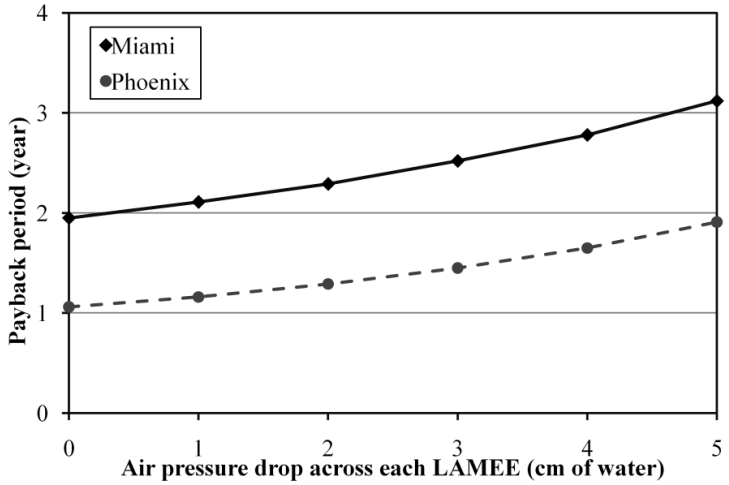

Figure 4.9. Payback period of the RAMEE in Miami and Phoenix as a function of pressure drop across each LAMEE.

Based on the results presented in Figure 4.9, the RAMEE system will have a payback period of 1-2 years in Phoenix and 2-3 years in Miami. Table 4.5 summarizes the life cycle cost (including investment and operation costs) of two alternative systems over 15 years of operation assuming 2 cm of water pressure drop across each LAMEE.

Table 4.5. LCC (including capital and operational costs) of the two HVAC system alternatives for a 15-year life-cycle.

	Saskatoon	Chicago	Miami	Phoenix
Without RAMEE (Thousands of $US)	961	1018	389	850
With RAMEE (Thousands $US)	701	901	354	763
% saving	27%	11%	9%	10%

4.6.4. Life Cycle Environmental Assessment (LCEA)

Similar to the life cycle cost analysis that addresses the expenses associated with a project during its life-cycle (including production, operation and disposal), life cycle environmental assessment (LCEA) deals with the impact of a system on the environment. Both approaches are similar in that they study the system over its life cycle rather than making a decision based on just the capital cost; however, they are different in their measuring metrics (i.e., money for LCC and environment for LCEA [4.35]). In this paper, the environmental impact of the two systems, i.e. VAV HVAC systems with and without the RAMEE on greenhouse gas emissions and climate change is studied. The tons of CO_2- equivalent emission is used to represent the climate change since CO_2 is the main greenhouse gas.

The mass of greenhouse gases emitted during the combustion of natural gas depends on the fuel composition and this may vary slightly from location to location. However, an average value is used for both US and Canada based on the data obtained from Canada's Clean and Renewable Energy Research Centre [4.36]. On the other hand, due to the variety of resources that different utilities use to generate electricity (e.g., hydro, nuclear, fossil fuel, etc.), the greenhouse gas emissions due to

electricity consumption varies dramatically for different locations. Table 4.6 presents the amount of emitted greenhouse gases associated with consuming natural gas and electricity in the different locations studied in this paper. Data obtained from Canada's Clean and Renewable Energy Research Centre [4.36] and US Environmental Protection Agency [4.37] are used to produce the results shown in this table. CO_2-equivalent is calculated using weighting factors (also called Global Warming Potential, GWP) of CO_2, N_2O and CH_4 as 1, 310 and 21, respectively [4.36].

Table 4.6. The greenhouse gas emission due to electricity and natural gas consumption in different locations.

	Natural gas				**Electricity**			
Location	CO_2 (t/TJ)	N_2O (kg/TJ)	CH_4 (kg/TJ)	**CO_2-equivalent (t/TJ)**	CO_2 (t/TJ)	N_2O (kg/TJ)	CH_4 (kg/TJ)	**CO_2-equivalent (t/TJ)**
Saskatoon	49.68	0.52	1.1	**49.86**	-	-	-	**234**
Chicago	49.68	0.52	1.1	**49.86**	194	3.2	2.3	**195.04**
Miami	49.68	0.52	1.1	**49.86**	166	2.1	5.8	**166.77**
Phoenix	49.68	0.52	1.1	**49.86**	165	2.3	2.2	**165.76**

Nyman and Simonson [4.35] studied the LCA of air-handling units with and without energy recovery systems and found that the emission of greenhouse gases during their operation in a 20-year life-cycle was typically 20 to 40 times greater than the emissions occurred during the manufacturing process of the units. Therefore, the LCA in this paper takes the environmental impacts of the systems during the operation only. Figure 4.10 compares the annual equivalent CO_2 emission by the HVAC system with and without the RAMEE for the hospital in different locations.

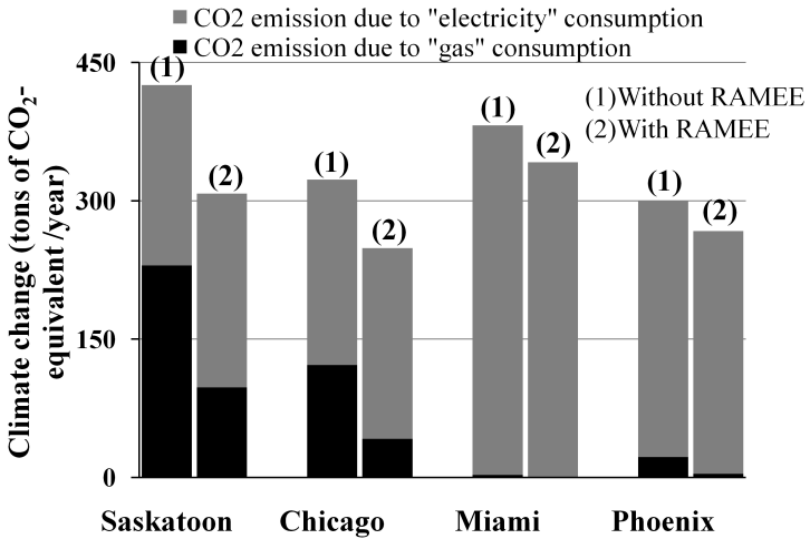

Figure 4.10. Annual equivalent emission of CO_2 from the hospital building with and without the RAMEE.

Figure 4.10 demonstrates the positive impact of energy recovery when a RAMEE is used to reduce the emission of greenhouse gases. By employing the RAMEE, the emission of CO_2-equivalent from the hospital building HVAC system can be reduced by about 25% and 10% in cold climates and hot climates, respectively. A typical mature tree absorbs CO_2 at a rate of 21.6 kg/year [4.38], and a new medium size car emits 3.3 tons of CO_2 per year (traveling 20,000 km/year, using regular gas with an automatic transmission; Natural Resources Canada 2010). Therefore, the carbon offset by purchasing the RAMEE for the hospital building is equal to planting 5450, 3440, 1850 and 1490 trees or removing 36, 23, 12 and 10 cars off the road in Saskatoon, Chicago, Miami and Phoenix, respectively.

4.6.5. Comparison of Two Case Studies

Rasouli et al. [4.20] studied the application of a RAMEE in an office building HVAC system simulated for different climates. In this section, a comparison of results between the two case studies of the RAMEE (i.e., the office building and the

hospital) is presented. Table 4.7 summarizes the differences and similarities between the characteristics of the two cases.

Table 4.7. Summary of the characteristics of each case study.

Area:	Office: 28800 m^2, 10-storey Hospital: 3150 m^2, 3-storey	**Heating system:**	Office: Radiator heating Hospital: VAV HVAC
Building envelope:	Similar, described in section 4.4	**Cooling system:**	Similar, VAV HVAC
Operation schedule:	Office: 6:00-22:00 Hospital: day-time: 6:00-22:00; night-time: 22:00-6:00	**Min. required total air change**	Office: N/A Hospital: 6 ACH day-time; 4 ACH night-time
Ventilation rate:	Office: 0.5 ACH Hospital: 2 ACH day-time; 1.3 ACH night-time	**Indoor RH**	Similar, below 60% when building is occupied
Indoor set-point temperature:	Office: 24°C at summer day-time; 22°C at winter day-time; 15°C night-time Hospital: 24°C in summer, 22°C in winter	**RAMEE's control and operating condition**	Similar, refer to Tables 4.1
Efficiency and pressure drop of HVAC equipment	Similar, specified in section 4.6	**Internal loads:**	Similar in loads but different operation schedules

Figure 4.11a presents the comparison of the total annual energy intensity for the buildings in different climates. The results show that the total energy intensity in the hospital without the RAMEE is 3.7, 3.1, 2.4 and 2.8 times greater than the office building in Saskatoon, Chicago, Miami and Phoenix, respectively. As a comparison to the TRNSYS simulation results, CBECS [4.19] has reported 2.8 times higher HVAC energy intensity in hospitals compared to office buildings in US in 2003 (i.e., 1472 MJ/m^2 in hospitals versus 533 MJ/m^2 in office buildings). Figure 4.11b shows the energy savings with RAMEE (including heating, cooling and fan energy) that is 48%, 45%, 8% and 17% in the hospital, and 30%, 28%, 5% and 10% in the office building in Saskatoon, Chicago, Miami and Phoenix, respectively.

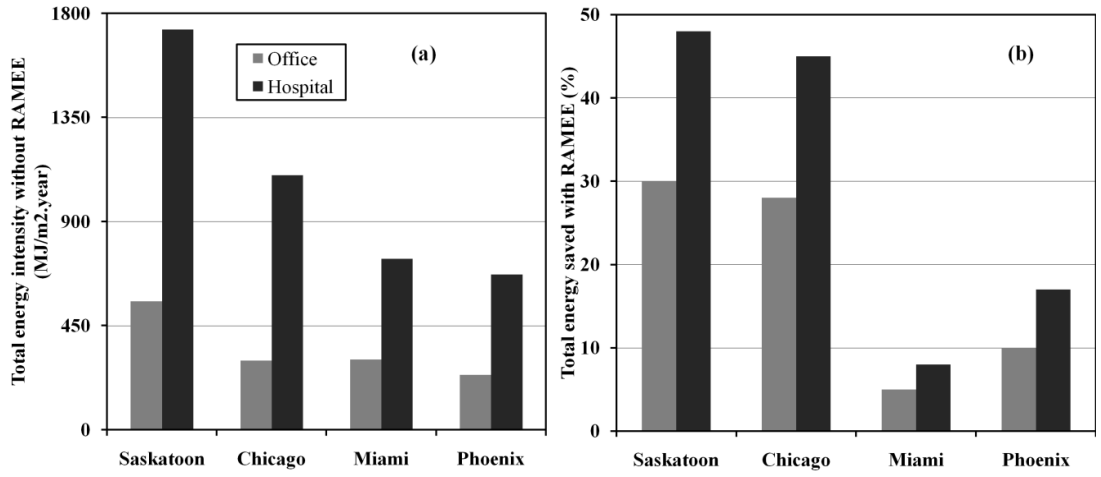

Figure 4.11. Comparison of (a) energy intensity of the HVAC system without the RAMEE and (b) energy saved with the RAMEE for two case studies in different climate.

Table 4.8 shows the comparison of operating average yearly *Cr** for the two case studies. The results show that the average *Cr** is very close for both buildings in each location. Therefore, average *Cr** seems to be a climate-dependent parameter (not a building-dependent parameter).

Table 4.8. Comparison of weighted average yearly *Cr for the two case studies in different locations.**

	Saskatoon	**Chicago**	**Miami**	**Phoenix**
Office	1.22	1.30	2.90	1.62
Hospital	1.22	1.37	2.99	1.64

Assuming similar air pressure drop of 2 cm of water across each LAMEE, the payback of the RAMEE in the hospital is about 2 years faster than the office building. In cold climates (Saskatoon and Chicago), the payback is immediate for hospitals and takes 1.8 to 2 years for office buildings. In hot climates (Miami and Phoenix), the payback may take 1.5 to 2.5 years for hospitals and about 4 to 4.8 years for office buildings.

4.7. Conclusions

The steady-state operation of a Run-Around Membrane Energy Exchanger (RAMEE) that transfers heat and moisture between outdoor ventilation and building exhaust air is described in the paper. The RAMEE effectiveness varies depending on outdoor conditions, indoor conditions, ventilation air flow rate (represented by *NTU*) and salt solution flow rate (represented by *Cr**). The RAMEE effectiveness can be optimized by changing these parameters; however, the salt solution flow rate is the only controllable variable for a given building in a given location. During the winter, the RAMEE should operate at the *Cr** which gives maximum sensible effectiveness. While in the summer, the RAMEE should be operated at the *Cr** resulting in maximum reduction of outdoor air enthalpy. The RAMEE is simulated in a hospital building using TRNSYS computer program joint with an Artificial Neural Network (ANN) that predicts the optimal salt solution flow rate (corresponding to Cr^*_{opt}). The hospital building is simulated in four different climates, i.e., Saskatoon (cold and dry), Chicago (cool and humid), Phoenix (hot and dry) and Miami (hot and humid). The simulation results showed about 58% to 65% annual heating energy saving in cold climates and 15% to 20% annual cooling energy saving in hot climates. Since the application of hourly optimal *Cr** requires an accurate control of the salt solution flow rate, the impact of applying average seasonal and yearly *Cr** values was studied. Also, the results show that operating the system under seasonal or yearly average *Cr** (that vary depending on the location) has a minimal impact on energy savings compared to the case that hourly optimal *Cr** is applied. The life cycle analysis results showed that the payback of the RAMEE is immediate in cold climates and reduces the equivalent emission of CO_2 (corresponding to the climate change) by 25%. In hot climates, the payback may take up to 2 to 3 years, and the RAMEE reduces the equivalent emission of CO_2 by 10%.

4.8. References of chapter 4

[4.1] C.J. Simonson, R.W. Besant, Heat and moisture transfer in desiccant coated rotary energy exchangers: Part I - Numerical model, HVAC & R research 3(4) (1997) 325-350.

[4.2] L.Z. Zhang, Y. Jiang, Heat and mass transfer in a membrane-based energy recovery ventilator, Journal of Membrane Science 163 (1999) 29-38.

[4.3] H. Fan, C.J. Simonson, R.W. Besant, W. Shang, Run-around heat recovery system using cross-flow flat-plate heat exchangers with aqueous ethylene-glycol as the coupling fluid, ASHRAE Transactions 111(1) (2005) 901-910.

[4.4] M. Seyed-Ahmadi, B. Erb, C.J. Simonson, R.W. Besant, Transient behavior of run-around heat and moisture exchanger system, Part I: Model formulation and verification, International Journal of Heat and Mass Transfer 52(25-26) (2009) 6000-6011.

[4.5] M. Seyed-Ahmadi, B. Erb, C.J. Simonson, R.W. Besant, Transient behavior of run-around heat and moisture exchanger system, Part II: Sensitivity studies for a range of initial conditions, International Journal of Heat and Mass Transfer 52(25-26) (2009) 6012-6020.

[4.6] A. Vali, C.J. Simonson, R.W. Besant, G. Mahmood, Numerical model and effectiveness correlations for a run-around heat recovery system with combined counter and cross flow exchangers, International Journal of Heat and Mass Transfer 52(25-26) (2009) 5827-5840.

[4.7] H.B. Hemingson, The impacts of outdoor air conditions and non-uniform exchanger channels on a run-around membrane energy exchanger, M.Sc. thesis, University of Saskatchewan, Saskatoon, SK, 2010.

[4.8] H.B. Hemingson, C.J. Simonson, R.W. Besant, Steady-state performance of a run-around membrane energy exchanger for a range of outdoor air conditions, Int. J. Heat Mass Transfer 54 (2011) 1814–1824.

[4.9] S. Akbari, H.B. Hemingson, D. Beriault, C.J. Simonson, R.W. Besant, Application of neural networks to predict the steady state performance of a Run-Around Membrane Energy Exchanger, Int. J. Heat Mass Transfer 55 (2012) 1628–1641.

[4.10] M. Afshin, C.J. Simonson, R.W. Besant, Crystallization limits of LiCl-water and MgCl2-water salt solutions as operating liquid desiccant in the RAMEE system, ASHRAE Transactions 116 (2010), Part 2, 494-506.

[4.11] K. Mahmud, G.I. Mahmood, C.J. Simonson, R.W. Besant, Performance testing of a counter-cross-flow run-around membrane energy exchanger (RAMEE) system for HVAC applications, Energy and Buildings 42(7) (2010) 1139-1147.

[4.12] B. Erb, C.J. Simonson, M. Seyed Ahmadi, R.W. Besant, Experimental Measurements of a Run-Around Membrane Energy Exchanger (RAMEE) with Comparison to a Numerical Model, ASHRAE Transactions 115(2) (2009).

[4.13] ASHRAE. 2008. ANSI/ASHRAE Standard 170-2008, Ventilation of Health Care Facilities. Atlanta: American Society of Heating, Refrigerating and Air-Conditioning Engineers, Inc.

[4.14] ASHRAE. 2010. ANSI/ASHRAE Standard 62.1-2010, Ventilation for Acceptable Indoor Air Quality (IAQ). Atlanta: American Society of Heating, Refrigerating and Air-Conditioning Engineers, Inc.

[4.15] M. Rasouli, C.J. Simonson, R.W. Besant. Applicability and optimum control strategy of energy recovery ventilators in different climatic conditions, Energy and Buildings 42(9) (2010) 1376-1385.

[4.16] T.P. McDowell, S. Emmerich, J. Thornton, G. Walton, Integration of Airflow and Energy Simulation using CONTAM and TRNSYS, ASHRAE Transactions 109(2) (2003) 757-770.

[4.17] M.J. Brandemuehl, J.E. Braun, The Impact of demand-controlled ventilation strategies on energy use in buildings, ASHRAE Transactions 105(2) (1999) 39-50.

[4.18] M. Orme, Estimates of the energy impact of ventilation and associated financial expenditures, Energy and Buildings 33(3) (2001) 199-205.

[4.19] EIA. 2003. Commercial Building Energy Consumption Survey, Energy Information Administration, U.S. Department of Energy.

[4.20] M. Rasouli, S. Akbari, H. Hemingson, R.W. Besant, and C.J. Simonson, Application of a run-around membrane energy exchanger in an office building HVAC system, ASHRAE Transactions, 117(2) (2011) 686-703.

[4.21] ASHRAE. 2004. ANSI/ASHRAE Standard 62-2004, Ventilation for Acceptable Indoor Air Quality (IAQ). Atlanta: American Society of Heating, Refrigerating and Air-Conditioning Engineers, Inc.

[4.22] R.S. Briggs, R.G. Lucas, T.Z. Todd, Climate classification for building energy codes and standards: Part 2 - Zone definitions, maps, and comparisons, ASHRAE Transactions 109(1) (2003) 122-30.

[4.23] L.Z. Zhang, J.L. Niu, Effectiveness Correlations for Heat and Moisture Transfer Processes in an Enthalpy Exchanger with Membrane Cores, Journal of Heat Transfer 124(5) (2002) 922-929.

[4.24] F.P. Incropera, D.P. Dewitt, Fundamentals of Heat and Mass Transfer, fifth edition, John Wiley & Sons, New York (2002) 642–681.

[4.25] I. Teke, O. Agra, S.A. Atayilmaz, H. Demir, Determining the best type of heat exchangers for heat recovery, Applied Thermal Engineering 30 (2010) 577-583.

[4.26] M. Rasouli, C.J. Simonson, R.W. Besant, Optimal control of energy recovery ventilators and their impact on energy and comfort, submitted to ASHRAE Transactions (2012).

[4.27] S.A. Klein, TRNSYS- A transient system simulation program, Engineering Experiment Station Report 38-13, Solar Energy Laboratory, University of Wisconsin, Madison (2000).

[4.28] J.W. Thornton, et al., TESS Libraries 2.0. Thermal Energy System Specialists, LLC. Madison, WI, USA (2009).

[4.29] ASHRAE. 2004, ANSI/ASHRAE Standard 55-2004, Thermal Environmental Conditions for Human Occupancy. Atlanta: American Society of Heating, Refrigerating and Air-Conditioning Engineers, Inc.

[4.30] Y. Yao, Z. Lian, W. Liu, Z. Hou, M. Wu., Evaluation program for the energy-saving of variable-air-volume systems, energy and buildings 39 (2007) 558-568.

[4.31] Mossman, M.J., et al., RSMeans Mechanical cost data, 33rd annual edition (2010).

[4.32] R.W. Besant, C.J. Simonson, Air-to-air energy recovery, ASHRAE Journal 42(5) (2000) 31-38.

[4.33] J.R. Turpin, Hybrid Systems Offer the Best of Both Worlds, *ACHRNews*, (2000) p. 18.

[4.34] CRC handbook of chemistry and physics. 1977. Cleveland, Ohio : CRC Press, c1977.

[4.35] M. Nyman, C.J. Simonson, Life cycle assessment (LCA) of air handling units with and without air-to-air energy exchangers, ASHRAE Transactions 110(1) (2004) 399–409.

[4.36] F. Aube, Guide for computing Co2 emissions related to energy use, CanmetENERGY Research Lab, Natural Resources Canada (2001).

[4.37] EPA. Power Profiler eGRID subregion and GHG emissions finder tool, US Environmental Protection Agency (2010).

[4.38] M. McAliney, Arguments for Land Conservation: Documentation and Information Sources for Land Resources Protection, Trust for Public Land, Sacramento, CA, (1993).

CHAPTER 5

SUMMARY, CONCLUSIONS, AND FUTURE WORKS

5.1. Summary

The Run-Around Membrane Energy Exchanger (RAMEE) is an air-to-air heat and moisture recovery system (composed of two Liquid to Air Membrane Energy Exchangers (LAMEEs) that are coupled with a salt solution flow) which can be used in Heating, Ventilating, and Air Conditioning (HVAC) systems of buildings to precondition the supply air stream. Like many other thermal systems (e.g. thermal solar panels, energy wheels, air conditioning systems, etc.), controlling the RAMEE to achieve the highest possible performance is important. The first step to develop a control algorithm for a specific system is to obtain a mathematical model representing the behavior of that system.

The objective of this thesis was to develop mathematical models to predict:

1. the *steady-state* performance of a RAMEE
2. the *transient* performance of a RAMEE

The neural network (NN) approach was implemented to achieve the objectives of this thesis.

After a short introduction in chapter 1, chapter 2 describes the NN model used to predict the steady-state performance (i.e. sensible and latent effectiveness) of the RAMEE. The importance of each design or operating parameter was investigated using appropriate sensitivity studies. Then, only the parameters that had a significant

effect on the RAMEE performance were included in the NN model. Sensitivity studies showed that the Number of Transfer Units (*NTU*), the solution to air heat capacity rate ratio (*Cr**), and the indoor and outdoor air conditions (i.e. temperature and humidity) had a significant effect on the steady-state performance of RAMEE while the effect of Entrance Ratio and Aspect Ratio had a small effect and could be neglected.

The training data set required for the steady-state NN model was generated using a finite difference numerical model which solves the physical governing equations for steady-state coupled heat and mass transfer through the RAMEE system and predicts the performance of the system for different input parameters. Two separate neural networks each with five inputs and one output (with two hidden layers of 10 neurons in each layer) were selected as the architecture with desired accuracy to predict the RAMEE sensible and latent effectiveness separately. The steady-state NN models were verified using numerical and experimental data. The root mean squared error (RMSE) between the numerical and NN models were 0.05 °C for sensible results and 0.02 g_v/kg_a for latent results, indicating satisfactory agreement for energy exchange calculations. Also the NN and experimental results agreed within the 95% uncertainty bound of experimental data.

New NN models to predict the transient performance of the RAMEE were developed in chapter 3 using a similar approach as in chapter 2. A transient numerical model (TNM) that can predict the behavior of the system for different initial, design, and operating parameters was used to determine the required data set for training the NN models. All parameters that could affect the transient performance of RAMEEs were introduced and the effect of each parameter was investigated individually. Finally, outdoor conditions, *NTU*, and *Cr** were included

in the model while the effect of initial conditions, geometrical parameters, and salt solution storage tanks volume were neglected. Two separate (i.e. sensible and latent) NN models with 12 inputs and one output were selected as representative models and the NN models were verified using numerical data. The mean absolute difference (average for all different test cities with different climates) between the results of transient numerical model and NN models were 0.5 °C for the sensible model and 0.2 g_v/kg_a for the latent model, which indicates satisfactory agreement for energy exchange calculations.

Chapter 4 presents a practical application of the NN models developed in chapter 2. The NN models were optimized to find the optimum effectiveness (i.e. the effectiveness that results in the maximum energy savings) of the RAMEE in each hour. These optimum effectiveness values were used in the TRNSYS computer program to find the maximum possible energy savings by implementing an optimally controlled RAMEE in a conventional hospital HVAC system. The optimized RAMEE reduces the annual heating energy by 58% to 66% in cold climates, and the annual cooling energy by 10% to 18% in hot climates. The RAMEE can also reduce the required capacity of the heating system by 45% in cold climates, and the required capacity of the cooling system by 25% in hot climates. The same analysis for the application of a RAMEE system in the HVAC system of an office building (presented in Appendix A) shows up to 43% heating energy saving in cold climates, and up to 15% cooling energy saving in hot climates.

5.2. Conclusions

According to the investigations presented in this thesis the following conclusions can be made:

1. It is concluded that the implemented neural network (NN) models in chapter 2 are able to predict the steady-state effectiveness of the RAMEE. A completely unseen test set of 9000 data points which covers a wide range of parameters (i.e. *NTU* from 1 to 15, *Cr** from 0.4 to 5, and outdoor and indoor conditions covering different climates) is used to test the accuracy of the NN models numerically. Also, an experimental validation for an extreme experimental case with H^*=-0.68 is presented.
2. The sensible and latent effectivenesses for the continuous yearly transient operation of the RAMEE are predicted using two separate NN models. A training data set of approximately 50000 points, generated using the TNM, is used to train the NN models using a back-propagation algorithm to minimize the error between the outputs of the TNM and the NN models. Finally, a 12-16-16-1 configuration is concluded to result in a NN model of satisfactory accuracy for either sensible or latent energy transfer in the RAMEE.
3. Such a fast and non-iterative mathematical model (NNs) can be used as a computational component in commercial building energy simulation packages to estimate the possible annual energy savings using a RAMEE. Also NN models are useful to get a quick idea of system behavior in order to modify the operation or design parameters.
4. The NN models are some multivariable mathematical functions, describing the behavior of RAMEE, and depending on the application can be simply optimized using common optimization algorithms.
5. An optimally controlled RAMEE: results in great savings in cold climates (up to 60% in annual heating energy), significantly decreases the annual cooling energy in hot climates (up to 20%), downsizes the cooling or heating

equipments, increases the indoor air quality, and improves the health of occupants.

5.3. Limitations and Future Works

This M.Sc. thesis has shown an attempt to predict both the steady-state and transient performance of the RAMEE using an alternative method (NNs) with specific advantages over traditional numerical solutions. During the development of the NN models, some limitations and simplifying assumptions were applied that require further study to make the results of this thesis more practical and useful.

1. The validity range of the steady-state NN models can be expanded significantly by including number of mass transfer units (NTU_m) in the NN inputs. The NTU_m mainly depends on membrane water vapor permeability. After including NTU_m in the inputs, the NN models will be able to predict the steady-state performance of counter flow RAMEEs with different membranes and air and solution channel thicknesses. In order to cover the effect of NTU_m in the steady-state models, the training data set should be expanded by adding new data points with different NTU_m values than the existing training set.
2. The limitations for transient NN models are:
    A. Fixed temperature and humidity ratio values are assumed for indoor air.
    B. The effect of initial conditions has not been included in NN models since the focus of chapter 3 is the non-stop yearly operation of RAMEE.
    C. The NN models are developed for a specific design of counter flow RAMEE. Therefore, major modifications in geometrical design,

membrane properties, storage tank volume, or flow configuration may require new training data sets and new NN models.

Each of the above mentioned limitations can be a topic for further study.

3. The transient NN models are developed to cover different climates. This decreases the accuracy of the NN models. For significantly better results, sophisticated NN models that are simpler and highly accurate can be developed for each specific climate or location. In this case, the NN models will have less difficulty to map the data since it will be easier to model a specific weather pattern than a few different weather patterns at the same time.
4. Any modifications like expanding the range of input parameters, significantly changing the aspect and entrance ratios, or changing the salt solution type (with something other than $MgCl_2$ or LiBr) may require re-training the existing models or developing new NN models using appropriately modified training data sets.
5. In chapter 4 and Appendix A it was assumed that the RAMEE is always operating close to steady state condition. The validity of this assumption can be double checked by repeating the TRNSYS simulations using transient NN models of chapter 3 instead of steady-state NN models of chapter 2.

APPENDIX A

MANUSCRIPT #4

Application of a Run-Around Membrane Energy Exchanger in an office building HVAC system

M. Rasouli, S. Akbari, H. Hemingson, R.W. Besant and C.J. Simonson

Abstract

A Run-Around Membrane Energy Exchanger (RAMEE) has been introduced in the literature as a novel energy recovery system that transfers heat and moisture between the ventilation and exhaust air. The RAMEE consists of two separate (supply and exhaust) flat-plate exchangers made of water vapor permeable membranes, and coupled with an aqueous salt solution. In this paper, the application of a RAMEE in an HVAC system is investigated. The paper discusses the dependency of RAMEE performance on ventilation air and salt solution flow rates and indoor and outdoor air conditions and describes how to control the RAMEE in different operating conditions (summer, winter and part-load). An Artificial Neural Network (ANN) that is able to predict the optimal system performance was developed in previous research. The ANN results are used for TRNSYS computer simulation of the RAMEE system when operating in an office building in four different climates. The results show up to 43% heating energy saving in cold climates, and up to 15% cooling energy saving in hot climates. Cost analysis proves the important role of pressure drop across the exchangers in life cycle cost, and predicts payback period ranging from 2 to 5 years for the RAMEE.

1. Introduction

Recent research has presented a strong relationship between indoor air quality (IAQ) and occupants' productivity [A.1-A.3]. On the other hand, studies have indicated a higher demand for energy when a higher ventilation flow is introduced to a conditioned space [A.4-A.6]. Therefore, HVAC system operating conditions and equipment sizes should be optimized to provide a satisfactory level of productivity and thermal comfort while HVAC energy consumption is minimized.

Energy Recovery Ventilators (ERVs) reduce the energy required to condition ventilation air by transferring heat (and moisture) between conditioned exhaust air and outdoor ventilation air. The pre-conditioning of this outdoor air reduces the energy required by HVAC systems, while thermal comfort is satisfied. In general, ERVs can be divided into two groups: i.e., heat recovery systems which transfer only sensible heat, and heat and moisture recovery systems (also called energy exchangers) which transfer both sensible and latent energy. Heat pipes, flat plate heat exchangers and rotary heat wheels only transfer heat between the supply and exhaust airstreams, however, they are common due to their low pressure drop and convenient maintenance [A.7]. The main disadvantage of heat recovery systems is that they cannot transfer moisture. Energy wheels and permeable flat plate exchangers can transfer both heat and moisture. For example, an energy wheel coated with a desiccant can transfer both heat and moisture between two air streams [A.8-A.9]. Flat plate exchangers constructed with water permeable membranes can transfer heat and moisture between the airstreams [A.10].

All above mentioned devices require that the supply and exhaust ducts to be side-by-side which usually imposes higher ducting costs. In addition, contaminant carryover in rotary wheels and cross-flow leakage of air through seals are concerns

in some types of buildings such as health care facilities and laboratories. The extra ducting cost and the contaminant transfer could be avoided if the exhaust and supply air ducts were separated. In this paper, a literature review on a novel Run-Around Membrane Energy Exchanger (RAMEE) which is capable of transferring both heat and moisture between remote supply and exhaust ducts is presented. Since the performance of a RAMEE depends on the ventilation air and salt solution flow rates and indoor and outdoor air conditions, which continuously change throughout the year, appropriate control of the RAMEE system is needed. Therefore, an investigation on the optimum operation of a RAMEE during summer, winter and part-load conditions is conducted. As a case study, an office building equipped with a RAMEE is simulated in different climates using the TRNSYS [A.11] computer program, and the potential cooling and heating energy savings are presented. A Life Cycle Cost Analysis (LCCA) is performed over a 15-year period to study the economics of the RAMEE system compared to a conventional HVAC system with no energy recovery.

2. Run-Around Membrane Energy Exchanger (RAMEE)

In this section, an overview of the literature is presented to introduce the RAMEE. A schematic of exchangers and the flow diagrams of a HVAC system equipped with a RAMEE is described. The parameters affecting the RAMEE effectiveness are discussed.

2.1. Exchanger Design

A Run-Around Membrane Energy Exchanger (RAMEE), shown in Figure A.1a, which exchanges both heat and water vapor between the exhaust air and un-conditioned outdoor ventilation air has been proposed to overcome the limitations of

currently available ERVs [A.12]. The RAMEE system consists of two separate exchangers with a salt solution coupling liquid that is pumped in a closed loop between the two exchangers. Each exchanger, which is called a liquid to air membrane energy exchanger (LAMEE), is a flat plate energy exchanger constructed with vapor permeable membranes that allow the transmission of water vapor but not liquid water. The salt solution loop couples these two LAMEEs in the RAMEE, and the air and salt solution may flow in cross flow [A.13-A.14], counter/cross flow [A.15-A.16] or counter flow [A.17] arrangement through each of the two LAMEEs placed into the supply and exhaust streams. However, the flow arrangement that combines high performance with practical header design is the cross/counter flow arrangement as shown in Figure A.1(b). It should be noted that the numerical simulation results of a counter flow LAMEE are used in this paper [A.16]. However, the manufacturer may consider a counter/cross flow due to the limitation in separating the flow inlets. The numerical model of the RAMEE system shows that a good cross/counter flow will reduce the RAMEE effectiveness by less than 2% compared to a counter flow design at the same operating condition [A.18].

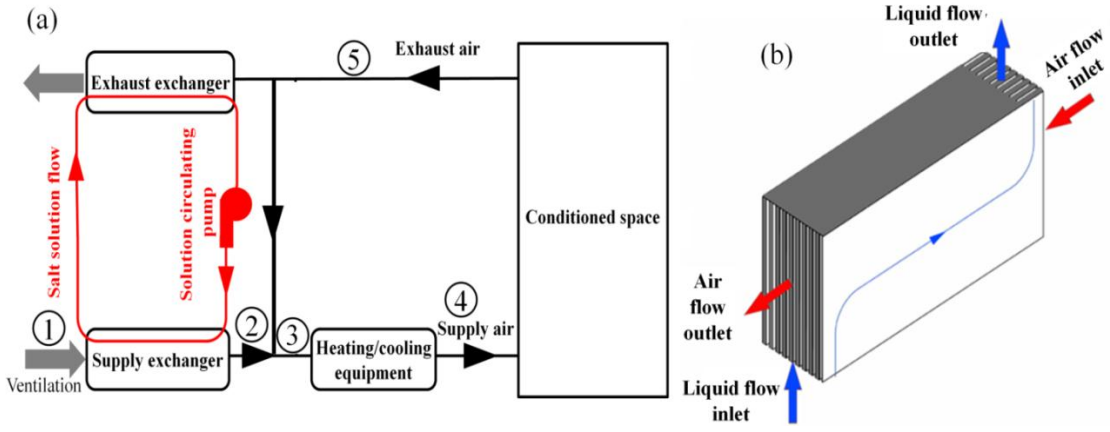

Figure A.1. Schematic diagram of a (a) HVAC system equipped with a RAMEE, and (b) air and solution flow in a LAMEE.

The RAMEE system uses the exhaust air to precondition the ventilation air and decreases the energy consumption and the size of the heating/cooling equipment.

For example, during the summer when the outdoor air is warm and humid, the desiccant salt solution gains heat and moisture from the ventilation air stream in the supply exchanger. The solution is then pumped into the exhaust exchanger where it releases this heat and moisture to the exhaust air stream. This loop cools and dehumidifies the outdoor ventilation air in summer. During winter, the salt solution gains heat and water vapor from the conditioned exhaust air when passing through the exhaust exchanger. This solution then releases both heat and moisture while it flows through the supply exchanger and thus pre-conditions (i.e., heats and humidifies) the ventilation air before it enters to the heating equipment.

2.2. System Performance

Based on the numerical model developed in previous research [A.16-A.17] for a RAMEE system with equal supply and exhaust air flow rates, the RAMEE effectiveness in transferring heat (ε_s), moisture (ε_l) and enthalpy (ε_t) is a function of three dimensionless groups, i.e., *NTU* (number of heat transfer units), NTU_m (number of mass transfer units) and *Cr** (ratio of salt solution heat capacity to that of the air) as defined below:

$$\varepsilon_s = \frac{T_1 - T_2}{T_1 - T_5} \tag{A.1}$$

$$\varepsilon_l = \frac{W_1 - W_2}{W_1 - W_5} \tag{A.2}$$

$$\varepsilon_t = \frac{h_1 - h_2}{h_1 - h_5} \tag{A.3}$$

$$NTU = \frac{UA}{\dot{m}_{air} C_{p,air}} \tag{A.4}$$

$$NTU_m = \frac{U'A}{\dot{m}_{air}} \tag{A.5}$$

$$Cr^* = \frac{\dot{m}_{sol}C_{p,sol}}{\dot{m}_{air}C_{p,air}} \tag{A.6}$$

In addition, the system performance strongly depends on the condition of outdoor ventilation air, and slightly depends on the indoor air conditions which might vary between summer and winter indoor set-points [A.17].

2.2.1. Impact of *NTU* and *Cr** on RAMEE Performance

Equation A.4 shows that *NTU* is directly related to the heat exchange surface area of each exchanger and represents the size of the RAMEE. The higher the *NTU*, the higher the effectiveness (shown in Figure A.2(a)) [A.17]. *Cr** characterizes thermal capacity rate of the liquid flow compared to the thermal capacity rate of the air flow in the RAMEE system and is similar to *Cr* used in the literature to describe the thermal capacity rate ratio for run around heat exchangers [A.18]. As shown in Figure A.2(b), effectiveness increases from zero as *Cr** increases from zero until it reaches the peak value. The optimum *Cr** at which the peak performance is achieved depends on the type of ERV. For instance, the maximum effectiveness of a run-around heat and moisture recovery system operating at the AHRI summer test conditions [A.19] occurs approximately at *Cr**=3 (for equal supply and exhaust air flow rates), while a run-around heat recovery system has its peak effectiveness at *Cr*=1 [A.20].

Hemingson et al. [A.17] used a numerical model to predict the RAMEE effectivenesses in different outdoor conditions and these results showed good agreement with heat transfer theory. They indicated that the RAMEE effectiveness increases with *NTU* (as shown in Figure A.2(a)) and it follows the same trend as

expected by analytical solutions and empirical correlations [A.21-A.22]. The system has a significantly higher sensible effectiveness and slightly higher latent effectiveness when its *NTU* is increased. Also, increasing NTU_m leads to a considerable increase in latent effectiveness and a slight increase in sensible effectiveness. The system performance varies with *Cr** until it reaches the optimal value where the peak performance is achieved. This is schematically shown in Figure A.2(b) for a specific outdoor condition. It should be noted that the dependency of the RAMEE effectiveness on *Cr** varies with outdoor condition and is discussed in the next section.

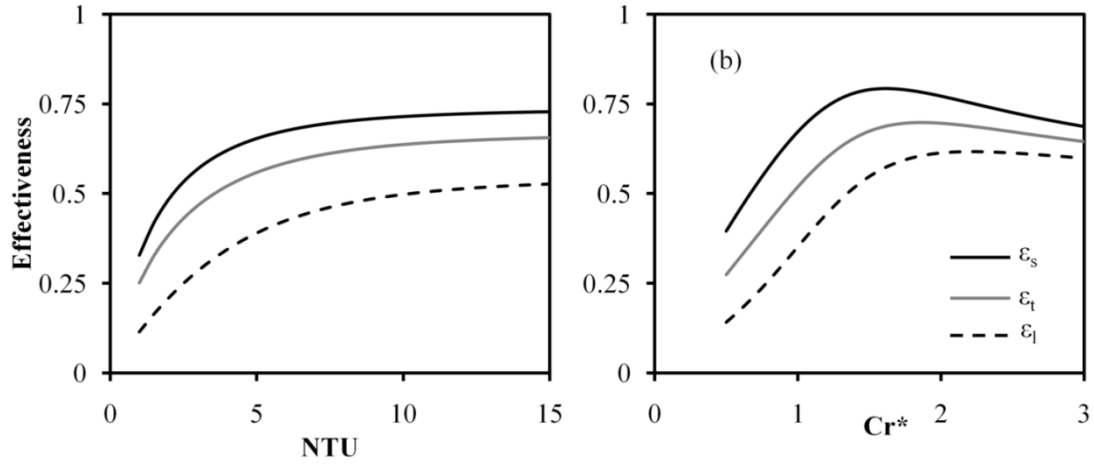

Figure A.2. Variation of RAMEE effectiveness as a function of *NTU* and *Cr for outdoor condition at 5°C and 5 g/kg and indoor condition at 22°C and 9.3 g/kg (a) NTU (at *Cr**=1.3) and (b) Cr* (at *NTU*=10).**

2.2.2. Impact of Indoor and Outdoor Conditions on RAMEE Performance

Hemingson et al. [A.17] showed the influence of outdoor air temperature and humidity on the effectiveness of the RAMEE. The main reason for the dependency of RAMEE effectiveness on outdoor conditions is the impact that outdoor temperature and humidity will have on the liquid desiccant and the fact that heat and moisture transfer are coupled. The moisture transfer between the two fluid streams in each LAMEE releases/absorbs phase change energy and increases/decreases the desiccant temperature and consequently the sensible effectiveness. The change in

desiccant temperature and humidity due to heat and moisture transfer affects the latent effectiveness of the system as well. Hemingson et al. [A.17] concluded that as the temperature difference between outdoor and indoor air increases (either summer or winter), the latent effectiveness increases. Also, the greater the humidity ratio difference between the indoor and outdoor air, the higher the heat transfer. Figure A.3 presents the RAMEE effectiveness for five different outdoor conditions for *NTU*=10 where the summer/winter indoor conditions are chosen from the AHRI test conditions [A.19].

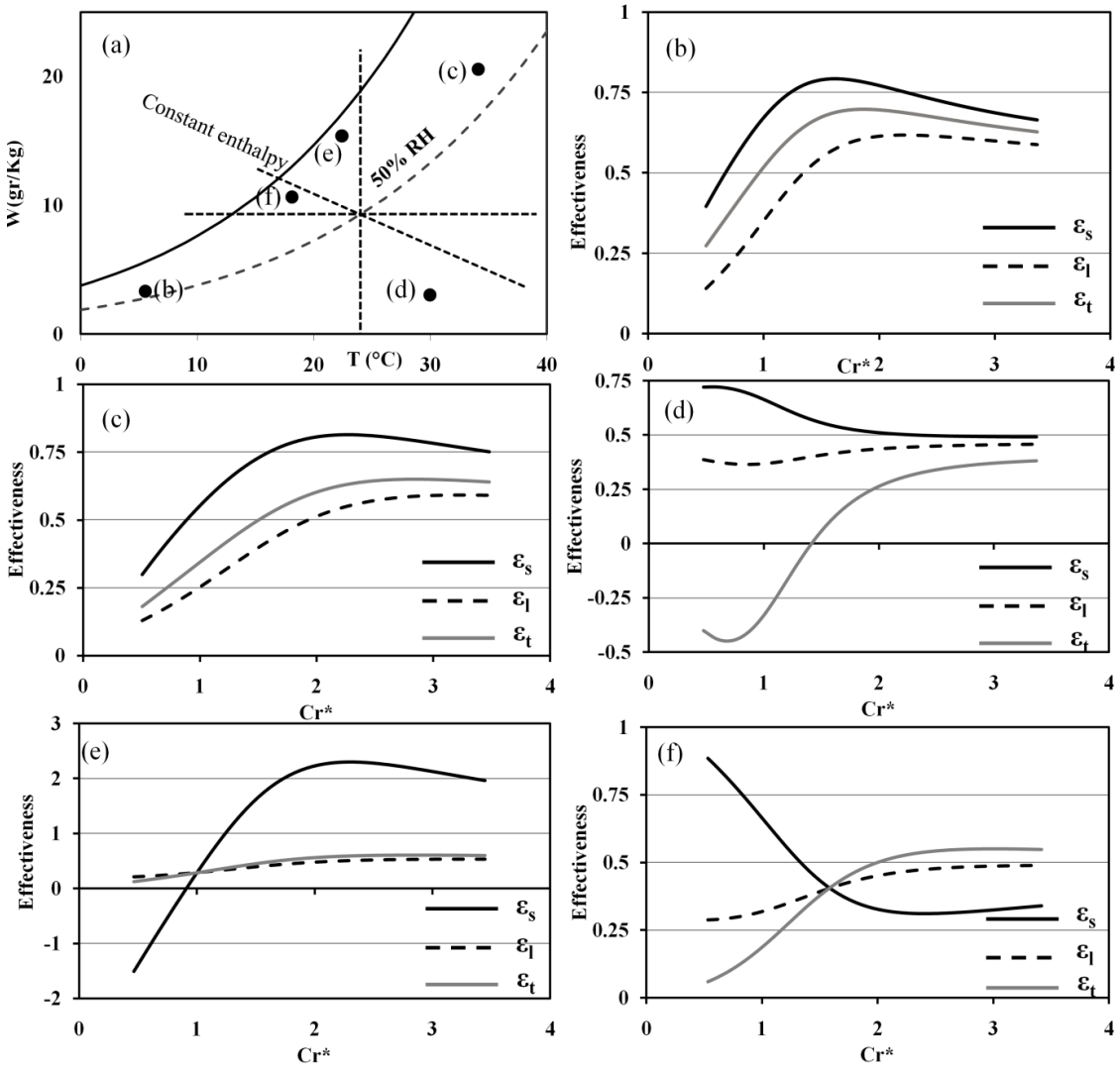

Figure A.3. RAMEE effectiveness versus *Cr for five different outdoor conditions (*NTU*=10) (a) the psychometric chart, (b) cold-dry (5°C and 5 g/kg), (c) hot-humid (35°C, 20g/kg), (d) hot-dry (30°C, 2g/kg), (e) cool-humid, high enthalpy (22°C, 15g/kg), and (f) cool-humid, low enthalpy (19°C, 10g/kg).**

Figure A.3 shows that the optimal *Cr** (i.e., the *Cr** at which the maximum RAMEE effectiveness is achieved) varies significantly with outdoor condition. *Cr**, as defined in Equation (A.3), depends on ventilation air and salt solution flow rates. For a given building, where ventilation rates are maintained at a constant rate specified by standards [A.23-A.24], *Cr** remains only a function of the salt solution flow rate. Therefore, the salt solution flow rate should be controlled to give the optimal *Cr** at all outdoor conditions.

Regarding the impact of indoor condition, Hemingson et al. [A.17] found that changing the indoor conditions between summer and winter indoor temperature and humidity set-points has a minimal impact on RAMEE performance (about 0.3% change in total effectiveness).

3. RAMEE Control

As mentioned in the previous section, the RAMEE effectiveness depends on *NTU*, *Cr** and indoor and outdoor air conditions. Among these variables, only *NTU* and *Cr** are controllable and the optimal operation of the RAMEE system requires proper control of these variables. The design *NTU* is determined during the exchanger design and manufacturing process. But, it can be changed by changing the ventilation air flow rate (e.g., bypassing a fraction of ventilation air) during the operation of the RAMEE. The operating *Cr** can be controlled via adjustment of salt solution or ventilation air flow rates by the operator during the operation of the RAMEE.

NTU represents the size of the RAMEE system, and the greater the *NTU*, the higher the effectiveness. On the other hand, increasing the size of the system increases the manufacturing costs [A.25]. Therefore, *NTU* should be large enough to give a reasonable effectiveness, but not extremely large which may cause excessive

production cost. A design *NTU* of 10 is found feasible in the literature [A.25] and is used for this study. However, it may change as the ventilation rate might change during the operation of the RAMEE. The following sub-sections discuss the appropriate control of *Cr** and *NTU* to achieve the optimal performance of the RAMEE system in different operating conditions (i.e., summer, winter and part-load).

3.1. Heating Season (Winter)

When the outdoor temperature is lower than the HVAC system indoor set-point, and the internal heat loads and solar radiation gains do not satisfy the space heating demand, the heating system needs to be operated. Due to a low outdoor air temperatures and moisture content, conditioning the outdoor ventilation air during cold weather requires heating and possibly humidification.

Previous research [A.9] and [A.26-A31] has studied the savings using different types of ERVs in various climates and have found that the operation of ERV is beneficial especially for cold weather conditions. For instance, Rasouli et al. [A.28] simulated an office building in different climates and showed that ERVs with sensible effectiveness values in the range of 55%-95% may save 15-30% of annual heating energy for buildings in cold climates. They showed that in a typical office building in the US, the sensible heating accounts for most (about 96%) of the annual HVAC heating energy consumption while humidification accounts for less than 4% of the annual heating energy when the goal is to maintain an indoor humidity of 30% RH. Since humidification energy is small and many buildings don’t have humidification system, the focus on the winter is to reduce the sensible heating energy.

As shown in Figure A.3, the *Cr** at which maximum sensible, latent and total effectiveness occur depends on the outdoor conditions. As indicated by Rasouli et al. [A.28], minimizing the sensible heating load of the HVAC system is the main concern during the winter, therefore, the optimal *Cr** is the *Cr** at which the sensible effectiveness is maximum (*Cr** of about 1.5 in Figure A.3(b)). Applying such an optimal *Cr** does not sacrifice the latent effectiveness, and gives a latent effectiveness that is only slightly lower than its peak value. The moisture transfer from exhaust air to the outdoor ventilation air should improve the indoor humidity during the winter when outdoor air is mostly dry and humidification is not provided by the HVAC system. Studies have shown that absenteeism in schools and offices may be reduced when the indoor humidity is increased in the winter [A.32-A.33].

3.2. Cooling Season (Summer)

Research on ERVs in the cooling season has shown that reducing the annual cooling energy requires proper control of the ERV ([A.29] and [A.34-A.35]). In general, the present control strategies can be categorized into two groups: (i) temperature-based controls which allow the ERV to operate only if the outdoor air temperature is greater than the indoor air, and (ii) enthalpy-based controls which allow the ERV to operate only if it can reduce the enthalpy of outdoor air. Rasouli et al. [A.29] compared the present control strategies and proposed an optimal ERV control. Based on their results, an ERV should be operated only if it can reduce the enthalpy of outdoor ventilation air, and the greater the reduction of outdoor air enthalpy the lower the coil cooling load. Therefore, as defined in Equation (A.3), the RAMEE system should be operated at maximum absolute total effectiveness when the outdoor enthalpy is greater than the indoor, and should have minimum (and negative) total effectiveness when the outdoor enthalpy is lower than the indoor.

For a better explanation, refer to the performance of the RAMEE in four different summer outdoor conditions presented in Figure A.3(c), (d), (e), and (f). For cases (c) and (e), where the outdoor enthalpy is greater than the indoor enthalpy, the RAMEE should be operated at maximum positive total effectiveness (i.e., *Cr** of about 2.5). Such *Cr** maximizes both heat and moisture transfer (cooling and dehumidification) for the hot-humid case (Figure A.3(c)). But, it maximizes the moisture transfer (dehumidification) and minimizes the heat transfer (heating) for the cool-humid case (Figure A.3(e)). When the outdoor enthalpy is lower than the indoor enthalpy and the cooling is still required, the RAMEE should be operated only if a negative total effectiveness can be achieved by adjusting the appropriate *Cr**. Therefore, for case (d), the RAMEE should be operated at *Cr** of about 0.8 where the minimum (and negative) total effectiveness is achieved. Such *Cr** maximizes the heat transfer (cooling) and minimizes the undesirable moisture transfer (humidification). In case (f), however, the RAMEE should be turned off, because no *Cr** value gives negative total effectiveness values.

3.3. Economizer

During the heating and cooling season, HVAC system energy consumption increases as the outdoor ventilation rate increases [A.4-A.5]. Therefore the outdoor air flow is typically maintained at the minimum rate that satisfies ASHRAE ventilation standard requirements [A.23]. However, during cool summer days when the internal loads and solar gains necessitate the operation of the cooling system, free cooling can be provided by increasing the outdoor air flow rate. In such outdoor conditions, the RAMEE should be turned off (to prevent heating of the cool outdoor air) and an economizer should be employed to introduce 100% outdoor air to meet a portion (or all) of the building cooling load. This will reduce (or even eliminate) the

cooling load and improves the indoor air quality. Seem and House [A.36] introduced a strategy to control economizers based on minimization of coil cooling load. Their results showed that the outdoor ventilation flow should be increased when the outdoor enthalpy and outdoor temperature are lower than the indoor. In practice, the introduction of 100% outdoor air when the outdoor temperature is slightly lower than the indoor temperature may not be beneficial, because the additional fan power may exceed the cooling energy savings. Therefore, in this paper, 100% outdoor air is provided when the outdoor enthalpy is lower than the indoor enthalpy and the outdoor temperature is between 14°C and 20°C. To prevent thermal discomfort, if the outdoor temperature falls below 14°C, a fraction of the exhaust air is recirculated and mixed with the outdoor air to maintain minimum of 14°C supply temperature.

3.4. Part-Load Operation

During cool summer days when the outdoor temperature is lower than the indoor temperature, a cooling system might be still required to meet the internal heat loads and solar radiation gain. The supply temperature is determined based on the building cooling load and the required ventilation air flow rate. In case the outdoor temperature is below the required supply temperature, the outdoor air needs to be heated up to the desired supply temperature. As an alternative, an ERV could be operated to heat the ventilation air, however, full-load operation of the ERV may overheat the outdoor air to temperatures greater than the desired supply temperature. This require the cooling of overheated air, and in such conditions, the ERV should be operated in part-load operating condition (i.e., not in full capacity of transferring heat and moisture).

Depending on the type of ERV, different methods can be used to adjust the effectiveness to the desired value. For example, adjusting the wheel speed for energy

wheels, decreasing the flow rate of the fluid streams (ventilation or exhaust) or by-passing a fraction of the ventilation air can give the required effectiveness for other ERVs. For the RAMEE system, considering the parameters affecting the system effectiveness, adjusting *NTU* or *Cr** are the two available strategies to control the part-load operation. Considering Equations (A.4) and (A.6), *Cr** and *NTU* are functions of salt solution and ventilation air flow rate, therefore the system effectiveness could be changed by changing the flow rate of any of these two streams. Between the two available options, adjusting *NTU* is simpler because the RAMEE effectiveness is more predictable with changing *NTU* (i.e., effectiveness increases with *NTU*), but the effectiveness has a complex behavior with changing *Cr** as shown in Figure A.3 By-passing a fraction of ventilation air, as shown schematically in Figure A.4, decreases the heat transfer from exhaust air to the cool ventilation air and prevents overheating. The bypass fraction should be adjusted carefully to give the desired supply temperature.

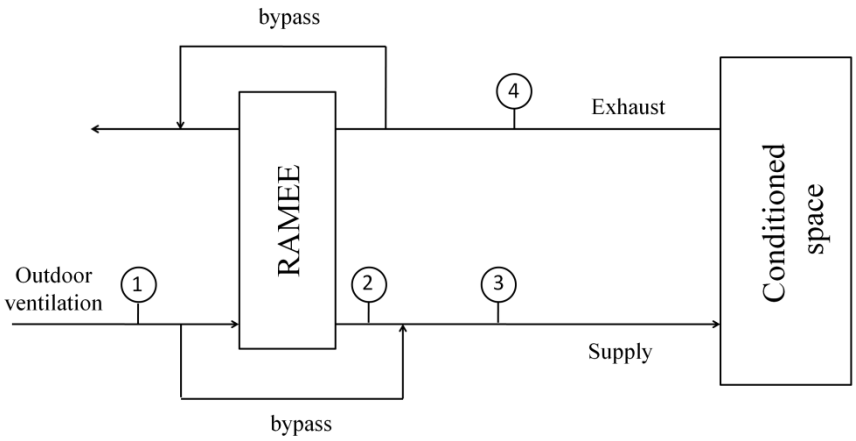

Figure A.4. Schematic of the RAMEE system operating under part-load condition.

For given indoor and outdoor conditions and a known ventilation rate (i.e., minimum standard requirement), the condition at state (3) is a function of RAMEE effectiveness, and the fraction of ventilation air bypassing the RAMEE:

$$T_3 = \frac{\dot{m}_{bypass}.T_1 + \dot{m}_2.T_2}{\dot{m}_{bypass} + \dot{m}_2} \quad \text{(A.7)}$$

Where T_2 is the condition of outdoor air leaving the RAMEE and can be stated as:

$$T_2 = T_1 - \varepsilon_s(T_1 - T_4) \quad \text{(A.8)}$$

And, assuming no air leakage in the exchangers:

$$\dot{m}_{bypass} + \dot{m}_2 = \dot{m}_1 = Ventilation\ rate\ (constant) \quad \text{(A.9)}$$

The condition at state (3) can be specified as a function of RAMEE effectiveness and bypass fraction by substitution of Equations A.8 and A.9 into Equation A.7:

$$T_3 = T_1 + \varepsilon_s(1 - R)(T_4 - T_1) \quad \text{(A.10)}$$

where, R is the bypass fraction and is defined as:

$$R = \frac{\dot{m}_{bypass}}{\dot{m}_1} \quad \text{(A.11)}$$

Equation A.13 can be re-arranged to determine the bypass fraction:

$$R = 1 - \frac{T_3 - T_1}{\varepsilon_s(T_4 - T_1)} \quad \text{(A.12)}$$

Equation (A.12) determines the by-pass fraction as a function of indoor, outdoor and supply temperature and the RAMEE optimal sensible effectiveness at the given operating condition.

In conclusion, the operation of RAMEE in different outdoor conditions is shown on the psychometric chart in Figure A.5. States (3) and (4) refer to the condition of the supply air and indoor air, respectively.

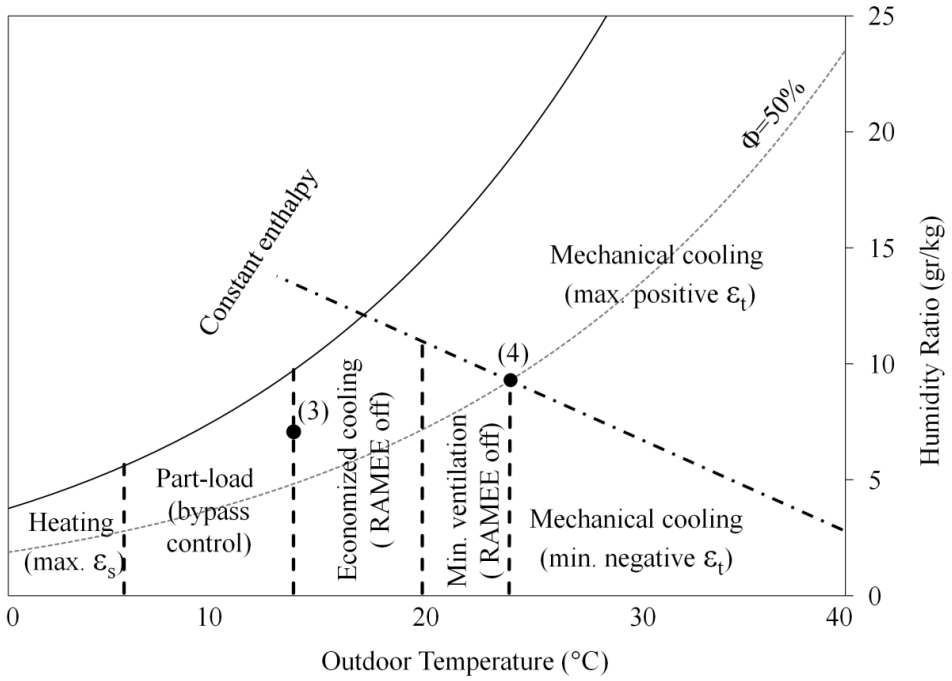

Figure A.5. Operating condition of the RAMEE system in different outdoor condition.

4. Model Specification

4.1. Building Description

The RAMEE system is simulated in a 10-storey office building with total floor area of 28,800 m^2 (310,000 ft^2), representing 3.34% of the existing U.S. office buildings [A.37]. The building description is taken from a study carried out at Pacific Northwest National Lab and includes the building parameters required for an energy analysis. The original building is constructed in Fort Worth, Texas, and only has about 2 cm (0.8 in) of insulation which gives a thermal resistance of 0.78 m^2 K/W (4.43 h ft^2 F/BTU). In order to have a building that could fairly represent a typical building in different locations, walls, slabfloor and roof are improved by adding insulation layers. Walls are made of light weight concrete, an insulation layer and gypsum board that gives a total thermal resistance of 2.72 m^2 K/W (15.45 h ft^2 F/BTU). The roof is made of built up roofing, insulation and aluminum siding that gives a total thermal resistance of 3.64 m^2 K/W (20.68 h ft^2 F/BTU) and the slab

thermal resistance is 3.45 m^2 K/W (19.60 h ft^2 F/BTU). The windows are changed from single pane (as specified in the original PNL report) to double pane windows. The building has about 30 W/m^2 (9.5 BTU/h ft^2) of internal heat gains based on PNL report. An occupant density of 5 People/100 m^2 (≈ 0.47 people/100 ft^2) is assumed that gives an outdoor ventilation air flow rate of 0.5 ACH (11.3 m^3/s; 24,000 CFM), limited to occupied hours (7am to 9pm), to meet the ASHRAE ventilation requirement [A.23].

4.2. HVAC System

The cooling system operating in the described building is a variable air volume HVAC system (VAV HVAC) that supplies air at 14°C (57.2 F) or higher when the building is occupied. The RAMEE system pre-conditions the ventilation air, and the cooling unit completes the air-conditioning process and provides the supply air at the required temperature and humidity to maintain the indoor conditions at the average ASHRAE comfort temperature (i.e., 24°C (75.2 F) in summer) [A.38]. The cooling system may sensibly cool the supply air if it is dry enough to provide a satisfactory indoor humidity, but dehumidification is provided to prevent indoor humidity ratios above 12 g/kg (0.012 lb/lb) (about 64% RH at specified indoor temperature).

The heating system consists of radiators that operate with hot water (natural convection) and are installed inside the building. The radiant heating system mainly addresses the building loads and maintains an indoor temperature of 22°C (71.6°C) in the winter [A.38]. Outdoor ventilation air is provided when the building is occupied and the RAMEE system along with an auxiliary heating system heats the ventilation air up to 14°C (57.2 F) to prevent thermal discomfort. During unoccupied

hours, no ventilation air is provided, and the radiant heating system does not operate unless the indoor temperature falls below 15°C (59 F).

The outdoor ventilation rate is maintained at the minimum standard requirement (i.e., 0.5 ACH) when the building is occupied, unless economized cooling is available. During economizer operation, the outdoor ventilation rate can increase up to 4 ACH. The ventilation rate is reduced to 50% and 25% of the design flow rate on Saturdays and Sundays due to lower occupancy, respectively.

4.3. Climatic Conditions

The described office building is studied in Saskatoon (Saskatchewan, cold-dry climate), Chicago (Illinois, cool-humid climate), Miami (Florida, hot-humid climate) and Phoenix (Arizona, hot-dry climate) as the four North American cities that represent different climate zones [A.39]. Figure A.6 shows the yearly distribution of outdoor conditions for each location in three main regions on the psychometric chart; i.e., Region 1 includes low outdoor temperatures when heating is required (i.e., the HVAC system is in heating mode), region 2 includes outdoor conditions when economized cooling is available (lower temperature and lower enthalpy than the indoor), and region 3 includes high temperature and humidity outdoor conditions where cooling and possibly dehumidification is required. The pie graph associated with each building location presents the fraction of a year that the HVAC system operates in each specific region. Typical Meteorological Year (TMY 2 weather data format) [A.40] which contains typical hourly weather data required for yearly building energy analysis is used for this study.

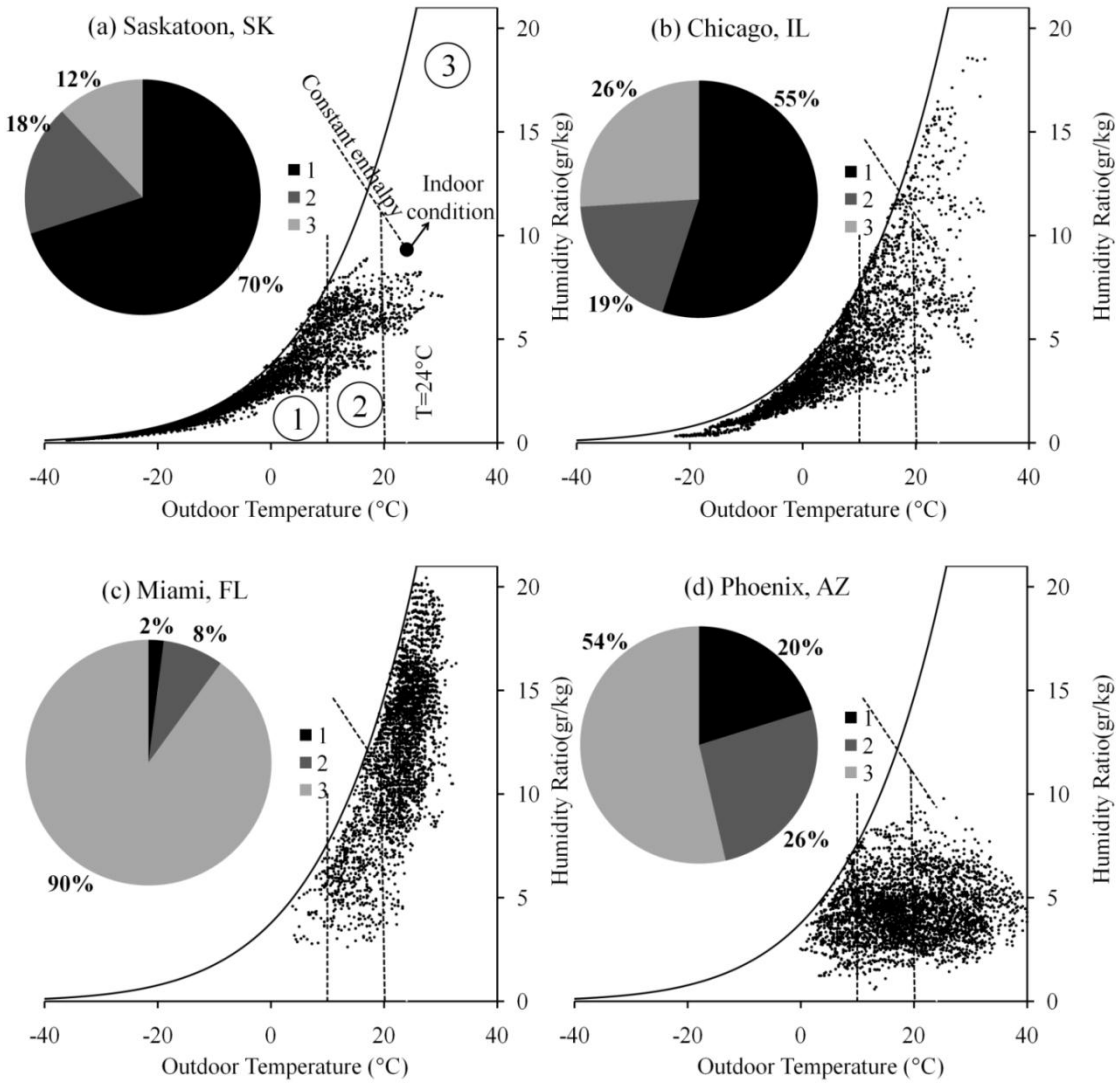

Figure A.6. TMY2 yearly distribution of hourly outdoor conditions and HVAC system operation when heating is required (1), economized cooling is available (2) and cooling is required (3) in (a) Saskatoon, (b) Chicago, (c) Miami and (d) Phoenix.

4.4. Simulation Program

The numerical solution of heat and mass transfer in the RAMEE system for steady-state and balanced air flow rates was developed in previous research [A.12], [A.16], and [A.17]). Akbari et al. [A.41] developed an Artificial Neural Network (ANN) that is able to predict the RAMEE performance. The neural network was subjected to direct pattern search optimization algorithm that is able to find the optimal operating *Cr** at any given condition. The thermal system (including the HVAC system, RAMEE and the building) is simulated using the TRNSYS building

energy simulation tool [A.11] equipped with the Second version of TESS libraries [A.42] working in conjunction with MATLAB 2010 programming language. Figure A.7 schematically shows the dataflow between the TRNSYS model and the ANN.

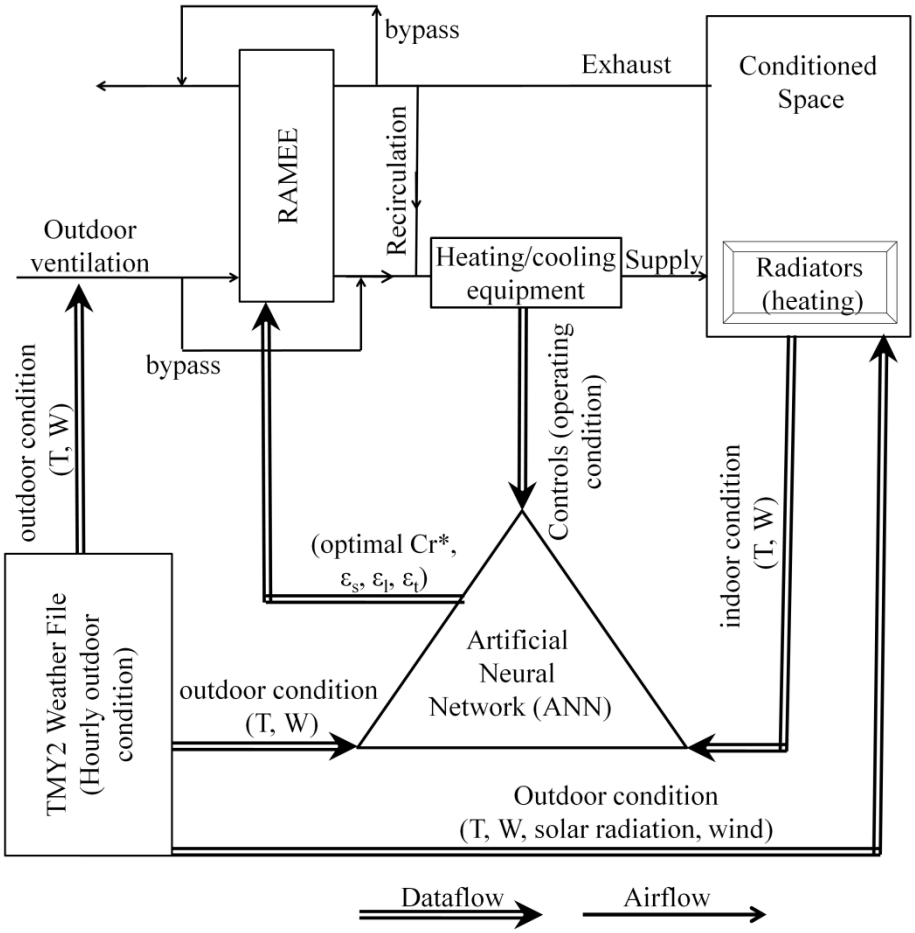

Figure A.7. Schematics of the dataflow between the TRNSYS model and the ANN.

At any specific hour, the TRNSYS simulation gives the hourly building loads based on internal loads, infiltration rate and outdoor condition (temperature, humidity, solar radiation, wind, etc.). Assuming that the RAMEE system is not employed, the condition and flow rate of the supply air to the conditioned space that meets the space loads, minimum ventilation requirement, and the indoor comfort conditions, and the hourly heating/cooling loads are calculated. Based on the indoor and outdoor conditions the TRNSYS model (and the assumed NTU of 10), the ANN predicts the optimal *Cr** and the sensible and latent effectiveness associated with

such optimal *Cr**. The sensible and latent effectiveness are input to the TRNSYS model of the RAMEE system. The operation of RAMEE system under specified effectivenesses preconditions the outdoor ventilation air and reduces the heating/cooling loads. It should be noted that the operation of RAMEE may slightly change the indoor condition compared to the base case. Such a change in indoor condition can affect the system effectiveness and requires iterations to determine the modified system effectiveness based on new indoor conditions. Iterations between the TRNSYS and ANN models are not conducted here, because typical variations in indoor conditions may change the RAMEE effectiveness by less than 0.3% [A.17].

5. Results and Discussions

In this section, the TRNSYS simulation results of the RAMEE employed in different climates are presented. The results mainly focus on the impact of the RAMEE on annual energy consumption and equipment sizes for both heating and cooling seasons at each location. As mentioned before, the ANN predicts the hourly optimal *Cr** at which the RAMEE system should operate to have the peak performance. The optimal *Cr** varies from hour to hour as the outdoor (and possibly indoor) conditions change. Figure A.8 shows the hourly values of optimal *Cr** during one year in each location.

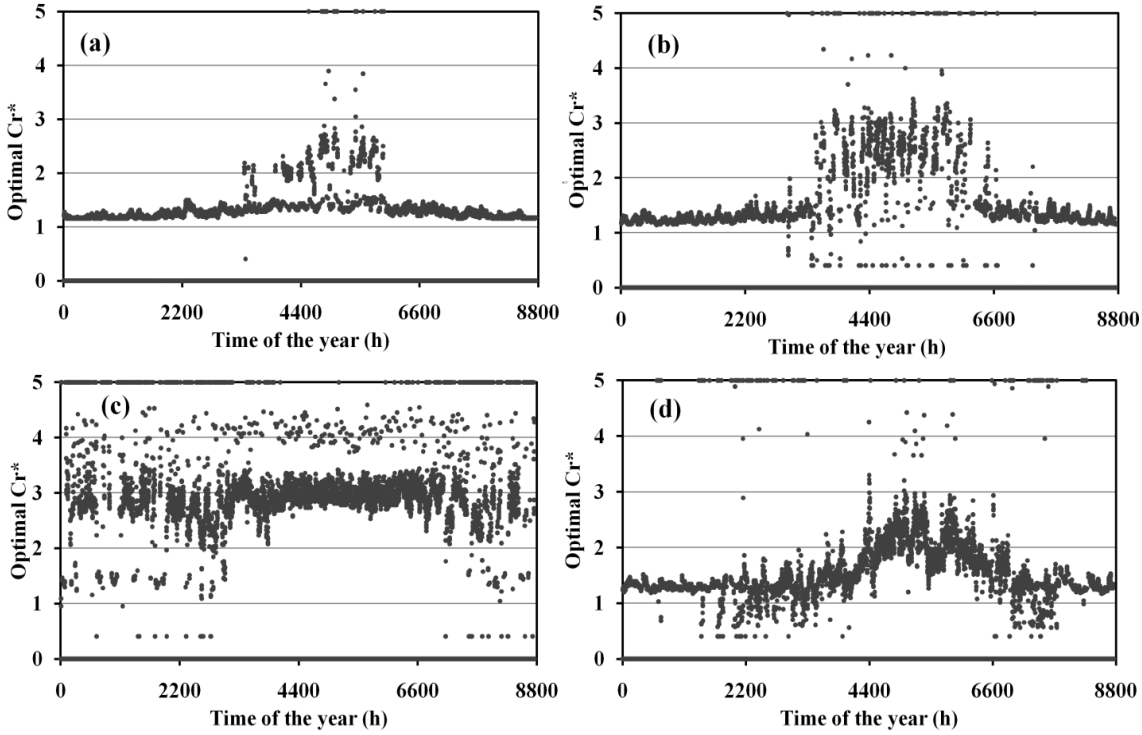

Figure A.8. Yearly variation of hourly optimal Cr* values for different climatic conditions, (a) Saskatoon, (b) Chicago, (c) Miami, and (d) Phoenix.

As is shown in Figure A.8, the optimal *Cr** (Cr^*_{opt}) is higher in the summer than in the winter. For cold climates (Saskatoon and Chicago), the average Cr^*_{opt} is close to 1.2, where for Miami as representative of hot and humid climate, the optimal hourly *Cr** is close to 3 for most of the year. As shown in Equation (A.6), *Cr** is a function of ventilation air and salt solution flow rates. Having the ventilation rate set at the minimum ASHRAE requirement, the solution flow rate has to be controlled to achieve the optimal *Cr**. In the next sections, the annual cooling and heating energy saved due to the use of the RAMEE when operating under hourly optimal *Cr** is presented.

5.1. Heating Season

The results for annual heating saving and reduction in the size of heating system when the RAMEE is operating under hourly optimal *Cr** (i.e., the *Cr** that gives the maximum sensible effectiveness) are presented in Figure A.9.

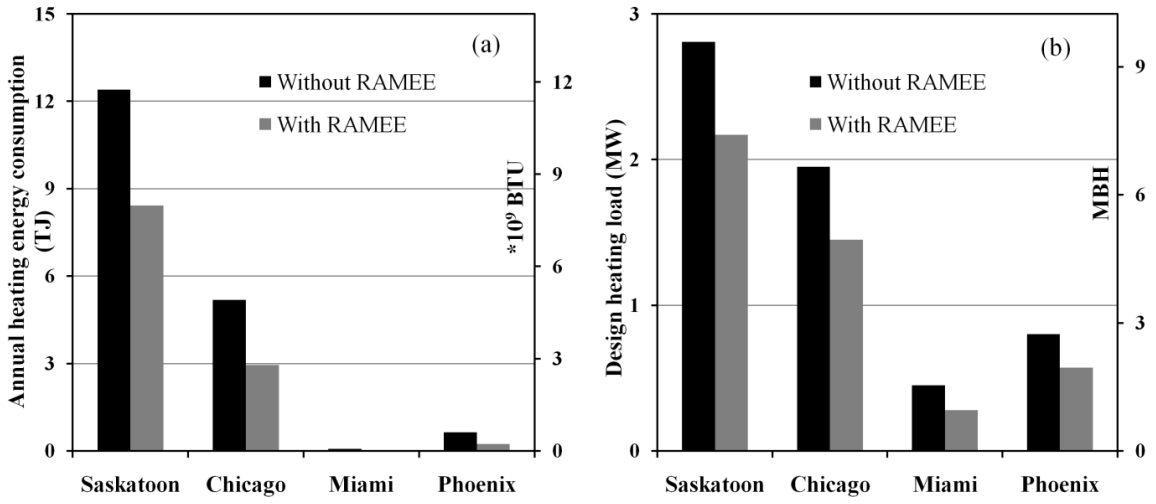

Figure A.9. Impact of the RAMEE on (a) annual heating energy consumption and (b) the size of heating equipment.

The simulation results presented in Figure A.9, indicate that the operation of the RAMEE under optimal *Cr** leads to 32%, 43%, 74% and 63% annual heating energy saving in Saskatoon, Chicago, Miami and Phoenix, respectively. The size of heating equipment is also reduced by 23%, 26%, 38% and 29% in Saskatoon, Chicago, Miami and Phoenix, respectively. The results obtained from a series of TRNSYS simulations of constant effectiveness ERVs indicated that such savings could be achieved if a constant effectiveness ERV with sensible effectiveness of about 77% was employed in the same building during the heating season.

5.2. Cooling Season

The results from the TRNSYS simulation of the RAMEE operating in the office building during the cooling season are presented in Figure A.10. The results show that the RAMEE with economizer reduces the annual cooling energy by 39%, 21%, 8% and 15% in Saskatoon, Chicago, Miami and Phoenix, respectively. The cooling energy saved in Saskatoon (cold climate) is mostly due to the presence of economizer, which saves about 30% of the cooling energy, rather than the RAMEE itself, which saves about 9% of annual cooling energy. This is because Saskatoon

represents a cold climate and free cooling is available for a majority of the time in cooling season (Figure A.6). On the other hand, the savings with the RAMEE account for the majority of cooling energy saved in Miami and the RAMEE system alone reduces the cooling energy by 7%, and adding an economizer results in an additional 1% energy saving. The size of the cooling equipment is reduced by 5% in Saskatoon and Phoenix, and by 10% in Miami and remains unchanged in Chicago.

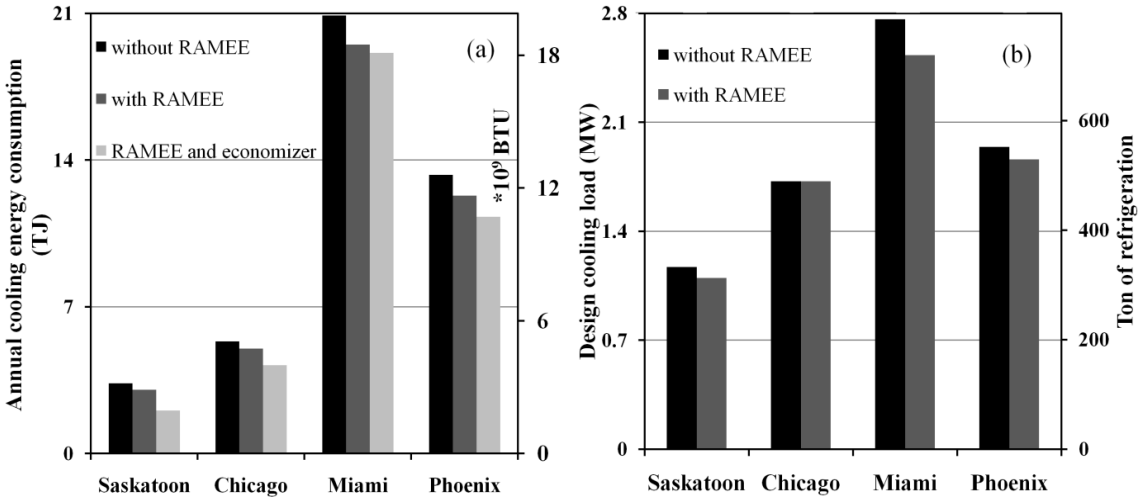

Figure A.10. Impact of the RAMEE system on (a) annual cooling energy consumption and (b) the size of cooling equipment.

It should be noted that Commercial Building Energy Consumption Survey (CBECS) has reported an average energy intensity of 533 MJ/m^2.year (46.9 Thousand BTU/ft^2.year) for HVAC system energy consumption in US office buildings [A.43]. In this research, the energy intensity of the studied office building varies depending on the climate and for the base case it is found 555, 300, 304 and 237 MJ/m^2.year (48.8, 26.4, 26.7 and 20.9 Thousand BTU/ft^2.year) for Saskatoon, Chicago, Miami and Phoenix, respectively. These results are lower than the CBECS average value except for Saskatoon. This could be due to the fact that existing buildings may have equipments operating at lower efficiencies compared to the high-efficient heating and cooling equipments used in this paper (i.e., boiler with 88% nominal combustion efficiency, cooling unit with COP of 3 and fans of 60%

efficiency). In addition, as mentioned previously, the building envelope was improved by using double pane glasses (instead of single pane glasses that are used in the original building) and adding 10 cm (4 in) and 15 cm (6 in) of insulation to walls and roof, respectively. Having the RAMEE and an economizer employed in the office building, the total energy intensity was reduced by 30%, 32%, 5% and 12% in Saskatoon, Chicago, Miami and Phoenix, respectively.

6. Control Based on Average *Cr** Values

For any specific outdoor condition, the implementation of optimal *Cr** requires an accurate control of salt solution flow rate to achieve the desired *Cr** value. As shown in Figure A.8, a scatter variation of optimal hourly *Cr** between 1 and 5 is observed; however, the optimal *Cr** stays fairly constant during each season. For example in Chicago, the optimal *Cr** fluctuates around an average value of 1.2 during the winter and increases to about 2.4 during the summer. Therefore, it may be possible to use a constant salt solution flow rate (*Cr** value) during each season (or during the entire year) rather than having the *Cr** value change every hour. Table A.1 shows the seasonal and yearly weighted averaged values of *Cr** for each location for the office building and its associated standard deviation. The standard deviation is higher for cooling season as the optimal *Cr** has a more scatter variation with *Cr** in summer (shown in Figure A.8). The weighted average *Cr** is defined as:

$$Cr^*_{ave} = \frac{\sum_{i=1}^{8760} Cr^*_{opt,i} \cdot Q_i}{\sum_{i=1}^{8760} \cdot Q_i} \tag{A.13}$$

Where: $Cr^*_{opt,i}$ and Q_i are the optimal *Cr** and energy transfer via the RAMEE system (positive values for both heating and cooling) at i^{th} hour, respectively.

When employing the seasonal average *Cr** value, the *Cr** switches between the heating and cooling set-points according to the season. But, with the yearly average value, the RAMEE system operates with constant *Cr** throughout the year.

Table A.1. Seasonal and yearly weighted average *Cr and associated standard deviation for the office building in each location.**

	Seasonal average *Cr**		**Yearly average**
	Winter (heating)	Summer (cooling)	Heating and cooling
Saskatoon	1.21±0.05	2.19±0.17	1.22±0.29
Chicago	1.24±0.05	2.41±0.31	1.30±0.46
Miami	1.43±0.01	2.91±0.38	2.90±0.41
Phoenix	1.29±0.02	1.76±0.51	1.62±0.54

Table A.2 presents the annual cooling and heating energy savings when the RAMEE system operates under specified average *Cr** values. In order to highlight the effect of implementing average *Cr** values on RAMEE savings, the energy savings with economizer are not included in the cooling savings.

Table A.2. Annual energy saved with the RAMEE system operating with selected average *Cr values.**

	Annual heating energy saved			**Annual cooling energy saved**		
	Optimal *Cr**	Seasonal *Cr**	Yearly *Cr**	Optimal *Cr**	Seasonal *Cr**	Yearly *Cr**
Saskatoon	32%	32%	32%	9%	9%	8%
Chicago	43%	43%	43%	6%	6%	5%
Miami	74%	74%	67%	7%	7%	7%
Phoenix	63%	62%	61%	8%	8%	7%

Based on the results obtained from the TRNSYS simulation of the studied office building (Table A.2), the annual cooling and heating energy savings are nearly the same whether hourly or average *Cr** values are used. Such an insignificant change in annual energy savings can be explained by considering the behavior of the RAMEE effectiveness as a function of *Cr** presented in Figure A.3. As shown in the figure, changing the *Cr** around the optimal value does not influence the RAMEE effectiveness significantly (sensible effectiveness in the winter and total

effectiveness in the summer). For instance, for typical summer conditions presented in Figures A.3c and 3.3e, the total effectiveness is fairly constant for *Cr** values ranging from 2 to 3. Therefore, applying an average *Cr** value instead of the hourly optimal value does not reduce the total effectiveness and consequently the cooling energy saved significantly. As an advantage of implementing yearly average *Cr** value, there is no need to vary the salt solution flow rate as seasons change; however, a negligible reduction in annual savings is observed compared to seasonal average *Cr** approach.

7. Life Cycle Cost Analysis (LCCA)

A Life Cycle Cost Analysis (LCCA) of the RAMEE system is performed to study the system from an economic point of view. The LCCA is carried out for three different alternatives; i.e., the base case where the VAV HVAC system is not equipped with an economizer or ERV, the second alternative that is the VAV HVAC system equipped with the RAMEE, and a case where the HVAC system is equipped with an economizer and the RAMEE. The LCCA is carried out over a 15-year life cycle and the present value method (all expenses converted to the present equivalent value) is used. The LCCA includes capital costs and operation costs. The capital costs (or investment costs) include all the expenses before the project begins to operate and includes the cost of heating and cooling equipment, supply and exhaust fans and the RAMEE. The operational costs are defined as all the expenses that occur during the operation of the system throughout its life cycle and include the energy costs to run the HVAC equipments. The main assumptions for this LCCA approach are: no demolition cost or residual value for the alternative systems, and no extra cost for the maintenance of the RAMEE system. RSMeans Mechanical Cost Data [A.44] that includes the required information about HVAC system equipment

cost is used to estimate the investment costs. Also, the local energy prices in each city are used to calculate the operational costs.

A gas-fired boiler with nominal efficiency of 88% is selected as the heating unit (to satisfies the minimum combustion efficiency of 80% required by ASHRAE standard 90.1: [A.45]). RSMeans Mechanical Cost Data [A.44] suggests an average investment cost of about $68.3/KW ($20/MBH) for cast-iron gas-fired boilers operating in the range of power outputs required for the studied building. An air-cooled air conditioning unit with coefficient of performance (COP) of 3 is selected as the cooling unit (to satisfies ASHRAE standard 90.1 minimum requirement of 2.78 COP [A.45]). The capital cost of the cooling unit based on RSMeans Mechanical Cost Data [A.44] for direct-expansion water chillers is considered to be on average 171$/KW ($600/ton). Centrifugal type HVAC fans that cost $851/$m^3$/s ($0.4/CFM) are used for the LCCA in this study. RSMeans Mechanical Cost Data [A.44] estimates an investment cost of about $1.5/CFM for energy wheels, however, technical papers in the field of air-to-air energy recovery ventilators [A.46-A.47] have expected the manufacturing cost of an ERV as high as $5/CFM. In this paper, the investment cost of the RAMEE is considered $3/CFM.

Table A.3 compares the capital costs for different alternatives. It should be noted that the addition of an economizer to an HVAC system does not change the design heating load. Also, the design cooling load occurs at high temperature outdoor conditions that are out of the economizer's operating range; therefore, the design cooling load remains unchanged when an economizer is employed. The capacity of supply and exhaust fans is similar for all three alternatives. Therefore, the investment cost of RAMEE is similar to the case which RAMEE works with an economizer. In Tables A.3 and 3.4, for simplification, Alt. 1 refers to the base case

HVAC system that is not equipped with a RAMEE, Alt. 2 refers to the HVAC system equipped with a RAMEE and Alt. 3 refers to the HVAC system equipped with a RAMEE and an economizer.

Table A.3. Summary of equipment capacity and HVAC equipment costs for the selected office building.

		Saskatoon		Chicago		Miami		Phoenix	
		Alt. 1	Alt. 2 Alt. 3	Alt. 1	Alt. 2 Alt. 3	Alt. 1	Alt. 2 Alt. 3	Alt. 1	Alt. 2 Alt. 3
Equip. Size	Heating system, KW	2814	2169	1948	1453	449	279	799	569
	Cooling system, KW	1168	1104	1720	1720	2757	2532	1941	1857
	Fan capacity, m^3/s	90	90	95	95	96	96	127	127
Equip. Cost	Heating system, Thousand $US	192.2	148.1	133	99.2	30.7	19.1	54.6	38.9
	Cooling system, Thousand $US	199.2	188.4	293.4	293.4	470.4	432	331.2	316.8
	Cost of fans, Thousand $US	76	76	80.4	80.4	81.6	81.6	108	108
	Cost of RAMEE, Thousand $US	0	72	0	72	0	72	0	72
Total investment, Thousand $US, ($US/m^2)		**467.4 (16.2)**	**484.5 (16.8)**	**506.8 (17.6)**	**545.0 (18.9)**	**582.7 (20.2)**	**604.7 (21.0)**	**493.8 (17.1)**	**535.7 (18.6)**

Table A.4 shows the comparison of three alternatives in operational costs of heating and cooling equipment and the fan energy consumption excluding the pressure drop across the RAMEE system. The fan power is a function of air flow rate, the pressure drop in the supply and exhaust ducting and the fan efficiency. The pressure drop across the ducting system and fan efficiency are assumed to be 4 in. water and 60%, respectively.

Although the RAMEE system reduces the energy consumption of heating and cooling equipment, it imposes an extra pressure drop that increases the energy consumed by the fan(s). Therefore, the life cycle cost of the RAMEE system will be dependent upon the pressure drop across the exchangers.

Table A.4. Summary of annual energy consumption and energy cost of different alternatives excluding the fan energy consumption due to the pressure drop in the RAMEE.

Location	Saskatoon			Chicago			Miami			Phoenix		
Alt. #	Alt 1	Alt 2	Alt 3	Alt 1	Alt 2	Alt 3	Alt 1	Alt 2	Alt 3	Alt 1	Alt 2	Alt 3
Heating energy (TJ/year)	14.1	9.6	9.6	5.9	3.3	3.3	0.1	0.02	0.02	0.7	0.3	0.3
Cooling energy (TJ/year)	1.1	1.0	0.7	1.8	1.7	1.4	7.0	6.5	6.4	4.4	4.1	3.8
Fans (TJ/year)	0.80	0.80	0.89	0.99	0.99	1.08	1.74	1.74	1.78	1.76	1.76	1.86
Natural gas, Thousand m^3/year	373	253	253	156	88	88	2	0.6	0.6	19	7	7
Natural gas, Thousand $US/year	21.4	14.9	14.9	39.8	23.6	23.6	0.6	0.5	0.5	6.8	2.8	2.8
Electricity, TJ/year	1.92	1.81	1.58	2.77	2.66	2.48	8.71	8.24	8.15	6.19	5.86	5.63
Electricity, Thousand $US/year	73.9	69.9	66.0	154.5	148.2	147.8	103.3	98.2	97.9	109	103.2	100.7
Total energy cost, $US/year	**95.3**	**84.8**	**80.9**	**194.3**	**171.8**	**171.4**	**103.9**	**98.7**	**98.4**	**115.8**	**106.0**	**103.5**

Figure A.11 summarizes the LCCA for three alternatives in different locations as a function of pressure drop across each LAMEE. As expected, the greater the pressure drop across the exchangers, the higher the life cycle cost.

Payback Period (*PBP*) is a measure to determine the amount of time it takes the consumer to recover the extra investment cost to purchase the high-efficient alternative as a result of lower operation cost [A.48]. The *PBP*, as defined in Equation A.14, is the ratio of extra investment cost to purchase the more efficient option to the decrease in annual operation costs.

$$PBP = \frac{\Delta IC}{\Delta OC} \tag{A.14}$$

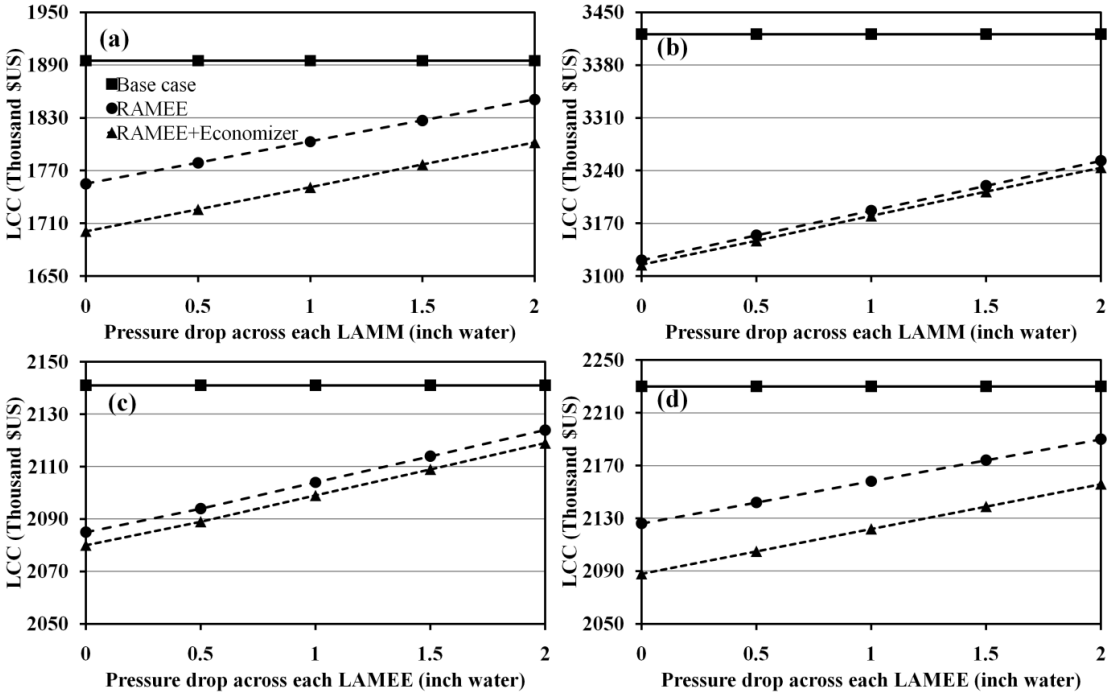

Figure A.11. LCC of the three alternative systems as a function of pressure drop across the RAMEE system in (a) Saskatoon, (b) Chicago, (c) Miami and (d) Phoenix.

Where, *IC* and *OC* stand for investment costs and operational costs, respectively. The *PBP* of employing alternative 3 (i.e., the RAMEE system along with an economizer) in different locations, assuming a total pressure drop of 0.8 in. water across each exchanger (as expected by the manufacturer) is presented in Table A.5.

Table A.5. Payback period of RAMEE and economizer in different locations.

Location	Saskatoon	Chicago	Miami	Phoenix
***PBP*(years)**	1.8	2.0	4.8	4.0

8. Conclusions

The operation of a Run-Around Membrane Energy Exchanger (RAMEE) that is able to transfer heat and moisture between outdoor ventilation and building exhaust air is described in this paper. The RAMEE control varies depending on outdoor condition and whether the building needs heating or cooling. When the HVAC system is on heating mode, the RAMEE operates with maximum sensible

effectiveness. However, a fraction of ventilation air should be bypassed if the full-load operation at maximum sensible effectiveness overheats the outdoor air (also called part-load operation). When the HVAC system is in the cooling mode, the RAMEE should operate with maximum total effectiveness. Using an Artificial Neural Network (ANN) that is trained based on a numerical solution of heat and moisture transfer in the RAMEE, the optimal system performance (optimal hourly *Cr** and associated sensible and latent effectiveness) is predicted when the RAMEE system operates in a 10-storey office building. This building represents 3.34% of US office building stock, and is simulated using the TRNSYS computer program in four different North American locations representing major climatic conditions; i.e., Saskatoon (cold and dry), Chicago (cool and humid), Phoenix (hot and dry) and Miami (hot and humid). The simulation results showed 32% and 43% annual heating energy saving in Saskatoon and Chicago as representatives of cold climate. During the cooling season, the RAMEE operates under maximum absolute total effectiveness (to maximize the reduction of outdoor air enthalpy) and results in about 8% and 15% cooling energy saving when it operates along with an economizer in Miami and Phoenix as hot climates. Since the application of hourly optimal *Cr** requires an accurate control of the salt solution flow rate and causes a transient response, the impact of applying average seasonal and yearly *Cr** was studied. The results show that operating the system under seasonal average *Cr** (i.e., constant salt solution flow rate throughout each season) that switches between cooling and heating season set points has a minimal impact on energy savings. The life cycle cost analysis showed that the pressure drop across the exchangers plays an important role in payback of the RAMEE system. Based on manufacturer's estimation on

RAMEE's pressure drop, the payback period of the RAMEE system was found to be about 2 years in cold climates and 4 to 5 years in hot climates.

9. References of Appendix A

[A.1] L. Fang, G. Clausen, P.O. Fanger, Temperature and humidity: important factors for perception of air quality and for ventilation requirements, ASHRAE Transactions 106 (2) (2000) 503-510.

[A.2] R. Kosonen, F. Tan. The effect of perceived indoor air quality on productivity loss, Energy and buildings 36(10) (2004) 981-986.

[A.3] O. Seppänen, W.J. Fisk, Some quantitative relations between indoor environmental quality and work performance and health, Proceedings of the 10th International Conference on Indoor Air Quality and Climate, Beijing, China, (2005) p.4.

[A.4] M.J. Brandemuehl, J.E. Braun, The Impact of demand-controlled ventilation strategies on energy use in buildings, ASHRAE Transactions 105(2) (1999) 39-50.

[A.5] T.P. McDowell, S. Emmerich, J. Thornton, G. Walton, Integration of Airflow and Energy Simulation using CONTAM and TRNSYS, ASHRAE Transactions 109(2) (2003) 757-770.

[A.6] M. Orme, Estimates of the energy impact of ventilation and associated financial expenditures, Energy and Buildings 33(3) (2001) 199-205.

[A.7] R.W. Besant, C.J. Simonson, Air-to-air exchangers, ASHRAE Journal 45(4), (2003) 42-52.

[A.8] C.J. Simonson, R.W. Besant, Heat and moisture transfer in desiccant coated rotary energy exchangersm, Part I - Numerical model, HVAC & R research 3(4) (1997) 325-350.

[A.9] C.J. Simonson, Heat and energy wheels, Encyclopedia of Energy Engineering and Technology, Volume 2, Edited by Barney Capehart, CRC Press,Boca Raton, FL, (2007) 794-800.

[A.10] L.Z. Zhang, Y. Jiang, Heat and mass transfer in a membrane-based energy recovery ventilator, Journal of Membrane Science 163 (1999) 29-38.

[A.11] S.A. Klein, TRNSYS- A transient system simulation program, Engineering Experiment Station Report 38-13, Solar Energy Laboratory, University of Wisconsin, Madison (2000).

[A.12] H. Fan, C.J. Simonson, R.W. Besant, W. Shang, Run-around heat recovery system using cross-flow flat-plate heat exchangers with aqueous ethylene-glycol as the coupling fluid, ASHRAE Transactions 111(1) (2005) 901-910.

[A.13] M. Seyed-Ahmadi, B. Erb, C.J. Simonson, R.W. Besant, Transient behavior of run-around heat and moisture exchanger system, Part I: Model formulation and verification, International Journal of Heat and Mass Transfer 52(25-26) (2009) 6000-6011.

[A.14] M. Seyed-Ahmadi, B. Erb, C.J. Simonson, R.W. Besant, Transient behavior of run-around heat and moisture exchanger system. Part II: Sensitivity studies for a range of initial conditions, International Journal of Heat and Mass Transfer 52(25-26) (2009) 6012-6020.

[A.15] K. Mahmud, G.I. Mahmood, C.J. Simonson, R.W. Besant, Performance testing of a counter-cross-flow run-around membrane energy exchanger (RAMEE) system for HVAC applications, Energy and Buildings 42(7) (2009) 1139-1147.

[A.16] A. Vali, C.J. Simonson, R.W. Besant, G. Mahmood, Numerical model and effectiveness correlations for a run-around heat recovery system with combined counter and cross flow exchangers, International Journal of Heat and Mass Transfer 52(25-26) (2009) 5827-5840.

[A.17] H.B. Hemingson, C.J. Simonson, R.W. Besant, Steady-state performance of a run-around membrane energy exchanger for a range of outdoor air conditions, Int. J. Heat Mass Transfer 54 (2011) 1814–1824.

[A.18] A. Vali, Modeling a Run-around Heat and Moisture Exchanger Using Two Counter/Cross Flow Exchangers, Master's thesis, University of Saskatchewan, Saskatoon, Sk, Canada, 2010.

[A.19] ANSI/AHRI Standard 1060. 2005. Standard for Rating Air-to-Air Exchangers for Energy Recovery Ventilation Equipment, Air-Conditioning and Refrigeration Institute, Arlington.

[A.20] A. London, W. Kays, The Liquid-Coupled Indirect-Transfer Regenerator for Gas-Turbine Plants, Trans. ASME 73, (1951) 529-542.

[A.21] L.Z. Zhang, J.L. Niu, Effectiveness Correlations for Heat and Moisture Transfer Processes in an Enthalpy Exchanger with Membrane Cores, Journal of Heat Transfer 124(5) (2002) 922-929.

[A.22] F.P. Incropera, D.P. Dewitt, Fundamentals of Heat and Mass Transfer, fifth edition, John Wiley & Sons, New York, (2002) 642–681.

[A.23] ASHRAE. 2004. ANSI/ASHRAE Standard 62-2004, Ventilation for Acceptable Indoor Air Quality (IAQ). Atlanta: American Society of Heating, Refrigerating and Air-Conditioning Engineers, Inc.

[A.24] ASHRAE. 2008. ANSI/ASHRAE Standard 170-2008, Ventilation of Health Care Facilities. Atlanta: American Society of Heating, Refrigerating and Air-Conditioning Engineers, Inc.

[A.25] I. Teke, O. Agra, S.A. Atayilmaz, H. Demir, Determining the best type of heat exchangers for heat recovery, Applied Thermal Engineering 30 (2010) 577-583.

[A.26] M.T. Fauchoux, C.J. Simonson, D.A. Torvi, The effect of energy recovery on perceived air quality, energy consumption, and the economics of an office building, ASHRAE Transactions 113(2) (2007) 437-449.

[A.27] J. Liu, W. Li, J. Liu, B.Wang, Efficiency of Energy Recovery Ventilator with Various Weathers and Its Energy Saving Performance in a Residential Apartment, Energy and Buildings 42(1) (2010) 43-49.

[A.28] M. Rasouli, C.J. Simonson, R.W. Besant, Applicability and optimum control strategy of energy recovery ventilators in different climatic conditions, Energy and Buildings 42(9) (2010) 1376-1385.

[A.29] M. Rasouli, C.J. Simonson, R.W. Besant, Optimal control of energy recovery ventilators and their impact on energy and comfort, submitted to ASHRAE Transactions (2012).

[A.30] M. Rasouli, S. Akbari, H. Hemingson, R.W. Besant, C.J. Simonson, Application of a run-around membrane energy exchanger in an office building HVAC system, ASHRAE Transactions, 117(2) (2011) 686-703.

[A.31] M. Rasouli, C.J. Simonson, R.W. Besant, Energetic, economic and environmental analysis of a health-care facility HVAC system equipped with a run-around membrane energy exchanger, submitted to AHRAE Transactions (2012).

[A.32] G.H. Green, The effect of indoor relative humidity on absenteeism and colds in schools, ASHRAE Transactions 80 (1974) 131–141.

[A.33] K.W. Tham, Effects of temperature and outdoor air supply rate on the performance of call center operators in the tropics, Indoor Air 14 (2004) 119–125.

[A.34] S.A. Mumma, Dedicated outdoor air-dual wheel system control requirements, ASHRAE Transactions 107(1) (2001) 147-155.

[A.35] L.Z. Zhang, J.L. Niu, Energy requirements for conditioning fresh air and the long-term savings with a membrane-based energy recovery ventilator in Hong Kong, Energy 26(2) (2001) 119–135.

[A.36] J.E. Seem, J.M. House, Development and evaluation of optimization-based air economizer strategies, Applied Energy 87 (2010) 910–924.

[A.37] R.S. Briggs, D. Crawley, D. Belzer, Analysis and categorization of the office building stock. GRI-87/0244 (1987) by Battelle, Pacific Northwest Laboratory, for Gas Research Institute (1987).

[A.38] ASHRAE. 2004. ANSI/ASHRAE Standard 55-2004, Thermal Environmental Conditions for Human Occupancy. Atlanta: American Society of Heating, Refrigerating and Air-Conditioning Engineers, Inc.

[A.39] R.S. Briggs, R.G. Lucas, T.Z. Todd, Climate classification for building energy codes and standards: Part 2 - Zone definitions, maps, and comparisons, ASHRAE Transactions 109(1) (2003) 122-30.

[A.40] W. Marion, K. Urban, User's Manual for TMY2s, National Renewable Energy Laboratory (1995).

[A.41] S. Akbari, H.B. Hemingson, D. Beriault, C.J. Simonson, R.W. Besant, Application of neural networks to predict the steady state performance of a Run-Around Membrane Energy Exchanger, Int. J. Heat Mass Transfer 55 (2012) 1628–1641.

[A.42] J.W. Thornton, et al., TESS Libraries 2.0. Thermal Energy System Specialists, LLC. Madison, WI, USA (2009).

[A.43] EIA. 2003. Commercial Building Energy Consumption Survey, Energy Information Administration, U.S. Department of Energy.

[A.44] M.J. Mossman, et al., RSMeans Mechanical cost data, 33rd annual edition (2010).

[A.45] ASHRAE. 2004. ANSI/ASHRAE Standard 90.1-2004. Energy Standard for Buildings Except Low-Rise Residential Buildings, Atlanta: American Society of Heating, Refrigerating and Air-Conditioning Engineers, Inc.

[A.46] R.W. Besant, C.J. Simonson, Air-to-air energy recovery, ASHRAE Journal 42(5) (2000) 31-38.

[A.47] J.R. Turpin, Hybrid Systems Offer the Best of Both Worlds, ACHRNews, (2000) p. 18.

[A.48] G. Rosenquist, K. Coughlin, L. Dale, J. McMahon, S. Meyers, Life-cycle cost and payback period analysis for commercial unitary air conditioners, Energy Analysis Department, Environmental Energy Technologies Division, Ernest Orlando Lawrence Berkeley National Laboratory, University of California at Berkley, (2004) LBNL-54244.

APPENDIX B

REQUIRED DATA TO REPRODUCE THE NN NETWORKS

B.1. Nonlinear model of a neuron

A simple mathematical model of the first neuron in the first hidden layer (Fig. 7) is presented in Fig. B1.

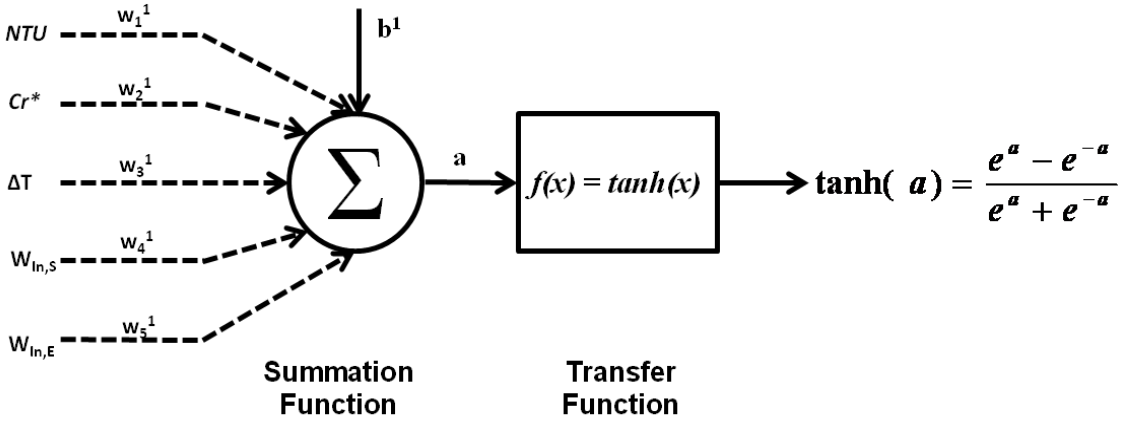

Figure B.1. Block diagram for the first neuron in the first hidden layer of the steady-state neural models.

The input signals, corresponding weights and biases, and the output of this neuron which is one of the inputs of the neurons in the next layer are shown in the Fig. B1. According to the notation was used to present weights and biases in appendix B2:

$$iw_{\{1,i\}} = \begin{pmatrix} 0.19859 & -1.8995 & -0.050675 & 0.0087069 & 0.046394 \\ 0.55701 & 0.3513 & -0.096322 & -0.43183 & -0.014339 \\ -0.19905 & -0.29534 & 0.049543 & 0.051683 & -0.066359 \\ 0.047809 & 0.15776 & 0.020629 & 0.0027475 & -0.00025207 \\ 0.4518 & -1.5997 & 0.036601 & 0.13825 & -0.037164 \\ 0.30161 & -0.074799 & -0.033415 & 0.052818 & -0.015584 \\ -0.0032581 & 0.27176 & 0.013249 & -0.0017261 & -0.0035854 \\ 0.17796 & 0.76575 & 0.27456 & -0.2898 & -0.21276 \\ 2.7969 & -0.014024 & 0.13183 & 0.015218 & 0.0067013 \\ -2.5942 & 0.13637 & 0.13636 & -0.022977 & 0.0034435 \end{pmatrix}$$

where,

$$iw_{\{1,i\}} = \begin{pmatrix} w_1^1 & w_2^1 & w_3^1 & w_4^1 & w_5^1 \\ w_1^2 & w_2^2 & w_3^2 & w_4^2 & w_5^2 \\ w_1^3 & w_2^3 & w_3^3 & w_4^3 & w_5^3 \\ w_1^4 & w_2^4 & w_3^4 & w_4^4 & w_5^4 \\ w_1^5 & w_2^5 & w_3^5 & w_4^5 & w_5^5 \\ w_1^6 & w_2^6 & w_3^6 & w_4^6 & w_5^6 \\ w_1^7 & w_2^7 & w_3^7 & w_4^7 & w_5^7 \\ w_1^8 & w_2^8 & w_3^8 & w_4^8 & w_5^8 \\ w_1^9 & w_2^9 & w_3^9 & w_4^9 & w_5^9 \\ w_1^{10} & w_2^{10} & w_3^{10} & w_4^{10} & w_5^{10} \end{pmatrix}$$

therefore,

w_1^1=0.19859, w_2^1=-1.8995, w_3^1=-0.050675, w_4^1=0.0087069, and w_5^1=0.046394.

According to this,

$a = w_1^1 \times NTU + w_2^1 \times Cr^* + w_3^1 \times \Delta T + w_4^1 \times w_{In,S} + w_5^1 \times w_{In,E} + b^1$ and the output of this neuron is equal to *tanh(a).*

B.2. Required data to reproduce the steady-state neural networks

The order of the inputs and corresponding units are as follows:

1) *NTU*, dimensionless parameter, value should be between 1 and 15
2) Cr^*, dimensionless parameter, value should be between 0.4 and 5
3) $\Delta T = T_{In,S} - T_{In,E}$ (°C)
4) $W_{in,s}$, supply inlet humidity ratio (kg_v/kg_a)
5) $W_{in,E}$, exhaust inlet humidity ratio, value should be between 0 to 0.012 (kg_v/kg_a)

** Output units are °C and kg_v/kg_a for sensible and latent NNs respectively.

Table B.1 shows the architecture and properties of steady-state sensible and latent networks.

Table B.1. Architecture and configuration of the steady-state NN models.

Number Of Inputs	5
Number Of Outputs	1
Number Of Hidden Layers	2
Number Of Neurons In each Hidden Layer	10
Number Of Neurons In Output Layer	1
Network Type	Fully Connected With Biases For All Neurons
Hidden Layers Transfer Function	Tangent Hyperbolic (Tangent Sigmoid)
Output Layer Transfer Function	Linear

B.2.1.Weights and biases of the steady-state sensible model:

$iw_{\{1,i\}}$:

0.19859	-1.8995	-0.050675	0.0087069	0.046394
0.55701	0.3513	-0.096322	-0.43183	-0.014339
-0.19905	-0.29534	0.049543	0.051683	-0.066359
0.047809	0.15776	0.020629	0.0027475	-0.00025207
0.4518	-1.5997	0.036601	0.13825	-0.037164
0.30161	-0.074799	-0.033415	0.052818	-0.015584
-0.0032581	0.27176	0.013249	-0.0017261	-0.0035854
0.17796	0.76575	0.27456	-0.2898	-0.21276
2.7969	-0.014024	0.13183	0.015218	0.0067013
-2.5942	0.13637	0.13636	-0.022977	0.0034435

$lw_{\{2,1\}}$:

-0.20211	-0.018959	0.0014601	1.9937	0.17699	-0.2603	-1.3075	0.011486	-0.42727	-0.10778
-2.5418	0.29917	1.0085	-6.7817	0.58411	0.095943	5.2114	-0.16214	1.107	3.3736
0.30516	-1.4597	-3.014	9.0806	-0.0077565	-3.6437	7.9961	0.74935	-0.76664	-1.9835
0.62544	-1.6614	-3.2256	9.8435	0.21877	-5.5294	9.2042	0.73679	-1.3001	-3.0227
0.19498	0.093785	0.23791	-0.53926	-0.18744	-5.739	0.74539	-0.064332	-7.0494	-2.4595
-0.24399	1.3098	1.3983	-4.3862	-0.84845	2.6108	9.1807	-0.033177	3.3937	5.8874
1.965	-0.12833	3.7921	0.27585	-0.9182	-0.83747	-1.5919	0.46186	2.7132	-3.9601
1.2391	0.011038	0.45671	0.42337	-0.90527	-0.72088	1.1208	-0.035813	-1.4319	-3.6435
-0.9247	-0.58362	-3.4638	-0.55482	-0.85346	4.0863	7.2509	-0.68601	1.5156	0.22306
-0.29898	-1.1106	-0.70939	7.3714	0.89185	-1.6913	-11.4691	-0.8235	-4.9862	-6.8673

$lw_{\{3,2\}}$:

19.2295	0.98581	-6.4213	4.789	7.1262	-1.9999	0.12296	3.0646	1.0968	-1.8246

$b_{\{1\}}$:

-2.014
-1.1277
0.42303
-0.030901
-1.3156
1.0397
-0.14857
-1.0683
4.4026
-4.1729

$b_{\{2\}}$:

0.37314
0.42003
8.4095
9.9614
11.0576
2.7345
-7.2423
-1.0131
-0.30632
-4.6882

$b_{\{3\}}$:

-7.3236

B.2.2. Weights and biases of the steady-state latent model:

$iw_{\{1,i\}}$:

-0.37319	0.19729	-0.0333	0.11523	0.16561
-0.56216	2.1161	-0.21931	-0.52022	0.14793
0.17564	0.19331	-0.02797	-0.22456	-0.14622
-0.10529	0.007498	0.045048	-0.00495	-0.00123
-0.13019	1.5748	0.019242	-0.04555	0.001231
0.018708	-1.258	-0.10701	0.031246	0.018157
-0.5447	0.005239	-0.0002	-0.05299	0.017865
-1.3027	0.040076	0.017709	0.089089	-0.07678
-0.0865	0.00986	0.039782	0.010949	-0.01164
-0.39433	-3.5122	-0.10761	0.047614	0.040074

$lw_{\{2,1\}}$:

-0.58332	0.19004	5.1174	14.4156	2.9211	6.3148	-9.0278	4.4717	-13.6667	-0.24206
-3.7422	0.5046	-11.2486	2.9143	-1.3096	0.028233	-4.2129	-6.133	-2.9818	-0.60127
-1.194	0.079094	-4.2338	-8.7684	-3.1933	-4.8529	7.1723	-1.2265	6.9083	0.91086
0.41364	0.0268	-3.1323	-9.6768	0.12714	2.2281	6.9637	-4.126	8.6684	2.0715
0.11528	0.071987	1.8762	2.7616	0.70402	0.91969	-5.3546	1.3077	-2.0334	0.84534
0.046937	-0.04151	-1.3869	-0.37227	0.70267	0.52573	-2.5485	-0.75901	-1.9673	-0.90664
0.074215	0.055709	1.5077	2.8915	-0.7393	1.4933	1.8872	0.82965	0.83967	0.64068
-0.04276	0.027669	1.1806	0.11884	-0.3479	-0.09446	1.1586	0.3676	1.5729	0.92266
0.016822	0.063011	-5.391	-0.21825	-1.9291	-2.1371	0.074534	-9.1461	-4.8209	-0.65391
-0.13397	-0.01931	-1.8547	-3.3105	0.34493	-1.3085	-5.9946	0.27003	2.6677	0.7802

$lw_{\{3,2\}}$:

-0.40614	0.86502	-0.96935	1.7124	-5.7103	11.1224	-5.3467	20.6634	-0.805	12.8668

$b_{\{1\}}$:

1.3042
1.7629
-1.3473
0.15486
1.2889
-1.7647
-1.7173
-2.7044
-0.06962
-4.0119

$b_{\{2\}}$:

0.55699
-18.3546
1.5114
6.7083
-0.47945
-5.1987
4.3993
3.4232
-15.8696
-8.6699

$b_{\{3\}}$:

12.7446

B.3. Data required to reproduce the transient neural networks

Units for the in are as follows:

1) *NTU*, dimensionless parameter, value should be between 1 and 13
2) *Cr**, dimensionless parameter, value should be between 1 and 5
3) The units for all inputs and outputs including temperature and humidity ratio values or temperature and humidity ratio differences are °C and g_v/kg_a respectively.

Table B.2 shows the architecture and properties of transient sensible and latent networks.

Table B.2. Architecture and configuration of the transient NN models.

Number Of Inputs	12
Number Of Outputs	1
Number Of Hidden Layers	2
Number Of Neurons In each Hidden Layer	16
Number Of Neurons In Output Layer	1
Network Type	Fully Connected With Biases For All Neurons
Hidden Layers Transfer Function	Tangent Hyperbolic (Tangent Sigmoid)
Output Layer Transfer Function	Linear

B.3.1.Weights and biases of the transient sensible model:

$iw_{\{1,i\}}$:

-0.058831	-0.027797	4.5091	-1.4908	2.4316	-4.2195	6.4725	-4.6348	0.23222	0.28811	-0.76517	1.1743
-0.44938	0.41272	0.49324	0.48591	0.11585	0.18385	-0.060641	-0.28539	-0.29515	0.69868	-0.85794	0.53774
-0.039332	0.049923	-0.24137	-0.00062026	-0.55638	0.61913	-0.89832	1.533	0.21171	0.10957	-0.007459	-0.24378
-0.38661	1.578	0.4037	0.53255	0.036522	0.22258	-0.098412	-0.2603	-0.35338	0.71617	-0.95969	0.63068
0.086759	0.023188	-1.1441	0.21228	1.1201	-1.0177	0.63242	0.072628	-0.84903	0.18941	0.025838	0.77725
-0.028342	-0.031982	-1.1121	0.43061	1.6612	-3.3077	6.6756	-4.2088	0.53075	1.0383	-0.74434	-0.58759
-0.15269	0.87889	0.078152	-0.019493	0.14322	-0.26893	0.42354	-0.42966	-0.059596	0.082831	-0.11142	0.043815
0.011007	0.029774	0.043526	0.36251	-2.0587	4.8853	-10.199	7.0264	-1.0345	-1.5278	1.4375	0.52607
0.004476	-0.0087709	-0.17624	1.4404	-0.50057	1.1331	-2.3144	1.6206	-0.32679	0.53178	-0.41095	-0.5777
0.063599	-0.73348	-0.13578	0.033025	-0.10785	0.23877	-0.32661	0.30427	0.046155	-0.036025	0.065906	-0.019752
-1.4298	-0.072005	-0.2782	0.085069	0.11487	-0.22991	0.32335	-0.2667	-0.062987	0.087883	-0.1605	0.12884
2.6281	-0.41145	0.31312	-0.42068	0.42136	0.94267	-1.3578	0.533	-0.39224	0.8655	-0.50148	-0.21886
-0.12573	0.14402	-1.2116	-0.15751	-4.4521	2.4623	0.57413	-3.8844	2.0929	1.1447	-0.83645	0.4965
-0.072184	0.0086125	0.85237	-0.27822	-1.1984	1.3964	-1.4445	0.65588	0.62	-0.36264	0.19776	-0.44558
0.00090591	0.01267	-0.23166	-1.0988	0.18097	-0.56991	1.4633	-1.0053	0.34679	-0.47651	0.41279	0.33001
-1.9089	-0.047788	0.58839	0.085893	-0.02128	-0.11581	0.10567	0.0057413	-0.042748	0.095224	-0.14182	0.091517

$lw_{\{2,1\}}$:

-14.6179	-17.6618	-71.306	8.9869	0.98781	3.5623	10.2345	0.90799	5.0602	4.6834	-0.32966	-38.9166	-3.6446	-1.3637	0.26066	-35.8913
-4.5961	-1.5273	-0.35215	1.6806	-9.1672	3.1627	-2.0484	2.9662	-1.7335	-5.9128	3.5623	-7.6892	1.2703	10.7391	-1.8931	-13.1819
-6.4513	14.6578	-2.914	-6.2054	7.4225	1.6209	0.62581	1.8925	0.90999	6.6684	-14.7665	-9.7839	-1.4798	-4.4175	13.0207	-2.0723
-0.047797	2.595	-1.0767	-3.865	2.5307	1.5926	-1.0414	0.89881	-1.2313	-1.836	-11.549	-0.24498	-0.15231	5.0539	-1.7187	2.4369
-6.6817	0.7423	1.1933	1.0337	-4.7445	0.49345	1.0425	1.4461	-4.8427	2.6765	-36.5713	-0.45425	0.26829	-6.2274	-1.734	7.199
-0.05793	-0.79338	-0.59036	0.62597	0.19923	-0.94736	-0.5283	-0.90073	-2.1314	5.0307	-11.7168	0.058462	0.036164	-0.25858	-3.9607	-6.9893
0.0068174	-0.082149	-0.10871	-0.014976	0.23842	0.1405	0.16461	0.078508	-0.38655	0.33373	-8.225	-0.025553	-0.013227	0.49291	-0.49739	1.2481
24.1691	-1.8726	37.8914	-3.7694	-1.1714	-1.4795	-4.5504	-10.9115	1.2967	-16.6806	0.25831	-6.2882	5.6263	-8.8454	2.0632	-2.1608
11.7368	0.65348	-10.2874	-3.5817	-1.4339	-2.4059	3.87	-5.7233	-1.8794	4.4248	-4.8385	0.2036	-3.8822	-0.80604	-7.2406	-0.18142
-2.4266	-1.8904	-6.2216	0.1525	-2.5934	-2.4537	-1.6463	-3.7224	-0.0070375	-3.6953	-8.8837	-0.35994	-0.56859	3.9272	2.1825	-2.2528
-0.28497	-7.1543	-1.3215	1.3707	1.5035	-1.0229	0.81034	-1.4219	-8.0457	-3.0624	-4.8542	0.69365	0.038963	1.1296	-9.7412	-5.163
-7.4672	-7.5918	-20.494	6.9748	-3.4802	-0.76878	-3.019	23.4322	12.4635	6.0769	35.6517	-7.1413	4.3561	30.8113	1.1638	-21.7601
11.2421	4.9557	-10.6425	3.7031	-11.3481	2.7839	-5.2316	6.6534	-11.3111	-0.8418	26.4699	-4.3494	6.3349	-7.4798	5.2154	-18.4751
12.6998	-8.6045	7.0657	10.0554	1.3002	-4.7097	0.18886	2.0532	-1.2821	8.6295	13.3225	-3.7703	-9.8192	-5.4018	5.2289	-1.5631
-0.19316	2.387	3.3659	-3.4223	-1.5432	-2.0486	-0.23093	-0.62332	-1.0893	0.398	-6.8523	-0.3186	0.8801	-1.3307	-1.9942	-0.36755
1.512	-0.27552	0.079634	0.49943	-2.53	-1.4288	0.20504	-0.94451	0.057416	0.29035	16.4362	0.0099114	-0.066988	-5.562	2.8893	-5.9715

$lw_{\{3,2\}}$:

-0.0038227	0.0038079	0.0034739	-0.27963	-0.089507	-0.040618	4.6197	-0.0029999	0.011775	-0.011928	0.042645	-0.044141	-0.0049294	0.0027295	0.058892	-0.059199

$b_{\{1\}}$:

-1.7387
1.5576
0.65777
2.7507
1.1879
0.5149
0.60562
-0.31912
0.9097
-0.98298
-3.7555
1.4345
1.9753
-1.1243
-0.65397
-3.7643

$b_{\{2\}}$:

28.3702
6.7076
-6.5005
-6.5886
-22.566
-17.6047
-6.0652
-3.714
-8.93
-6.8154
-5.1515
1.1083
-6.5223
20.3692
-5.6616
8.5012

$b_{\{3\}}$:

-1.7165

B.3.2.Weights and biases of the transient latent model:

$iw_{\{1,i\}}$:

-0.19886	-0.092166	0.52368	-0.46268	0.082066	0.75129	-1.8276	2.2448	-0.18444	0.12555	-0.19832	0.46363
0.097573	0.023546	0.88029	0.68451	0.13785	-0.11936	0.24601	-0.21142	0.053058	-0.17224	0.11138	-0.092555
-0.010147	0.0059624	-0.49813	-0.29601	-0.3741	0.98635	-1.6246	1.2528	0.092277	-0.2551	0.28161	-0.23534
-0.41314	-0.23744	1.673	-0.3473	1.9008	-1.1472	0.58821	-1.1109	-0.020762	-1.6377	1.9035	-1.2574
0.64165	-0.0818	1.007	-0.80025	0.56847	-1.4007	2.5511	-2.0366	0.074294	0.096002	-0.31438	0.34182
0.027766	0.0084233	0.027184	0.40829	0.04136	-0.2274	0.37458	-0.31065	-0.044946	0.052167	-0.040321	0.0091233
0.076444	-5.0498	-0.25469	0.29563	-0.096078	0.20175	-0.32734	0.22478	-0.029317	0.021288	0.044478	-0.10575
0.13408	2.6383	0.34229	0.15458	0.26012	-0.48059	0.90677	-0.77766	-0.046741	0.12135	-0.16964	0.2073
-0.1394	-0.073716	1.2744	2.0032	0.84968	-1.2	1.6027	-1.2985	0.035769	0.04015	-0.5202	-1.5395
-0.35897	0.069278	0.17166	-0.20014	-0.47589	0.67778	-1.3687	0.98802	-0.035796	-0.12885	0.043844	-0.19837
-0.05946	-0.021451	1.1472	-1.087	0.69296	-1.1574	1.8293	-1.468	0.0054088	0.23494	-0.49124	0.53295
-0.060187	4.541	0.23268	-0.13122	0.091305	-0.20924	0.33484	-0.24912	0.0023139	0.011104	-0.056529	0.093049
-0.060284	-0.019248	1.0079	-1.0699	0.65982	-1.0857	1.6957	-1.3453	-0.0053526	0.23942	-0.47061	0.50845
0.22695	0.025803	-0.25253	-0.30326	-0.083205	0.29442	-0.5851	0.52227	-0.037842	0.084954	-0.048129	0.023295
-0.12096	-0.010965	-0.54019	-0.55177	0.015083	0.16944	-0.47681	0.60094	-0.094786	0.22383	-0.17338	0.14952
0.24186	-0.0077457	-0.0978	0.31607	0.11308	-0.16898	0.32761	-0.241	-0.0038634	0.048415	-0.022428	0.057314

$lw_{\{2,1\}}$:

102.1743	-25.8478	-98.1504	31.1194	-12.3844	-30.8141	-5.0451	11.5173	-11.8313	3.1156	66.9412	-12.0125	51.3057	40.8448	-54.834	85.1798
3.3092	-1.297	2.5935	-0.22589	1.0907	2.5992	-1.7199	0.043728	-0.6442	-1.0745	-0.69246	-2.2816	1.9195	-0.15444	-5.2537	-5.4583
24.108	11.8004	-7.7879	-10.9114	3.3011	1.1928	2.3516	1.4158	-1.311	-1.3147	-6.7299	5.0359	11.8595	20.2551	27.7038	-18.351
10.0218	0.23605	-3.7562	0.39679	0.40251	-2.2896	-3.1	-0.76625	-4.7406	-1.4659	1.4021	-0.17089	-3.4186	2.1784	-5.3908	-8.0347
5.8399	-2.0427	-3.0484	-3.1959	-0.72765	-2.5442	-0.88393	-0.14096	1.0979	-1.0564	-3.5905	-0.79602	4.2843	-5.8091	-0.14372	-0.62603
-1.6171	-2.9891	13.3046	-1.6432	-3.2326	-0.15512	0.17518	1.6005	-4.6015	-1.8551	3.14	1.8997	-0.88902	6.8157	-8.2876	7.2002
14.2517	-1.8881	0.67501	-4.6917	-8.5986	5.3627	0.031857	-4.8046	-2.9599	-1.7863	14.3234	-13.0469	-14.042	-0.99836	-8.6789	1.031
-0.90666	-4.5489	1.5655	-0.09048	-2.1318	2.6083	1.8174	0.90412	-1.8185	-1.3119	-2.5291	2.021	3.9301	3.5928	8.9767	-0.57365
30.1595	-7.0421	0.70326	-15.1157	-12.842	10.4606	-4.1905	-2.7721	8.4417	-6.208	-0.5864	21.469	-9.8608	11.1936	-23.4504	-28.5264
0.63369	-4.1278	-5.7034	0.033807	-2.889	-1.379	-3.2984	-2.9097	-0.58078	-1.3757	0.92397	-0.085487	-2.633	-12.4283	4.6665	-2.8158
-17.0668	4.9928	1.128	-0.85331	-0.94646	1.6608	-1.0546	0.56809	0.32944	-0.35846	5.9304	-1.353	7.2855	-2.4646	5.5523	3.3621
-20.692	-3.4243	-3.1808	4.9537	-0.96023	-0.41036	1.2714	-0.16329	1.2375	1.0413	1.0345	1.3259	-4.1939	-2.4914	-8.9262	2.5894
0.25545	-0.65716	2.5948	-0.37577	-1.8018	0.73174	-2.8304	0.281	-4.4022	-1.0403	2.7361	-3.5048	3.9247	1.511	8.0104	0.39557
-1.3594	-1.6454	12.244	0.27921	0.68995	3.4379	1.8842	0.99902	0.89755	-0.81465	-1.6298	-0.96928	4.1633	3.8569	3.1079	-0.58119
-9.6361	0.60059	-4.6391	-4.8661	0.91572	1.1403	1.2043	-4.2939	3.9249	-0.58227	7.1886	-8.4498	-6.0953	-6.7952	-7.8906	0.072419
5.764	0.023324	3.0842	-3.7803	2.8502	-0.59915	0.056978	-0.037398	1.6761	0.11324	-5.4425	0.010788	5.7199	-0.0013572	-1.5165	-1.1077

$lw_{\{3,2\}}$:

-0.002424	-1.8613	0.0042473	-0.20422	0.78328	0.019343	-0.18104	0.063481	0.033905	0.033404	0.1386	0.46976	-0.38519	-0.036312	0.29923	-3.2001

$b_{\{1\}}$:

3.4681
-1.1992
-1.8684
2.9612
2.4757
0.87211
-4.4284
2.3856
4.6341
-0.59166
0.15591
4.286
0.30599
1.3992
2.178
1.437

$b_{\{2\}}$:

-310.8106
4.7396
-50.2682
-0.12365
-2.1127
11.069
16.65
-11.7906
24.1689
4.3859
3.0376
22.7781
-8.2131
2.5922
19.0345
-0.16854

$b_{\{3\}}$:

0.90915

APPENDIX C

COMPUTER CODES DEVELOPED TO OPTIMIZE THE RAMEE PERFORMANCE

Main Optimization Code

```
function [ OptimumValues ] = optimization( in ) %main function,
in(1,i)=NTU, in(2,i)=delta T, in(3,i)=Woutdoor (kg/kg),
in(4,i)=Windoor (kg/kg), in(5,i)= optimization type: 1=maximum
positive sensible effectiveness, 2= maximum positive total
effectiveness, 3=minimum total effectiveness, 0=system is off
    options = psoptimset('TolFun',1.0000e-002);     %pattern search
function options
    z=size(in);                                     %z is a 1by2
function indicating the size of the input matrix "in"
    x(2) = 3;
    y=3;                        %initial optimum value for Cr*
    for i=1:z(2)                %algorithm is being repeated for
each column of the "in" matrix. each column is the inputs for
optimization function for one hour. Number of columns is equal to
number of hours being optimized.
        if (in(5,i)==1)     %5th row of the "in" matrix is equal to
1, 2, 3, or 0 indicating the definition of optimization in that
specific hours
            [x,fval,exitflag] =
patternsearch(@SenPS,[in(1,i);y;in(2,i);in(3,i);in(4,i)],[],[],[],[]
,[in(1,i);.4;in(2,i);in(3,i);in(4,i)],[in(1,i);5;in(2,i);in(3,i);in(
4,i)],[],options);  %first optimization function, target function is
SenPS which returns -1*sensible effectiveness of the RAMEE by
running the NN models. pattrnsearch function can only find the
minimum of the target function not the maximum.
            OptimumValues(5,i) = -1*fval;   % Returns the maximum
positive sensible effectiveness value
            OptimumValues(4,i) = x(2);      % Returns the Optimum
Cr* that results in the maximum positive sensible effectiveness
            OptimumValues(6,i) = exitflag;  % Exitflag to make sure
the patternseach algorithm converged properly
            elseif (in(5,i)==2)
            [x,fval,exitflag] =
patternsearch(@TotPPS,[in(1,i);y;in(2,i);in(3,i);in(4,i)],[],[],[],[
],[in(1,i);.4;in(2,i);in(3,i);in(4,i)],[in(1,i);5;in(2,i);in(3,i);in
(4,i)],[],options); %second optimization function, target function
is TotPPS which returns -1*total effectiveness of the RAMEE by
running the NN models.
            OptimumValues(5,i) = -1*fval;   % Returns the maximum
positive total effectiveness value
            OptimumValues(4,i) = x(2);      % Returns the Optimum
Cr* that results in the maximum positive total effectiveness
            OptimumValues(6,i) = exitflag;  % Exitflag to make sure
the patternseach algorithm converged properly
            elseif (in(5,i)==3)
            [x,fval,exitflag] =
patternsearch(@TotNPS,[in(1,i);y;in(2,i);in(3,i);in(4,i)],[],[],[],[
],[in(1,i);.4;in(2,i);in(3,i);in(4,i)],[in(1,i);5;in(2,i);in(3,i);in
(4,i)],[],options); %third optimization function, target function is
TotNPS which returns total effectiveness of the RAMEE by running the
NN models.
```

```
            OptimumValues(5,i) = fval;      % Returns the minimum
total effectiveness value
            OptimumValues(4,i) = x(2);      % Returns the Optimum
Cr* that results in the minimum total effectiveness
            OptimumValues(6,i) = exitflag;  % Exitflag to make sure
the patternseach algorithm converged properly
        end
    OptimumValues(1,i) = in(1,i);   %NTU
    OptimumValues(2,i) = in(2,i);   %DT
    OptimumValues(3,i) = in(3,i);   %Wout
        if (in(5,i)==0) %if control is zero returns system is off
and returns -10 as Cr*, Effectiveness, and Exitflag
            OptimumValues(4,i) = -10;
            OptimumValues(5,i) = -10;
            OptimumValues(6,i) = -10;
        end
    end
OptimumValues;
end
```

Sensible effectiveness target function (SenPS)

```
function [E] = OptimumEffectiveness( z )    %Loads the sensible
steady-state network and returns the sensible effectiveness
    load C:\Nets\netS
    E=-(sim(netS,z)/z(3));
end
```

Negative latent effectiveness target function (TotPPS)

```
function [Et] = OptimumEffectiveness( z )   %Loads the sensible and
latent steady-state networks and returns the -1*total effectiveness
    load C:\Nets\netS
    load C:\Nets\netL
    Et=-(((sim(netS,z)/z(3))+(2500*(z(4)-
z(5))/z(3))*(sim(netL,z)/(z(4)-z(5))))/(1+(2500*(z(4)-z(5))/z(3))));
end
```

Positive latent effectiveness target function (TotNPS)

```
function [Et] = OptimumEffectiveness( z ) %Loads the sensible and
latent steady-state networks and returns the total effectiveness
    load C:\Nets\netS
    load C:\Nets\netL
    Et=(((sim(netS,z)/z(3))+(2500*(z(4)-
z(5))/z(3))*(sim(netL,z)/(z(4)-z(5))))/(1+(2500*(z(4)-z(5))/z(3))));
end
```

APPENDIX D

COPYRIGHT PERMISSIONS

This Appendix includes the copyright permission from the publisher of manuscript #1 and 4 and co-authors who contributed in manuscripts # 2 and 3.

D.1. Manuscript #1

For previously published manuscripts that form a part of a thesis, written permission from the publisher (copyright holder) is required by the College of Graduate Studies and Research (CGSR). For manuscripts published by Elsevier, the authors retain the right to include their publication in a thesis without requesting a written permission:

"*As an author, you retain rights for a large number of author uses, including use by your employing institute or company. These rights are retained and permitted without the need to obtain specific permission from Elsevier. These include: the right to include the article in full or in part in a thesis or dissertation (provided that this is not to be published commercially); the right to use the article or any part there of in a printed compilation of works of the author, such as collected writings or lecture notes (subsequent to publication of the article in the journal); and the right to prepare other derivative works, to extend the article into book-length form, or to otherwise re-use portions or excerpts in other works, with full acknowledgement of its original publication in the journal*."

This information is available at the publisher's website at: http://support.elsevier.com/app/answers/detail/a_id/565/session/L3RpbWUv , Feb. 27, 2012.

D.2. Manuscript #2

For previously published manuscripts that form a part of a thesis, written permission from the publisher (copyright holder) is required by the College of Graduate Studies and Research (CGSR). For manuscripts published by Elsevier, the authors retain the right to include their publication in a thesis without requesting a written permission:

"*As an author, you retain rights for a large number of author uses, including use by your employing institute or company. These rights are retained and permitted without the need to obtain specific permission from Elsevier. These include: the right to include the article in full or in part in a thesis or dissertation (provided that this is not to be published commercially); the right to use the article or any part there of in a printed compilation of works of the author, such as collected writings or lecture notes (subsequent to publication of the article in the journal); and the right to prepare other derivative works, to extend the article into book-length form, or to otherwise re-use portions or excerpts in other works, with full acknowledgement of its original publication in the journal*."

This information is available at the publisher's website at: http://support.elsevier.com/app/answers/detail/a_id/565/session/L3RpbWUv , May 11, 2012.

D.3. Manuscript #3

For unpublished manuscripts, written permission from co-authors is required by CGSR to include the manuscript in a thesis.

Copyright Permission Request Form

I am preparing the publication of manuscript titled:

Energetic, economic and environmental analysis of a health-care facility HVAC system equipped with a Run-Around Membrane Energy Exchanger

to be published as the forth chapter of my M.Sc. thesis, and to be submitted to the Department of Mechanical Engineering at the University of Saskatchewan. The authors contributing in the completion of this manuscript are as follows:

Mohammad Rasouli, Soheil Akbari, Carey J. Simonson, Robert W. Besant

I am requesting permission to use the materials described in aforementioned manuscript in my M.Sc. thesis and all subsequent editions that may be prepared at the University of Saskatchewan. Please indicate agreement by signing below:

Yours truly,

Soheil Akbari

Feb. 27, 2012

Permission granted by:

Signature:

Date:

Copyright Permission Request Form

I am preparing the publication of manuscript titled:

Energetic, economic and environmental analysis of a health-care facility HVAC system equipped with a Run-Around Membrane Energy Exchanger

to be published as the forth chapter of my M.Sc. thesis, and to be submitted to the Department of Mechanical Engineering at the University of Saskatchewan. The authors contributing in the completion of this manuscript are as follows:

Mohammad Rasouli, Soheil Akbari, Carey J. Simonson, Robert W. Besant

I am requesting permission to use the materials described in aforementioned manuscript in my M.Sc. thesis and all subsequent editions that may be prepared at the University of Saskatchewan. Please indicate agreement by signing below:

Yours truly,

Soheil Akbari

Feb. 27, 2012

Permission granted by:

Signature:

Date:

Copyright Permission Request Form

I am preparing the publication of manuscript titled:

Energetic, economic and environmental analysis of a health-care facility HVAC system equipped with a Run-Around Membrane Energy Exchanger

to be published as the forth chapter of my M.Sc. thesis, and to be submitted to the Department of Mechanical Engineering at the University of Saskatchewan. The authors contributing in the completion of this manuscript are as follows:

Mohammad Rasouli, Soheil Akbari, Carey J. Simonson, Robert W. Besant

I am requesting permission to use the materials described in aforementioned manuscript in my M.Sc. thesis and all subsequent editions that may be prepared at the University of Saskatchewan. Please indicate agreement by signing below:

Yours truly,

Soheil Akbari

Feb. 27, 2012

Permission granted by:

Signature:

Date:

D.4. Manuscript #4

For previously published manuscripts that form a part of a thesis, written permission from the publisher (copyright holder) is required by the College of Graduate Studies and Research (CGSR). For manuscripts published by ASHRAE TRANSACTIONS, the authors retain the right to include their publication in a thesis without requesting a written permission:

"ASHRAE retains exclusive copyright of papers published in HVAC&R Research and ASHRAE Transactions. Works published by ASHRAE are final and complete works.

Under ASHRAE copyright policies, authors retain the right for certain specific uses of their paper without requesting ASHRAE's permission. Only the "as published"

version of the paper may be used by the author. These uses are as follows:

• to make copies of the paper for their own personal use;

• to make copies and distribute copies of the paper to researchers or customers

of the author's employer for the personal use by such researchers

or customers;

• to post the paper as published by ASHRAE on the author's personal, institutional, or corporate website or server with a link to ASHRAE's website;

• to present the paper (after ASHRAE publication) at a meeting or conference and to distribute copies of such paper to the delegates attending the meeting with written permission from ASHRAE;

• to allow use of the paper by the author's employer for posting on the

employer's Web site, for use by the employer in training or educational courses offered by the employer, for internal research work that is conducted by the employer, and for internal publications published by the employer;

• to include the paper in full or in part in a thesis or dissertation;

• to include the paper in a printed compilation of works of the author, such as collected writings or lecture notes; and

• to prepare other derivative works, such as extending the paper into booklength form, or to otherwise re-use portions or excerpts in other works,

providing there is acknowledgement of its publication by ASHRAE.

Other uses must be authorized by ASHRAE. Authors should contact ASHRAE explaining their specific need and identifying the paper and ASHRAE publication in which the paper appeared."

This information is available in the Copyright Information section of ASHRAE Author's Manual which can be achieved using the following link: http://www.google.ca/url?sa=t&rct=j&q=ashrae%20transaction%20publication%20permission%20policy&source=web&cd=1&ved=0CCYQFjAA&url=http%3A%2F%2Fwww.ashrae.org%2FFile%2520Library%2FdocLib%2FPublic%2FInteractiveAuthorsManual2_18_11.pdf&ei=PVpNT4KKKKqG0AXct-TMAw&usg=AFQjCNF2vjSO1AvrQwq0DB1TUUgct6o4_w&sig2=yBSWCBYlni9AteRzcGj6wA&cad=rja

Feb. 27, 2012.